MODELING THE HIPPOCAMPUS: FINELY CONTROLLED MEMORY STORAGE USING SPIKING NEURONS

A Dissertation presented to
The Faculty of the Graduate School
University of Missouri – Columbia

In Partial Fulfillment
of the Requirement for the Degree
Doctor of Philosophy

---

by
Ali Hummos

Dr. Satish S. Nair, Dissertation Supervisor

May 2018

The undersigned, appointed by the dean of the Graduate School, have examined the dissertation entitled

MODELING THE HIPPOCAMPUS: FINELY CONTROLLED MEMORY STORAGE USING SPIKING NEURONS

presented by Ali Hummos,

a candidate for the degree of doctor of philosophy of Informatics,

and hereby certify that, in their opinion, it is worthy of acceptance.

Professor Carmen Chicone
Professor Chi-Ren Shyu
Professor Dong Xu
Professor Satish Nair

ACKNOWLEDGEMENTS

I would like to thank my family for their encouragement throughout this long journey. This work could not have been, without their love, support, and patience. I think all my colleagues and fellow scientists, their interactions helped shape my character and polish my knowledge. I would like to thank my advisor Dr. Nair, who guided through this journey me with his kindness and knowledge. I would like to thank my committee members for their direction and consideration, and taking that time to review my research.

TABLE OF CONTENTS

LIST OF FIGURES

LIST OF TABLES

ABSTRACT

The hippocampus, an area in the temporal lobe of the mammalian brain, participates in the storage of personal memories and life events. As such traumatic memories and the consequent symptoms of post-traumatic stress are thought to be stored or at least processed in the hippocampus. While a fundamental understanding of a traumatic memory is still elusive, studying the physiology and functional properties of the hippocampus are an essential first step. Towards that goal, I developed a detailed computational model of the hippocampus. The model included the important effects of the neuromodulator Acetylcholine that switches the hippocampal network between the memory encoding state and the memory retrieval state. In the first study, I examined the mechanisms for controlling runaway excitation in the model. The results indicated different mechanisms for controlling runaway excitation in the memory encoding state as opposed to the memory retrieval state of the circuit. These findings produced the first functionally-based categorization of seizures in animals and humans, and may inspire specific treatments for these types of seizures. The second study examined the underpinnings of the rhythmic activity of the hippocampus. These oscillations in the theta range (4-12 Hz) are theorized to play a major role in the memory functions and in processing sequences of events and actions in both place and time. We found the generation of theta rhythmic activity to be best described as a product of multiple interacting generators. Importantly, we found differences in theta generation depending on the functional state of the hippocampus. Finally, the third study detailed the rules of the complex interactions between these multiple theta generators in the circuit. Our results shed more light on the role of specific components in the hippocampal circuit to maintain its function in both health and disease states.

CHAPTER 1: INTRODUCTION AND OBJECTIVES

1.1 Background and Motivation

Survivors of traumatic events can suffer emotional consequence for decades, caused by the *memories* encoded in their brains. The hippocampus, an area in the temporal lobe of the brain, is intimately associated with the storage of personal events, and is believed to be important for the storage and persistence of traumatic memories.

A mechanism for the storage and recall of series of events emerged after the discovery of place cells in the hippocampus. These neurons respond selectively to position in space (O'Keefe and Dostrovsky 1971), and the sequential activity of a few of them can are present a trajectory in space. More recent research has also expanded this view to a general ability to learn and retrieve sequences of events in both space and time (Poldrack and Rodriguez 2003; Eichenbaum 2000). The ability to store sequences of events in their spatial context underlies the hippocampal involvement in episodic memory.

Storage and retrieval of memories impose opposite constraints on the hippocampal circuit (Marr 1971). Acetylcholine, a cholinergic neuromodulator, can modulate the function of the hippocampus based on its slowly changing levels. High levels set the dynamics of the network to optimize the encoding of new information whereas low levels optimize for retrieval of previously stored information (Michael E. Hasselmo, Wyble, and Wallenstein 1996; M E Hasselmo, Schnell, and Barkai 1995).

To serve as a sequence generator, the hippocampus must represent sequences in a way that allows each step to activate or retrieve the next step in the sequence. Neurons in the hippocampus are richly interconnected through recurrent connections, making them capable of exciting each other. If step of a sequence was encoded by the activity of a neuron, then its outgoing connections can activate the next neuron in the sequence. This setup up is believed to be the substrate of the ability to store and recall sequences of activity, however, it also leaves the circuit prone to runaway excitation where neurons begin to excite each other exponentially through the rich recurrent connections. This dissertation describes work that examines the specific mechanisms in the hippocampal circuit that contains such runaway excitation.

Another important mechanism to encode sequences in time and space is to have an internal clocking device. Whether the hippocampus functions this way is still a controversy, but its activity does manifest rhythmically at theta (4-12 Hz) and gamma frequencies (> 30 Hz). This dissertation uses the same computational model to also examine the underpinnings of these oscillations.

Another highly studied yet elusive aspect of hippocampal function is the oscillatory activity recorded from the hippocampus during periods of activation. The dominant oscillatory frequency is in the 4-12 Hz band (labeled 'Theta' band) and the >30 Hz 'gamma' band (for review see, Buzsáki 2002; Buzsáki and Wang 2012).

This dissertation focuses on the modeling and analysis of the hippocampus at a cellular and systems level, to address some of the questions about runaway excitation and oscillatory activity. The following section details the organization of this dissertation.

1.2 Chapter Overview and Objectives

Chapter 2 – The rich recurrent connectivity between hippocampal neurons underlies the ability of the hippocampal CA3 region to retrieve previously learned pattern of activity (Marr 1971), but also leaves the area vulnerable to runaway excitation resulting in seizure episodes (aberrant spread of excessive electrical activity through brain tissue). The goal of our first study is to elucidate mechanisms that maintain this excitatory activity under control.

We found that distinct circuit mechanisms were responsible for controlling runaway excitation in the memory encoding circuit vs the memory retrieval circuit. These findings represent a fundamentally new approach to categorizing seizures based on the functional state of the brain. In support of our findings, we found disordered rats that show seizures only when required to learn their way around a novel environment.

Chapter 3 – Theta rhythms in the 4-12 Hz are the predominant oscillatory signature of the hippocampus. Their origins and function remain unknown. We used our hippocampal model to shed light on the generation of theta rhythmic activity in the hippocampus during spatial navigation and active exploration. Our results revealed a multitude of mechanisms active simultaneously and interactively to generate and maintain theta rhythmicity in the hippocampus. Additionally, we found again that there

are differences between the memory encoding and memory retrieval circuits that also extend to how they generate rhythmic activity.

Chapter 4 – We found the hippocampus to have multiple mechanisms acting in concert to generate its rhythmic activity. In this study we sought a deeper understanding into the rules that govern which mechanisms can substitute for one another and more interestingly, which mechanisms can interfere compete with other mechanisms. Towards that goal we presented a new conceptualization of mechanisms into categories including resonant and synchronizing mechanisms. This conceptual delineation enabled us to better predict the effects of inactivating certain mechanisms in experiments.

Chapter 5 – Summary and conclusions are presented to provide a coherent high-level picture of our work.

Appendix – Provide material that describes the mathematical details of our hippocampal model.

CHAPTER 2: Intrinsic mechanisms stabilize encoding and retrieval circuits differentially in a hippocampal network model

Ali Hummos, PhD student[1, 2], Charles Franklin, PhD student[3], Satish S. Nair, Professor[1, 3]
[1] Informatics Institute, [2] Department of Psychiatry, [3] Department of Electrical & Computer Engineering, University of Missouri, Columbia, Missouri.

Abstract

Acetylcholine regulates memory encoding and retrieval by inducing the hippocampus to switch between pattern separation and pattern completion modes. However, both processes can introduce significant variations in the level of network activity and potentially cause a seizure-like spread of excitation. Thus, mechanisms that keep network excitation within certain bounds are necessary to prevent such instability. We developed a biologically realistic computational model of the hippocampus to investigate potential intrinsic mechanisms that might stabilize the network dynamics during encoding and retrieval. The model was developed by matching experimental data, including neuronal behavior, synaptic current dynamics, network spatial connectivity patterns, and short-term synaptic plasticity. Furthermore, it was constrained to perform pattern completion and separation under the effects of acetylcholine. The model was then used to investigate the role of short-term synaptic depression at the recurrent synapses in CA3, and inhibition by Basket cell (BC) interneurons and oriens lacunosum-moleculare (OLM) interneurons in stabilizing these processes. Results showed that when CA3 was considered in isolation, inhibition solely by BCs was not sufficient to control instability. However, both inhibition by OLM cells and short-term depression at the recurrent CA3 connections stabilized the network activity. In the larger network including the dentate gyrus, the model suggested that OLM inhibition could control the network during high cholinergic

levels while depressing synapses at the recurrent CA3 connections were important during low cholinergic states. Our results demonstrate that short-term plasticity is a critical property of the network that enhances its robustness. Furthermore, simulations suggested that the low and high cholinergic states can each produce runaway excitation through unique mechanisms and different pathologies. Future studies aimed at elucidating the circuit mechanisms of epilepsy could benefit from considering the two modulatory states separately.

Introduction

The hippocampus plays an important role in memory storage and retrieval. Through the process of pattern completion, the CA3 region of the hippocampus aids in the retrieval of previously learned memory traces even from partial cues or noisy inputs (Marr, 1971). In contrast, the dentate gyrus (DG) functions to separate neural representations of similar memories (pattern separation), via a different circuit, to optimize their storage and later retrieval (Marr, 1971; for review, see Hunsaker and Kesner, 2013).

The recurrent connections in the hippocampal CA3 region are implicated in the retrieval of memories (Marr, 1971). However, it is also known that networks with high levels of recurrence are inherently unstable (Marr, 1971; Miles and Wong, 1983, 1987; Cossart et al., 2005; Beyeler et al., 2013). Excitatory activity in CA3 can be amplified and propagated throughout the network, creating a seizure-like response.

Furthermore, projections from DG to CA3 through the mossy fibers (MF) can also result in runaway excitation (Lawrence and McBain, 2003). Acetylcholine (ACh) has been proposed as a regulator of the circuit with high levels favoring pattern separation, and low levels facilitating pattern completion (Hasselmo et al., 1995). The neuromodulator ACh has a prominent role in encoding new memories and high cholinergic levels are induced by novelty and active exploration (Barry et al., 2012). It alters the circuit dynamics by lowering the synaptic efficacy at the recurrent connections in CA3 and by boosting transmission at MF synapses from DG to CA3. This combination, together with other effects on synapses and cell excitability, allows the network to encode separated representations of the current input while reducing interference from previously encoded memories (Hasselmo et al., 1995). These separated neuronal representations of memories

are created in DG and subsequently transmitted to CA3 through the sparse but powerful mossy fibers (Henze et al., 2002). Therefore, though the recurrent connections are suppressed during encoding, the impinging current from DG through these "detonator" synapses can also destabilize the CA3 network (Lawrence and McBain, 2003). Computational models of pattern separation and completion in the hippocampus have provided an important conceptual framework of how these processes might be regulated in the hippocampus (Treves and Rolls, 1992; Hasselmo et al., 1995) and have been validated experimentally (Rolls and Kesner, 2006; Leutgeb et al., 2007; Neunuebel and Knierim, 2014). Recent models have extended these results using spiking neurons (Meeter et al., 2004; Nolan et al., 2010). These models focused on the mechanisms and dynamics of memory storage and retrieval, and handled the instability in the network indirectly using a number of techniques such as normalizing total network activity (Treves and Rolls, 1992), using abstract models of feedback inhibition and attractor dynamics (Hasselmo et al., 1995), explicitly limiting the number of active cells (Meeter et al., 2004), and excluding recurrent connections from the model (Nolan et al., 2010). In the present study, we explicitly focus on intrinsic hippocampal mechanisms such as short-term plasticity (Abbott and Nelson, 2000), and interneurons (Lawrence and McBain, 2003), to investigate their roles in controlling neuronal excitability and the pathological states they might engender. Towards this end, we developed a biologically-realistic model of the hippocampus that included principal cells and two of the most common interneurons, basket cells (BC) and oriens lacunosum-moleculare (OLM) cells (Vida, 2010). Both interneuron types are well-studied and are differentially modulated by ACh (Lawrence et al., 2006). We matched experimentally reported behaviors, including

neuronal excitability, synaptic current dynamics, network spatial connectivity patterns, and short-term synaptic plasticity. The model suggested that OLM and BC inhibition and short-term synaptic plasticity contribute differently to network stability. Additionally, pattern separation and completion circuits in the hippocampus might produce instability through different dynamics, consequently requiring different mechanisms for their stabilization.

Methods

We developed a biologically realistic network model of the hippocampus that included networks for entorhinal cortex (EC), DG, and CA3 regions. The model is described next with the mathematical details and additional experimental data used provided in supplementary materials. The model was implemented using the NEURON software package (Carnevale and Hines, 2009). The code will be made available upon publication via the ModelDB public database (http://senselab.med.yale.edu/ModelDB/).

Single cell models

The model cells in CA3 were pyramidal cells and two of the most abundant interneuron types, BC and OLM cells (Vida, 2010). The model cells in DG were granule cells, BC, and Hilar Perforant Path-associated (HIPP) cells.

Single neurons were modeled using the Izhikevich formulation (2003, 2010). This formulation provides a reduced-order model that preserves many of the neuro-computational properties of more detailed biological models. We provide an overview below on how model neurons were matched to the salient features of electrophysiological recordings (Fig. 1). Section S2 in the supplementary materials has further experimental

data considered in developing the single cell models, and a listing of the model equations and parameters used.

For CA3 pyramidal cells, the resting membrane potential was set to -75 mv, spike threshold to -53 mv, and peak action potential voltage to 29 mv, as reported by Brown and Randall (2009). The remaining cell model parameters were tuned to match responses to both long and short current injections (Fig. 1, Table S1; Brown and Randall, 2009). Similarly, in developing the DG granule cells model, resting membrane potential, threshold, and peak action potential were set using data from Staley et al., (1992) and the model was then tuned to match current injection responses (Fig. 1, Table S1; Staley et al., 1992). OLM model passive properties were estimated from Ali and Thompson (1998), and the behavior of the cells was matched to current injections from the same study. In particular, we matched the spike frequency adaptation, the prominent slow after-hyperpolarization potential (AHP, Fig. 1), sag response, and rebound spikes (Fig. S1). For BC model, membrane properties (Table S1), current injection responses (Fig. 1), and finally current vs. firing rate relationship (Fig. S2) were matched to data reported by Buhl et al., (1996). Due to the striking similarity of OLM and HIPP cells (Katona et al., 1999), we used the same model for both cell types.

Neurons in the model had membrane potential values drawn from a random distribution. The initial voltage was drawn from a normal distribution with a mean 5 mv lower than their resting potential, and with a standard deviation of 10 mv. These values maintained the network stability at the beginning of simulations.

Network structure and connectivity

The rat hippocampus contains approximately 1.6 million cells (Hosseini-Sharifabad and Nyengaard, 2007). For computational efficiency, the numbers were scaled down while maintaining reported ratios (see section S3.1 of supplementary materials). The model DG region had 384 granule cells, and 32 each of BC and HIPP interneurons, while the model CA3 region contained 63 pyramidal cells and 8 each of BC and OLM interneurons (Seress and Pokorny, 1981; Kosaka et al., 1987; Baude et al., 2007; Hosseini-Sharifabad and Nyengaard, 2007).

The entorhinal cortex provides inputs to the hippocampus through the perforant pathway that projects to the entire hippocampal formation. The standard view describes a unidirectional connectivity with a direct pathway from EC to CA3 and an indirect pathway through DG (Fig. 2A, B) (Naber et al., 1997; Witter, 2010). The perforant path projections follow a lamellar organization across the longitudinal axis of the hippocampus, as follows: Lateral and posterior parts of the EC are connected to the dorsal parts of CA3 and DG, while the medial and anterior parts of EC project to the ventral parts of CA3 and DG. This lamellar organization transitions gradually from one extreme to the other on the longitudinal axis of the hippocampus, and a single neuron in EC can project to about 25% of the longitudinal length of CA3 (Witter, 2010). Projections from DG to CA3 (the indirect pathway) also follow a similar longitudinal organization; however, these projections target a more limited longitudinal extent (Fig. 2A, C; Witter, 2010).

Model cells were distributed in 3D space separated into the three regions, EC, DG, and CA3, with dimensions that approximate the respective dimensions of the rat hippocampus

(see section S3.2 of supplementary materials). Projections from EC to both pyramidal cells and BCs in DG and CA3 followed a lamellar pattern where neurons were most likely to connect to neurons in the center of their longitudinal neighborhood with a decreasing probability towards the periphery. This spatial connectivity was modeled using a Gaussian connection probability function that depended on the longitudinal distance between the two cells to be connected (Fig. 2C, D). The Gaussian function had a peak probability value of 0.4 and a standard deviation of 3 mm for the perforant path projections to both pyramidal and BCs in CA3 (Fig. 2C). Perforant path projections to DG had similar values as listed in table S3.

Similarly, MF projections from DG to CA3 followed the same lamellar pattern but with a more limited longitudinal extent by setting the standard deviation of the Gaussian probability function to 2 mm (Fig. 2C). In addition, to preserve the sparseness of the MF connections from DG to CA3, each DG granule cell connected to a maximum of two CA3 pyramidal neurons (Rolls and Kesner, 2006). Projections from DG granule cells to CA3 BCs are more diffuse and out-number projections to CA3 pyramidal neurons by a ratio of 10:1 (Acsady et al., 1998). Accordingly, DG projections to BC followed a Gaussian distribution with a peak probability of 0.2 and standard deviation of 3 mm (Fig. 2D). Recurrent CA3 connections generally reveal no spatial organization (Wittner et al., 2007), and therefore were distributed homogenously with a fixed probability of 0.3.

The dendritic projecting OLM cells are thought to be involved in feedback inhibitory loops (Maccaferri, 2005) and while they have a more limited axonal arborization (Buhl and Whittington, 2007) they make many more synapses compared to BCs (Sik et al., 1995). In contrast, BCs have a more diffuse axonal arborization with the highest

connection probability to pyramidal cells in their immediate neighborhood and a decreasing connection probability towards the periphery of their axonal arbors (Sik et al., 1995). Similarly, BCs project to neighboring OLM cells (Bartos et al., 2010). As before, we used a Gaussian function to approximate these spatial probabilities (Fig. 2E). We also assumed that BC projections to both pyramidal cells and to OLM cells shared the same spatial domain. Section S3.2 of supplementary materials has additional details.

In the reverse direction, OLMs receive reciprocal connections from the same pyramidal cells they projected to, in line with their function as local feedback cells (Maccaferri, 2005). On the other hand, principal cells in both DG and CA3 projected homogenously to BCs with a fixed probability of 0.15, consistent with the lack of specific topography reported at these projections (Wittner et al., 2006).

The network was constructed by generating connections randomly between cells while observing the connection probabilities and the spatial patterns of connectivity described above and in section S3.2 of supplementary materials. For each experiment, we performed 10 random initializations of the network and averaged the results. The spatial connectivity patterns are summarized in table 1, and parameters for synapses are listed in tables S3 and S4. Spontaneous firing rates of pyramidal cells in CA3 (Mizuseki et al., 2012) and granule cells in DG (Bower and Buckmaster, 2008) were matched to experimental reports in the full network.

Synaptic currents

Synaptic currents were modeled using the kinetic models described by Destexhe et al. (1998). The synaptic currents AMPA, NMDA, $GABA_A$, and $GABA_B$ were modeled and

their dynamics such as rise and decay time constants and delays were matched to available literature. In particular, CA3 pyramidal cell AMPA currents were fastest for MF inputs from DG and slowest for perforant path inputs from EC, while recurrent CA3 inputs from other pyramidal cells had intermediate values, as summarized in table 1 (Hoskison et al., 2004; Tóth, 2010). Additionally, inhibitory currents from OLM had slower dynamics compared to those from BC (Table 1; Bartos et al., 2010). Equations implemented are described in detail in section S4.1 in the supplementary material and parameters used are listed in tables S3 and S4.

Synaptic weights were assigned in accordance with literature where available (see tables 1, S3, and S4). The MF synapses were adjusted so that a train of spikes arriving at the synapse could cause a CA3 neuron to fire while a single spike could not (Henze et al., 2002). Recurrent CA3 collaterals were assigned a low initial weight, as an approximation of data showing that action potentials have a transmission probability of 4% at those synapses (Miles and Wong, 1986). Synapses from CA3 pyramidal to interneurons were set at a higher level considering that action potential transmission occurs at a ~60% success rate (Miles, 1990; Gulyás et al., 1993). Connections between granule cells and DG interneurons were adjusted to achieve sparse DG firing (Bower and Buckmaster, 2008). These assigned synaptic weights are listed in tables 1, S3, and S4. Synapses had initial weights chosen from a uniform random distribution, with a range from 50% to 100% of the assigned weight value.

Long-term synaptic plasticity

Classical Hebbian associative long-term potentiation (LTP) was shown at the perforant path synapses to DG (Bliss and Lomo, 1973) and to CA3 (Do et al., 2002; McMahon and

Barrionuevo, 2002). On the other hand, the characteristics of MF potentiation are controversial (Bliss et al., 2007), and so we only modeled short-term plasticity in the MF connections, as described below.

At GABAergic synapses, many forms of synaptic plasticity exist (for a review, see Maffei, 2011). Woodin et al., (2003) reported that activation of pre- and post-synaptic neurons in the hippocampus lead to LTP if the pre- and post-synaptic spikes were within 20ms of each other, LTD if within 50ms, and no change if longer. They also found this plasticity to be dependent on activation of postsynaptic L-type voltage dependent calcium channels (VDCCs).

To reproduce these experimental findings, long-term postsynaptic plasticity was implemented using a learning rule that used the concentration of a post-synaptic calcium pool at each modifiable synapse (Kitajima and Hara, 1997; Shouval et al., 2002; Li et al., 2009; Kim et al., 2013a, 2013b).

At excitatory synapses in our model, calcium entered post-synaptic pools via NMDA receptors, whereas at inhibitory synapses, calcium entered through VDCCs, and in addition, the postsynaptic pool also received Ca^{2+} from internal stores upon $GABA_B$ receptor stimulation (Gaiarsa et al., 2002). Such as scheme has been in other models by our group (Li et al., 2009; Kim et al., 2013a, 2013b). For both types of synapses, the synaptic weight depressed when calcium concentration of the pool was above a lower threshold and increased if the concentration exceeded an upper threshold. Equations and details related to the learning rule are provided in section S4.2 of the supplementary materials.

Short-term synaptic plasticity

In addition to long-term plasticity, model synapses also exhibited short-term synaptic plasticity that used the formulation proposed by Varela et al. (1997). We modeled the pronounced short-term facilitation at MF (Toth et al., 2000) and the frequency-dependent synaptic depression reported at the recurrent CA3 connections (Fig. 3; Hoskison et al., 2004).

In CA1, projections from pyramidal cells display short-term facilitation at synapses contacting OLM cells (Ali and Thomson, 1998), and short-term depression at those contacting BC cells (Ali et al., 1998). In the other direction, inhibitory currents from OLM cells to pyramidal cells show no short term facilitation or depression (Maccaferri, 2005), while inhibitory currents from BCs to pyramidal cells show depression (Hefft and Jonas, 2005). Equations and parameter values used to model these short-term plasticity patterns are provided in section 4.2 and table S5 of the supplementary materials, and model traces are compared with available experimental recordings in figure 3.

Acetylcholine effects

The neuromodulator acetylcholine activates two main classes of receptors, both of which are present in the hippocampus: muscarinic receptors that are coupled with a G-protein signaling cascade, and nicotinic receptors that are fast ionic channels. The hippocampus receives widespread volume transmission of cholinergic inputs from the septum-diagonal band complex (Woolf, 1991). To implement the effects of ACh on model neurons and synapses, we used a variable ‘ACh’ to represent the ACh level. The variable ACh had discrete values of 0 (low), 1 (baseline), and 2 (high).

Cholinergic stimulation has differential effects on synaptic transmission of different pathways in the hippocampus (Barry et al., 2012). Synaptic transmission through the perforant pathway projections to CA3 is suppressed by 50%, compared to a suppression by 85% at the recurrent connections in CA3 (Hasselmo et al., 1995; Kremin and Hasselmo, 2007). On the other hand, MF transmission is enhanced by 49% (Vogt and Regehr, 2001).

To model ACh effects on synapses, AMPA synaptic currents were scaled by the value of ACh. A parameter bACh determined the direction and magnitude of ACh effects on a particular synapse. Values of bACh for different synapses were set according to experimental results as summarized in table 1. The specific equations used to model these are listed in section S5.2 of supplementary materials.

In addition to the synapse specific effects, cholinergic stimulation enhanced cellular excitability and depolarized the resting membrane potential of principal cells, eliminated AHP, decreased spike frequency adaptation and induced rhythmic burst activity (Misgeld et al., 1989; Bianchi and Wong, 1994). Furthermore, effects on interneurons were subtype-dependent (McQuiston and Madison, 1999a, 1999b). Muscarinic stimulation of OLM interneurons depolarized the resting membrane potential, and lowered both spike frequency adaptation and AHP (Lawrence et al., 2006). In contrast, PV-BCs express low levels of nicotinic ACh receptors, and respond to muscarinic receptor activation with a limited resting membrane potential depolarization (Cea-del Rio et al., 2010; Cobb and Lawrence, 2010).

Effects of ACh on neurons were modeled by linearly scaling the neuronal model parameters by the ACh level as shown in figure S4 and detailed in section S5.1 of the supplementary materials. This setup produced a different set of parameter values for model neurons at low, baseline and high levels of ACh as listed in table S2. Considering the slow dynamics of ACh effects (onset time constant approximated between 1 and 2 s; Hasselmo and Fehlau, 2001), ACh level was set to a given value at the beginning of each experiment and had no dynamics.

Inputs and data analysis

Recordings from the hippocampus reveal a low spontaneous firing rate of 0.50 ± 0.78 Hz in CA3 (Mizuseki et al., 2012) and similar rates in DG (Bower and Buckmaster, 2008). Principal cells in CA3 and DG received random Poisson inputs to generate the spontaneous firing rates reported in vivo in the network.

To test the robustness in response to a wide range of input intensities, the network was challenged with 30 trials of increasing levels of input from EC. Each trial had a duration of 500 ms at the beginning of which a number of EC neurons were selected to receive one action potential each. Starting with trial 1 where one EC neuron was stimulated, one additional neuron received input for each subsequent trial until 30 neurons were stimulated at trial 30. This input structure was created so that a gradually increasing number of EC neurons fired one action potential at the beginning of the trial. This EC input was transmitted through the perforant pathway to the downstream CA3 and DG regions. For each neuron in CA3, the number of spikes fired during each trial was recorded, and the neuron was considered active if it had a z-score higher than 2.58 ($p <$

0.01, two tails), where z = (firing rate - mean spontaneous firing rate)/SD. For each experiment, we report the ratio of active to inactive neurons in CA3 to follow the dynamics of how rapidly cells are recruited into the pool of active cells, as intensity of input from EC increases.

Simulation details

The model was developed using the NEURON package and run on a PC with an Intel i7-core processer with an integration time-step of 0.1 ms (Carnevale and Hines, 2009). The recorded spike times were then analyzed using MATLAB (Mathworks).

As mentioned above, cell models had membrane potential values drawn from a random distribution. Additionally, network connectivity and initial synaptic weights were also drawn from random distributions. Accordingly, for each experiment, 10 simulations with different random initializations of the network were considered. Numbers reported in results are averages ±SD over data from these 10 different runs.

Model tuning and validation

The overall model was developed in stages: the single cell models, the properties of glutamatergic and GABAergic synapses, the intrinsic connections between cells, plasticity in appropriate connections, and, finally, neuromodulator effects. The following approach was used for modeling each of the above: (1) The experimental literature was mined, both to constrain the model and derive criteria to assess whether the model successfully reproduced the particular phenomena being modeled; (2) Iterative "tuning" of model parameters was performed until the model's behavior matched experimental observations; and (3) Validation of the model, which took two forms. First, the ability of

the model to reproduce the experimental data considered in its development. Second, the ability of the model to reproduce a set of experimental observations it was not designed to reproduce. The tuning and validation procedure used are described next.

Model Tuning: To further constrain the model and assess its functional capacity, we tuned it to perform pattern separation and pattern completion. The additional tuning required was mainly to adjust connection weights and LTP thresholds (Tables S3 and S4), to ensure practical neuron activity levels and synaptic learning rates.

Following Hasselmo et al. (1995), we ran the network through an encoding phase under high levels of ACh (= 2). In this encoding phase, an input pattern was constructed to consist of 10 randomly selected EC neurons (pattern 1), and the network was then presented with this input pattern for five 500 ms trials. For each trial, EC neurons in the pattern received inputs for 250 ms at 12 Hz.

After the encoding phase, we tested for retrieval in response to 10 input patterns that had decreasing amounts of overlap with the encoded pattern 1. The 10 probe patterns, numbered 2 to 11, were constructed as follows. Pattern 2 contained nine of the neurons in pattern 1 and an additional neuron selected randomly. Similarly, pattern 3 shared eight neurons with pattern 1 and included two other neurons selected randomly. With this logic, Pattern 11 had no neurons in common with pattern 1. To test for retrieval, all long-term plasticity was inactivated and we examined the output retrieved in response to probe patterns 2 to 11 under the lowered (retrieval) level of ACh (= 0).

In each retrieval trial, one of the eleven patterns was presented at EC, and the number of spikes each neuron fired during the trial was recorded. Subsequently, to form a trial "output" pattern for each area, the spike counts from all its principal cells were populated

into a vector that was normalized to a length of one. The correlation between the outputs of any two trials was then assessed by taking the dot product of the two corresponding output vectors. This correlation measure has a minimum value of 0 indicating that the two output patterns being compared had a non-overlapping set of neurons firing in each. Conversely, a correlation level maximum value of 1 indicates that the two vectors had the same set of neurons firing at the same rates.

For each area in the model, we calculated pair-wise correlation comparisons between the output from pattern 1 and the output from each of the patterns from 1 to 11. Figure 4 shows these pair-wise correlation values for EC, CA3 and DG averaged from 10 different randomly constructed model networks. Inputs arrived directly at EC neurons, thus, EC correlation levels reflect the similarity between input patterns. Correlation between CA3 output patterns were above EC correlation (Fig. 4A), indicating that CA3 was engaged in retrieval of stored patterns. For instance, input pattern 3 had a correlation of 0.8 with input pattern 1, whereas in CA3, the output from pattern 3 had a correlation of 0.98 with pattern 1, indicating that even for dissimilar inputs CA3 retrieved output that are more similar to the learned pattern 1. Thus, even with changes in the sensory input, CA3 may still retrieve a previously learned memory pattern. On the other hand, DG outputs revealed lower correlation relative to inputs, indicating that DG was predisposed to create distinct neuronal representations (Fig. 4A).

These results are consistent with computational theories of the division of labor between DG and CA3 (Treves and Rolls, 1992; O'Reilly and McClelland, 1994; Hasselmo et al., 1995; McClelland and Goddard, 1996) and recent experimental evidence (Lee and Kesner, 2004; Leutgeb et al., 2007; Bakker et al., 2008; Neunuebel and Knierim, 2014).

Model validation: Cholinergic transmission has been implicated in the modulation of activity in CA3 with high ACh favoring pattern separation and low ACh levels favoring pattern completion (Hasselmo et al., 1995; Rogers and Kesner, 2003; Meeter et al., 2004). Accordingly, to validate the model, we examined the effects of different levels on ACh on the dynamics during retrieval, and compared the results to reports in the literature. Averaged results from 10 random initializations of the network demonstrated that CA3 outputs in response to probe patterns 1-11 had significantly lower correlation levels to the encoded pattern 1 under high levels of ACh compared to low ACh levels (Fig. 4B), while DG correlation levels remained unchanged (not shown). These observations are in agreement with previous models (Hasselmo et al., 1995; Meeter et al., 2004; for review, see Newman et al., 2012) and experimental results (Ikonen et al., 2002; Rogers and Kesner, 2003, 2004).

Limitations: The Izhikevich neuron model formulation focuses on the dynamics around the resting state of the neuron and our modeling efforts aimed at reproducing the current injection responses such as spiking dynamics, adaptation and bursts. Model resting membrane potentials, threshold voltage, and peak action potential were matched to experimental values, but the input resistance was not. As cited, we did match current injection responses and so feel that the firing dynamics were modeled well. The Izhikevich formulation also allows for other currents to be added, further improving single cell characteristics, if required.

Also, we note that synapses from DG granule cells to CA3 parvalbumin-BCs exhibit short-term synaptic facilitation (Szabadics and Soltesz, 2009). However, inputs from MF to other types of interneurons such as Cholecystokinin-BC exhibit short-term depression.

Therefore, we assumed that the combined input from DG to both populations of BC cells would then effectively have no short-term dynamics. Accordingly, the MF synapses to BCs in the present model did not have any short-term plasticity.

Results

Our network model included the CA3 and DG regions of the hippocampus, with EC providing inputs to both regions (Fig. 2). The model also incorporated the effects of cholinergic modulation proposed by Hasselmo et al. (1995) and showed similar dynamics discussed next.

Under high levels of ACh, the DG formed distinct representations of input patterns, mainly due to the large numbers of DG granule cells. High ACh levels caused granule cells to fire at a higher rate through a more depolarized membrane potential, lower spike frequency adaptation, and lower AHP. This increased rate, combined with the prominent short-term facilitation at MF synapses, allowed high ACh levels to enhance the flow of information from DG to CA3. Furthermore, the high cholinergic state also suppressed synaptic transmission at the inputs from EC to CA3 and at the recurrent synapses in CA3; thereby decreasing any interference produced by similarity to any previously learned patterns during the encoding of new patterns. Additionally, the abundant connections from DG to CA3 BCs further increased the level of inhibition on CA3 pyramidal cells and reduced the activation of previously encoded memory patterns. In contrast, during the retrieval of stored patterns in the low cholinergic state, granule cells fired at a lower rate reducing their influence over CA3 pyramidal cells considerably. Low levels of ACh also boosted inputs to CA3 cells from EC and from other CA3 neurons. These effects

facilitated the retrieval of previously learned patterns as also shown in previous models (Barkai et al., 1994; Hasselmo et al., 1995; Hasselmo and Wyble, 1997).

The control that ACh exerts on the firing rate of granule cells, combined with the profound MF short-term facilitation, allowed ACh to gate the synaptic transmission from DG to CA3 effectively. Although this mechanism has been speculated based on experimental results (Vogt and Regehr, 2001), our model functionally implemented this particular mechanism and incorporated it into the framework established by Hasselmo et al. (1995) and Hasselmo and Wyble (1997).

During the development of the model, runaway excitation was a common phenomenon (Hasselmo et al., 1995). To prevent this spread of excitation we included several candidate mechanisms that were successful at stabilizing excitatory activity in the model without affecting the ability to encode and retrieve patterns as shown in figure 4. After developing and validating the model (fig.3), we used the model in its baseline state (prior to training with pattern 1), to investigate the specific roles of these intrinsic mechanisms in preventing runaway excitation after turning off plasticity and setting ACh to 'medium' level. We devised the following method for this analysis: EC neurons were projected to CA3 at increasing levels of activity, over 30 trials, as follows. Selected EC neurons were stimulated to fire one action potential at the beginning of a given trial. Starting with one neuron stimulated during trial 1, one additional EC neuron received stimulation for each trial, until thirty distinct neurons were stimulated during trial 30 (see Fig. 5A). This study resulted in several findings discussed in the following sections. We repeated the analysis using the model after it had learned pattern 1, and found similar results, as we describe later.

Recurrent connections create seizure-like instability

To characterize the unstable dynamics in CA3 created by its recurrent connections, DG was turned off and OLM and BC interneurons were disconnected. Additionally, short-term depression was removed from the recurrent connection synapses, all long-term plasticity was blocked, and ACh was set at the baseline 'medium' level. The EC neurons were then projected to CA3 at increasing levels of activity, over 30 trials. A typical EC firing pattern throughout the experiment is shown in figure 5A. Responses of CA3 neurons were then recorded without (Fig. 5B, D1) and with the recurrent connections in place (Fig. 5C, D2). As expected, CA3 population firing rate increased linearly with increasing inputs from EC, when the recurrent connections were disabled (Fig. 5E). In contrast, the population firing rate showed a sudden non-linear increase when the recurrent connections were present (Fig. 5E). These results are consistent with observations from earlier models (Traub et al., 1987).

While the population firing rate was helpful in detecting instability in the level of excitation, from a computational perspective, it is not the only relevant measure. We are interested in the ability of the model to form patterns of activity in response to inputs. A pattern is formed meaningfully, when only a subset of neurons are active. Towards this end, we quantified the ratio of neurons that were "active" for each input trial. A neuron was considered active in a trial if its z-score was higher than 2.58 (see methods). As expected, the activity ratio curve demonstrates the instability caused by recurrent connections (Fig. 5F) and the shape of the curve illustrates the difficulty recurrent connections pose in a model. Low inputs produce little response, and high inputs produce an unstable firing pattern where all cells fire, resulting in a very limited range for forming

distinct patterns of activity, i.e., limited capacity to handle variations in input level. Furthermore, the addition of recurrent connections changed the frequency at which bursts of different sizes occurred and caused a peak where bursts of four action potentials were more likely to occur (Fig. 5G).

Basket cells fail to control instability

As a first step to investigate the control of neuronal excitability in the CA3 network, we activated the fast spiking BCs in CA3, i.e., examined the behavior of the recurrent CA3 network with only BCs added. Considering the importance of BC firing rates at different levels of input, in addition to matching current injection behavior of BCs, we also matched the input-firing frequency curve for one of the BC interneuron reported by Buhl et al. (1996) (Figure S2). The reader is also reminded that connections in both directions from BC to pyramidal and vice versa exhibited short-term synaptic depression (Ali et al., 1998; Hefft and Jonas, 2005). Therefore, in this experiment, OLMs remained disconnected, short-term depression and long-term plasticity were blocked, and ACh was at the baseline 'medium' level. The network was tested with three levels of BC-to-pyramidal cells weights; low, medium, and high, with the weight values 0.1, 3, and 6 respectively.

Contrary to expectations, inhibition by BCs was unable to prevent instability in the CA3 network (Fig. 6A), and merely shifted the curve of the ratio of active neurons to the right with minimal effect on the profile of exponential increase. Even for high levels of BC inhibition, the minimal decrease in slope was not sufficient to stabilize the network during encoding and retrieval. We also determined the ratio of active BCs using z-scores

(Fig. 6B). Interestingly, despite receiving direct inputs from pyramidal cells that increased exponentially with number of trials, BCs continued to respond linearly with trials due to short-term depression at the pyramidal-to-BC synapses.

OLM interneurons and short-term depression in recurrent connections can control instability

We then asked whether OLM cells by themselves could provide the inhibition characteristics required to contain the instability in the CA3 network. To isolate the effects of OLM cells, we kept the same conditions as in the previous section except for disconnecting BCs and connecting OLM cells instead. As noted in methods, OLM cells received input from pyramidal cell with synapses exhibiting short-term facilitation (Ali and Thomson, 1998). This CA3 network was tested with low, medium and high levels of OLM inhibition (OLM to pyramidal weights 0.1, 3, 6, respectively). Despite their slow dynamics, OLM cells were surprisingly effective in controlling the instability (Fig. 7A). Higher levels of OLM inhibition moved the curve for the ratio of active pyramidal cells closer to linearity and decreased its slope below the curve for inputs increase (Fig. 7A). In addition, recruitment of OLM neurons into the 'active' pool showed a sudden nonlinear jump even for high levels of OLM inhibition during which pyramidal cells showed a near linear increase (Figs. 7A, B). This increased recruitment permitted OLM cells to contain instability in CA3 responses effectively.

To allow a qualitative comparison with results from optogentic silencing of BC and OLM cells in vivo (Royer et al., 2012), we calculated the change in the occurrence of bursts of different sizes when either OLM or BC inhibition was lowered from high to low.

Consistent with experimental findings (Royer et al., 2012), lowering OLM inhibition significantly increased the occurrence of bursts of five or more action potentials, whereas lowering BC inhibition modestly increased the frequency of bursts of two action potentials (Fig. 7C).

Next, we tested the effects of short-term depression in the recurrent CA3 connections as the sole stabilizing mechanism. For this, we disconnected BC and OLM cells and tested low, medium and high levels of short-term depression (d1 = 0.9, 0.7, 0.5, d2 = 0.98, 0.92, 0.86, respectively; equations in section S4.2 in supplementary materials). Note that the short-term depression parameters for medium levels were obtained by matching experimental recordings of recurrent CA3 connections (Fig. 3, Hoskison et al., 2004). Similar to the effects of OLM inhibition, simulations revealed that higher levels of short-term depression also decreased the rate of CA3 pyramidal cell recruitment below the rate of input increase (Fig. 8A). The magnitude of this effect was sufficient to increase the input range at which the model can form patterns to support encoding and retrieval.

Finally, activating either OLM inhibition or short-term depression alone at their 'baseline' levels, which were matched to experimental recordings, was not sufficient to reduce the rate of activity increase in CA3 below the rate of input increase at EC, and rather, higher than experimentally reported levels were necessary. Accordingly, a test with both mechanisms active at the experimentally reported 'baseline' levels revealed that the presence of both mechanisms reduces the rate of recruitment of pyramidal cells effectively (Fig. 8B).

High and low cholinergic states require different stabilizing mechanisms

The findings so far indicated that while BCs were incapable of stabilizing the CA3 network at baseline (medium) levels of cholinergic transmission, both inhibition by OLM cells and short-term depression at the recurrent connections did effectively control the instability. Our interest however extends to stabilizing the network in both low and high cholinergic states, where network instability might be more likely. Therefore, we next investigated the role of OLM inhibition and short-term depression in the full network, including DG, with all synapses and mechanisms active.

Recruitment of CA3 pyramidal cells was accordingly evaluated at low and high ACh levels, with either OLM inhibition or recurrent connections short-term depression active. Model runs revealed that for the low ACh case, short-term depression at the recurrent connections was the critical mechanism to maintain stability (Fig. 9A1) and the effect of OLM cells was no longer sufficient (Fig. 9A2). In contrast, for the high ACh case, short-term depression at the recurrent CA3 connections was by itself ineffective (Fig. 9B1), and OLM cells were the necessary mechanism to maintain stability (Fig. 9B2).

To further investigate these results, we looked at the distribution of burst sizes in CA3 and DG without the stabilizing effects of OLM inhibition and short-term depression (Figs. 10A, B). Interestingly, both low ACh and high ACh caused enhanced bursting in CA3, though with different patterns and different mechanisms, as follows. High ACh levels significantly enhanced MF transmission causing large currents to arrive at CA3 pyramidal cells. This pattern of excitation generated burst sizes that were distributed evenly but also included very long bursts of 20 and 30 action potentials. It is noteworthy

that applying a similar analysis as above to DG cells revealed that in response to high ACh, a limited number granule cells fired bursts of five to six action potentials, and consistent with the reported sparse activity in DG (Bower and Buckmaster, 2008), most granule cells were silent (fired 0 action potentials, Fig. 10B). Thus, these very long CA3 bursts were not merely transmitted from the upstream DG region, but rather were likely a product of the large excitatory currents arriving from MF synapses, combined with the ACh effects on CA3 pyramidal cells including membrane depolarization, reduced frequency adaptation, and reduced AHP.

The recurrent CA3 connections contributed but were not the main cause of runaway activity in CA3 during high ACh levels, and as expected, adding short-term depression to these connections did not correct the instability. In contrast, OLM inhibition mainly affected longer bursts of action potentials (Fig. 7C), making it suitable to control these very long bursts. The effects of three different levels of OLM inhibition on the distribution of burst sizes revealed an effective reduction in the occurrence of bursts with more than seven action potentials (Fig. 10C).

On the other hand, compared to baseline levels, low ACh levels shifted the CA3 firing to higher burst sizes. The pattern of enhanced excitation was similar to that generated by the recurrent connections (Fig. 5G), though larger in magnitude, due to the enhanced transmission at recurrent connections induced by low ACh.

The increase in average burst size caused by the enhanced recurrent connections was moderated by short-term depression at these synapses returning the network into a stable state (Fig. 9A1), whereas in the case of OLM interneurons, their slower dynamics

resulted in their inhibitory currents arriving after many CA3 pyramidal neurons had discharged bursts of action potentials (Fig. 10D). This revealed a critical result where the ability of OLM cells to contain the instability created by the CA3 recurrent connections depended on the strength of the synaptic transmission at the recurrents. Lower ACh reduced the cholinergic suppression of the recurrent connections and caused excitatory activity to spread rapidly between pyramidal cells well before OLM inhibition arrived (Fig. 10D), whereas at baseline ACh levels, OLM cells were able to fire in time to prevent pyramidal cells from exciting themselves into a runaway state.

We also considered whether the "trained" network (with pattern 1 encoded) might behave differently. To check this, we compared the stability profile of the trained network to the naïve network. In response to increasing inputs from EC the trained network had a slightly faster activation of CA3 pyramidal cells, but was otherwise identical in behavior (data not shown).

Taken together, these findings suggested that low ACh levels enhance CA3 recurrent connections leading to more sustained bursting in pyramidal cells, and short-term depression at these recurrent connections moderates this excitatory activity, whereas high ACh levels result in very long burst sizes that are optimally controlled by OLM inhibition (Fig. 11).

Discussion

We developed a biophysical model of the hippocampal DG and CA3 regions by matching biological data including single cell behavior, synaptic dynamics, connectivity patterns, and short- and long-term synaptic plasticity. Furthermore, the model was constrained to

reproduce the experimentally reported roles of CA3 and DG in pattern completion and separation, respectively. The recurrent connections in CA3 promote runaway excitation, and our results suggested that OLM inhibition and short-term depression at the recurrent connections were effective in preventing this instability, while BC inhibition by itself was not. In addition, our model extended the previously established distinctions between the low and the high cholinergic circuits (Hasselmo et al., 1995) by demonstrating different destabilizing and stabilizing mechanisms in these circuits (Fig. 11). An implication of these findings is that different forms of seizure activity could develop in each circuit through unique mechanisms.

Biologically constrained model of pattern completion and separation

Pattern separation and completion in the hippocampus is one of the most prominent computational theories that has been modeled extensively (Treves and Rolls, 1992; O'Reilly and McClelland, 1994; Hasselmo et al., 1995, 2002; Hasselmo and Wyble, 1997; Meeter et al., 2004; Kunec et al., 2005; Cutsuridis et al., 2010; Nolan et al., 2010). The role of cholinergic modulation in these processes has also been modeled using firing-rate neuron models (Hasselmo et al., 1995; Hasselmo and Wyble, 1997) and spiking neuron models (Barkai et al., 1994; Meeter et al., 2004). Hasselmo et al. (1995) considered the explosive growth of excitation in CA3, and revealed that cholinergic modulation itself along with local feedback inhibition aided in stabilizing the network.

Our network model extended previous work by adding components matched to neurophysiological data including two types of interneurons and short-term synaptic plasticity. The addition of these mechanisms allowed for a more detailed analysis of their

role in stabilizing excitatory activity in CA3 during low and high cholinergic states of the network.

In particular, short-term synaptic plasticity influenced the behavior of the model considerably. Based on in vitro studies, Vogt and Regehr (2001) suspected that due to the pronounced short-term synaptic facilitation at the MF synapses, cholinergic modulation can indirectly control MF synaptic transmission by modulating the firing rate of DG granule cells. Our model included these dynamics and showed an intact ability to encode and retrieve patterns of activity as regulated by cholinergic modulation (Fig. 4). Furthermore, short-term plasticity in the local connections between pyramidal cells and interneurons shaped the role of interneurons in stabilizing the CA3 network, and short-term depression in the connections between pyramidal cells themselves acted as a robust stability mechanism.

Depressing synapses limit efficacy of BC interneurons

Considering their rapid dynamics and fast inhibition, BC interneurons appeared well positioned to stabilize the network. However, our findings indicated that BC inhibition in a network of EC and CA3 merely shifted the CA3 input-output curve linearly and could not limit the unstable exponential growth in the recruitment of CA3 pyramidal cells (Fig. 6). These results are consistent with recent recordings from CA3 by Beyeler et al. (2013) that revealed a very limited role for perisomatic inhibitory currents in moderating the recruitment of hippocampal pyramidal neurons. In addition, a different study showed that

an increase in PV-BC inhibitory drive was insufficient to reduce the generation of epileptic discharges in a mouse model of epilepsy (Wyeth et al., 2010).

In our model, this inability of BC cells to control excitation was due to two factors. First, both BC-to-pyramidal (Hefft and Jonas, 2005) and pyramidal-to-BC connections (Ali et al., 1998) displayed short-term synaptic depression. Such dynamics render BC inhibition less relevant at higher firing rates during long bursts of action potentials that occur at the onset of instability. Second, compared to OLM cells, BCs receive less connections from pyramidal cells (Buhl and Whittington, 2007) and also provide fewer connections to pyramidal cells (Sik et al., 1995). The model suggests that these dynamics could explain the reported biological findings (Wyeth et al., 2010; Beyeler et al., 2013).

While our results showed that BCs did not have a significant role in stabilizing the CA3 network, preliminary results from a separate study indicated that they have a prominent role in selecting neurons in a hippocampal ensemble (unpublished data). Further studies are needed to clarify their role in the network.

Nonlinear mechanisms play a critical role in stabilization

Activity in CA3 when using only BCs suggested the need for a nonlinear mechanism where suppression of excitation remains modest during low activity levels but increases steeply as activity level increases. While depressing synapses at the recurrent collaterals seemed ideally suited for this task (Sussillo et al., 2007), OLM interneurons were not obvious candidates. Although they provide nonlinear inhibition due to their facilitating inputs, OLM cells exhibit slow membrane dynamics and slow inhibitory currents, project to dendrites, and receive limited direct input from sources other than pyramidal cells

(Maccaferri, 2005). However, the model showed that they were effective in limiting the spread of activity at baseline levels of synaptic transmission in recurrent connections.

More specifically, the ability of OLM inhibition to maintain stability of the network was dependent on the level of ACh. At low ACh levels, OLM inhibition failed to stabilize the network mainly due to the rapid spread of excitation through the recurrent connections. Due to the slow dynamics of OLM cells, their inhibitory current arrived at pyramidal cells after excitation has already spread through the network (Fig. 10D). In contrast, at baseline ACh levels, the recurrent connections were relatively suppressed and excitation spread at a slower rate. Therefore, at baseline ACh levels, OLM inhibition arrived in time to prevent the spread of excitation between cells and consequently maintained the stability of the network. Finally, at high ACh levels, the recurrent connections were highly suppressed and were not relevant to network instability. Strong inputs arrived through MF from DG granule cells leading to extended bursts in CA3, and OLM inhibition was well positioned to reduce these bursts and prevent runaway excitation.

Two distinct circuits in the hippocampus

While the presence of two circuits for encoding and retrieval in the hippocampus is well-established (Treves and Rolls, 1992; O'Reilly and McClelland, 1994; Hasselmo et al., 1995), our results extend this perspective. The existence of different dynamics and stability mechanisms revealed a more pronounced distinction between the two circuits (Fig. 11). While both circuits utilize the same physical implementation, the roles of the different components change significantly. In addition to the differences in stability

mechanisms reported here, a different study using our model suggested a parallel distinction in oscillatory mechanisms between the two circuits (unpublished data).

These findings suggested that failure of different mechanisms might be implicated in hyperexcitability or seizure-like behavior in the hippocampus during different levels of cholinergic transmission. Considering that levels of ACh are primarily increased with novelty and active exploration (Barry et al., 2012), our model predicts that certain types of seizures are induced by novelty and other types may be facilitated by familiarity. Indeed, rats receiving Domoic acid (an excitatory neurotoxin) during development go on to develop a "novelty-induced seizure-like syndrome" (Doucette et al., 2004; Perry et al., 2009). In these studies, rats developed stereotypical chewing, clonus, and other seizure-like behaviors when placed in a novel Morris water maze. Reports related to a possible familiarity-induced syndrome have numerous references to the 'déjà vu' phenomenon (an intense feeling of familiarity that precedes seizures in humans). However, the relationship between this phenomenon and the actual seizure-behavior remains poorly understood (Martin et al., 2012), which limits any conclusions about the direction of causality. Nonetheless, our model further predicts that the novelty-induced seizures would be a reflection of dysfunction of inhibitory interneurons, while the familiarity-induced counterpart could be due to pathology of excessive excitatory transmission at the recurrent collaterals.

Conclusions

Findings from our computational model shed light on how intrinsic hippocampal mechanisms might stabilize activity in CA3 during pattern completion and separation

phases. Specifically, nonlinear mechanisms such as depressing synapses at recurrent CA3 collaterals or inhibition by OLM interneurons were suited to prevent runaway excitation whereas inhibition by BC interneurons was insufficient. Pattern encoding and pattern retrieval occur through distinct circuits in the hippocampus with different destabilizing and stabilizing mechanisms. These results raise the possibility that different clinical interventions may be required to prevent seizure behavior during distinct modulatory states of the hippocampal network.

Figures

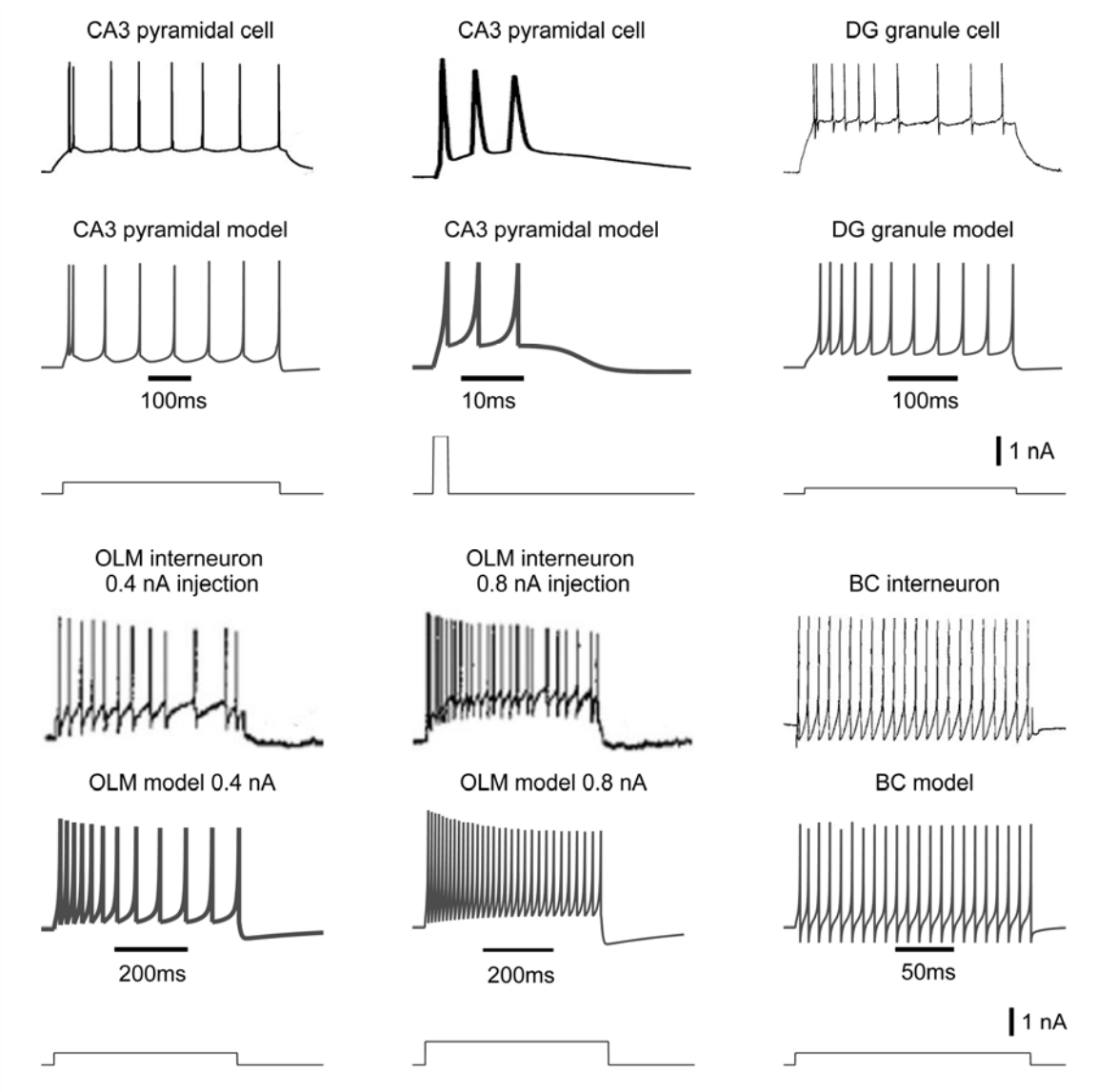

Figure 1 Matching neurons to biological recordings

In vitro current injection recordings of the cell types and their matching model cells. Current injections used in both experimental recordings and model are displayed underneath each pair of recordings and model traces. Sources for the experimental data: CA3 pyramidal cell (Brown and Randall, 2009), DG granule cell (Staley et al., 1992),

OLM cell (Ali and Thomson, 1998), and basket cell (Buhl et al., 1996). The parameter values for the model cells are in table S1 of supplementary materials.

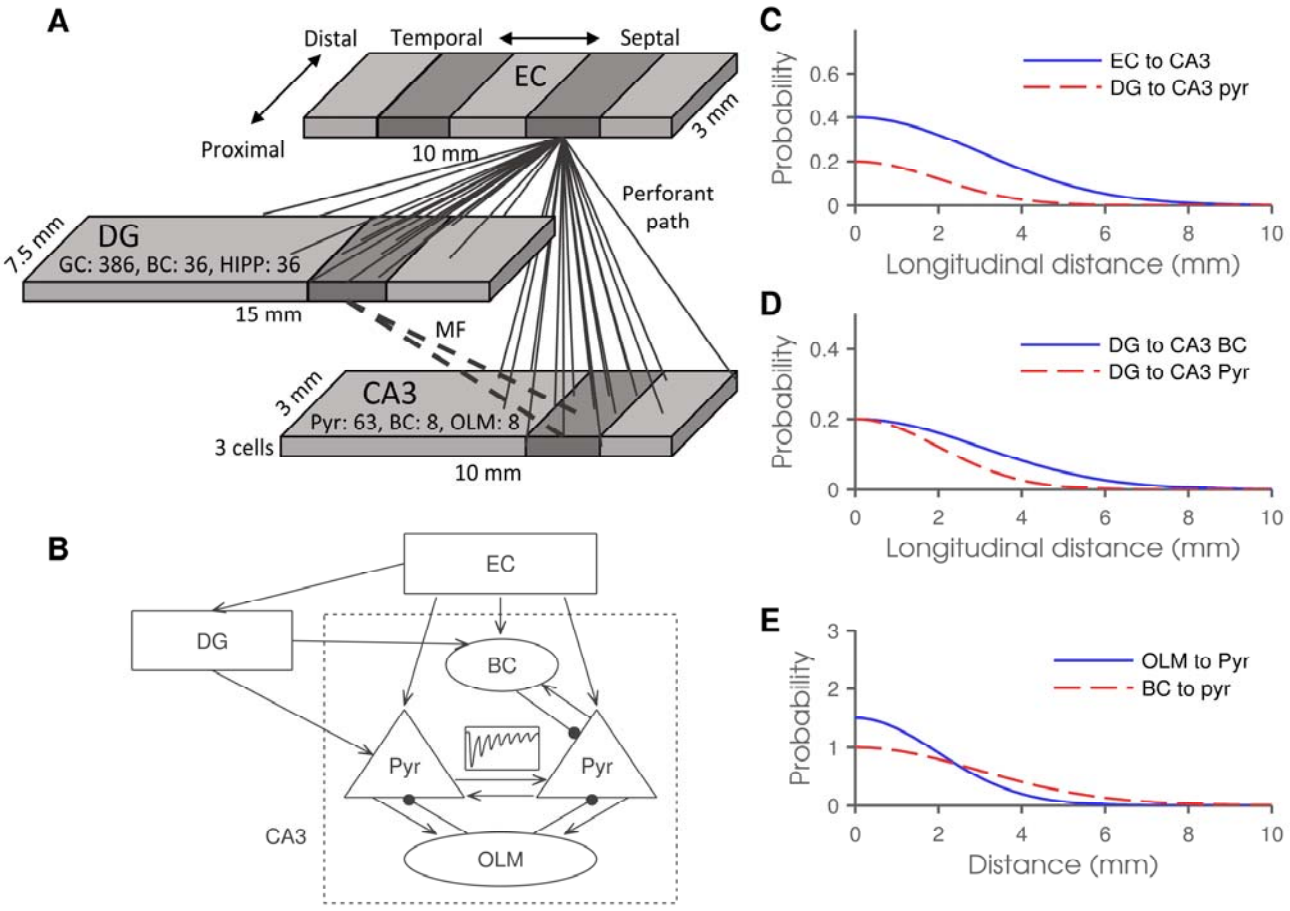

Figure 2 Network 3D structure and CA3 local circuitry.

A) Schematic of the network implemented showing the modeled regions EC, CA3 and DG with their dimensions, cell numbers, and lamellar connectivity pattern. Neurons in EC are more likely to send connections to DG and CA3 neurons in their longitudinal vicinity. Similarly, DG granule cells in the same longitudinal neighborhood are likely to project to CA3 neurons in the same lamella. Cells were compacted into three sheets of

cells, in the radial dimension, representing stratum-pyramidale in CA3 and the granular layer in DG.

B) Schematic with details of CA3 internal circuitry. Excitatory connections terminate in arrows and inhibitory ones in black filled circles.

C) Gaussian connection probability functions. The longitudinal organization of EC inputs to CA3 is compared to DG inputs. Inputs from DG had a more focused pattern of connectivity (see table S3 for parameter values).

D) Projections from MF to BCs had a wider longitudinal extent, compared to the ones from MF to CA3 pyramidal cells (pyr).

E) The probability of an interneuron connecting to a pyramidal cell depended on the distance between the two in the longitudinal and transverse planes. Note that probability for the OLM domain exceeded one to ensure that OLM cells made dense connections in their immediate neighborhood.

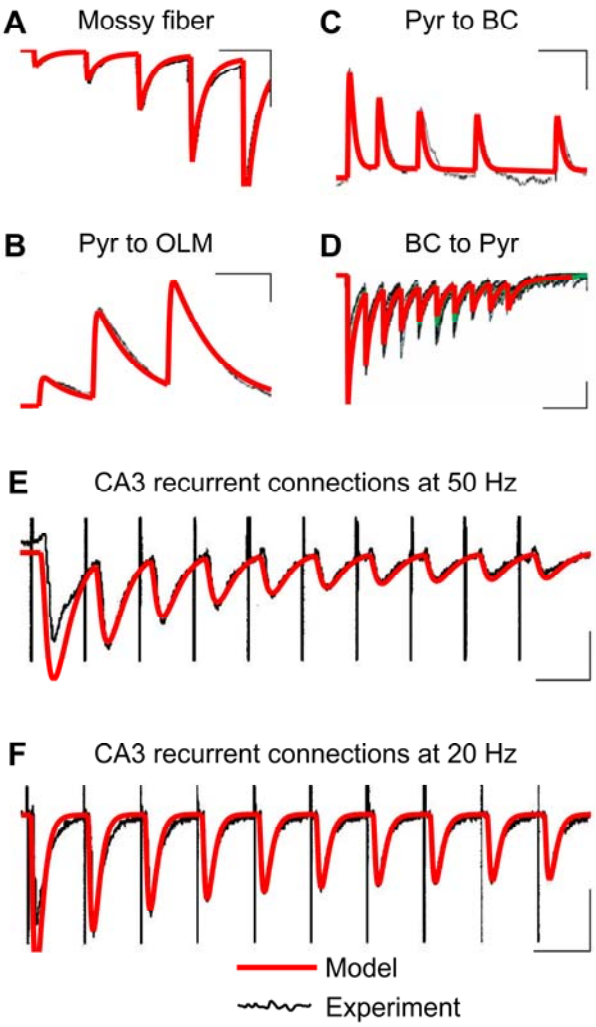

Figure 3 Matching short-term plasticity to experimental recordings.

Short-term plasticity was modeled using equations proposed by Varela et al., (1997) and parameter values were obtained by matching model to experimental recordings. Note that depending on available data, some panels display the post-synaptic cell membrane potential and others display the synaptic current. Parameter values used to reproduce data are listed in table S5.

A) Mossy fiber synaptic facilitation (Toth et al., 2000). (Scale bars: 50 ms, 100 pA).

B) CA3 Pyramidal cell to OLM interneuron (Ali and Thomson, 1998). (Scale bars: 20 ms, 1 mv).

C) CA3 Pyramidal cell to BC interneuron (Ali et al., 1998). (Scale bars: 30 ms, 0.5 mv).

D) BC interneuron to CA3 pyramidal cell (Hefft and Jonas, 2005). (Scale bars: 50 ms, 100 pA).

E, F) Recurrent CA3 connections stimulated at 50 Hz, and 20 Hz, respectively (Hoskison et al., 2004). Note that these connections displayed paired pulse facilitation, a phenomenon not included in our synapse model. Therefore, responses to the first stimulus in the train appear larger than the recordings. (Scale bars: 20 ms, 0.5 mv in E; 50ms , 0.5 mv in F).

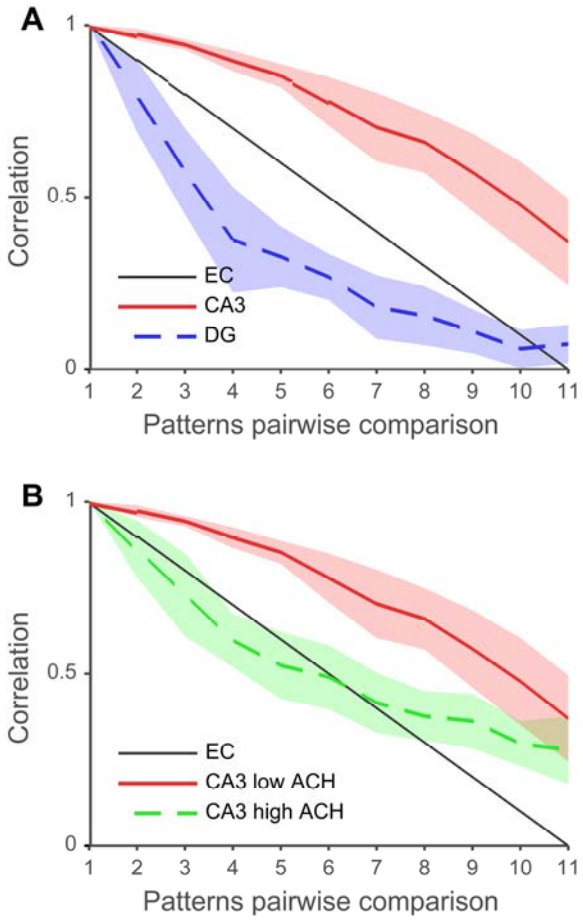

Figure 4 Pattern completion and separation in CA3 and DG.

The network learned pattern 1 for five trials under high levels of ACh. Subsequently, long-term plasticity was inactivated to test retrieval in response to inputs patterns 1 to 11. Output spikes were recorded at EC, CA3 and DG, and correlation was calculated between the output from pattern 1 and the output from each of the test patterns. Results were averaged over data from 10 randomly constructed networks and shaded areas indicate standard deviation.

A) Correlation of output patterns produced at EC, CA3 and DG in response to probe patterns 1-11. The correlation between input pattern 1 and the probe patterns at EC is shown as a reference point. Correlation values at CA3 pyramidal neurons lie well above the input correlation indicating a tendency towards pattern completion in CA3. Conversely, DG correlation values lie below input correlation levels indicating pattern separation.

B) The effects of low vs. high levels of ACh during retrieval on correlation levels in CA3.

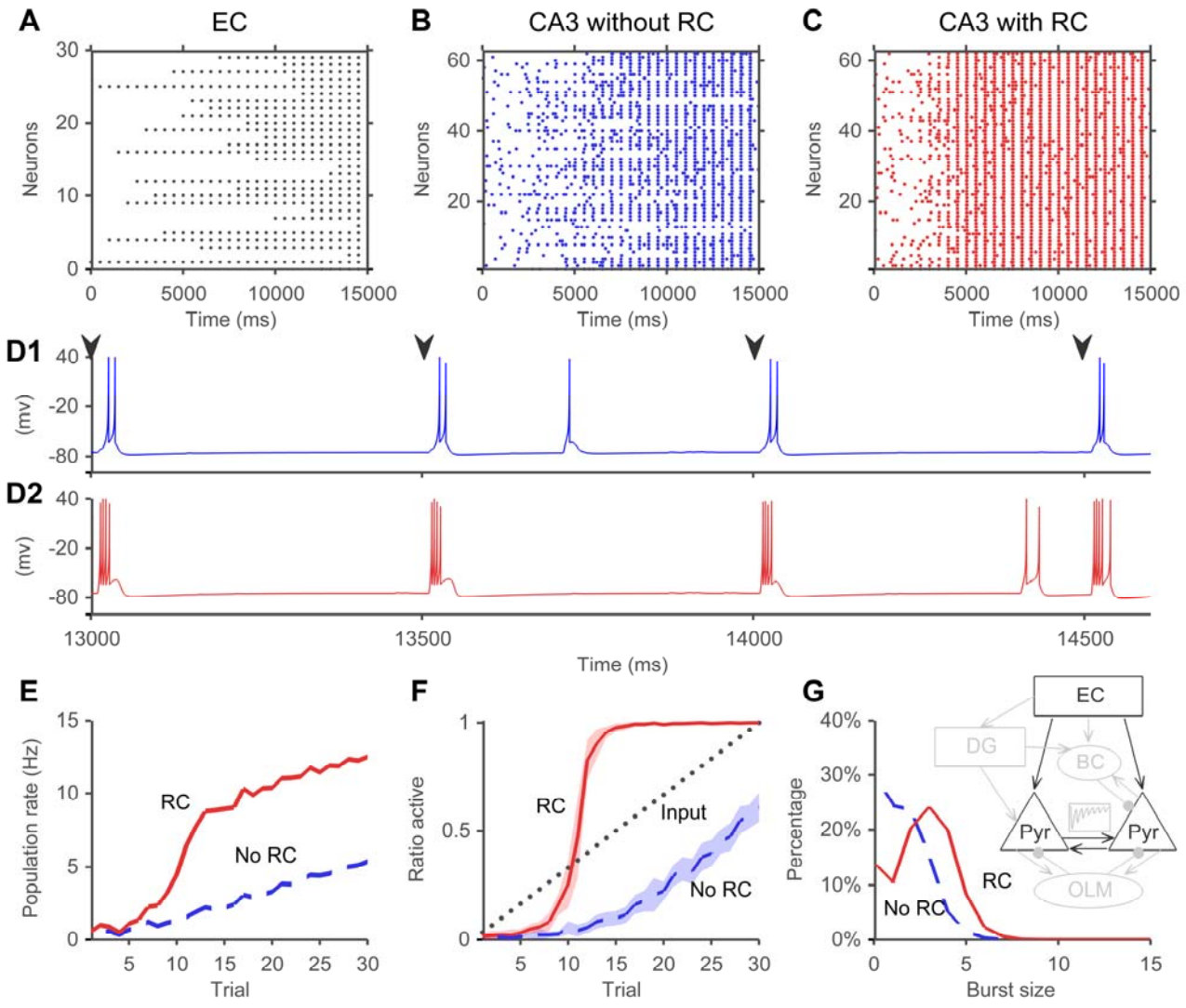

Figure 5 The effects of recurrent connections on excitation within CA3.

At the beginning of each trial, a stimulus of one action potential was delivered to a number of randomly selected of EC neurons, which projected to CA3. The number of EC neurons stimulated increased with each trial. The DG region and other cell types in CA3 were disconnected, with ACh at baseline levels and no short- or long-term plasticity.

A) Spike raster plot of EC neurons in response to structured inputs for 30 trials from a representative network. Each trial had a 500 ms duration, and for each trial, an increasing number of randomly selected EC neurons received a synaptic stimulus generating one action potential. As can be seen in the plot, only one EC neuron fired on trial 1 in the first 500 ms, two fired during trial 2, and so on, ending in 30 neurons firing on trial 30 in the last 500 ms of the simulation.

B) Spike raster plot of CA3 pyramidal neurons without the recurrent connections in response to the input presented at EC across 30 trials.

C) Spike raster plot of CA3 from a representative network with recurrent connections restored. Spikes are shown for the 30 trials of the experiment.

D) Membrane voltage traces from a representative neuron in the network without recurrent connections (D1) and with recurrent connections (D2). The traces show the membrane voltage response during trials 22 to 25, with arrowheads marking the beginning of each trial th.

E) Population firing rate histogram for CA3 without recurrent connections (dashed line) and with recurrent connections (solid line). Firing rate was calculated for each trial by averaging trial spike count from all CA3 pyramidal neurons and dividing by trial duration.

F) Ratio of active to inactive neurons in EC (dotted diagonal line), in CA3 without recurrent connections (dashed line) and in CA3 with recurrent connections (solid line).

Results are averages of data from 10 networks with different random seeds, and shaded areas represent standard deviation.

G) Changes in distribution of different burst sizes with and without recurrent connections. The distribution was obtained by pooling action potential counts from each neuron in each trial. The data were averaged from running 10 initializations of the network, and presented as a percentage of the total neuron-trial count for each burst size. Inset shows a schematic with model components used in this experiment. Active components are shown in dark lines, while inactive components are shown in light gray lines. RC: recurrent connections.

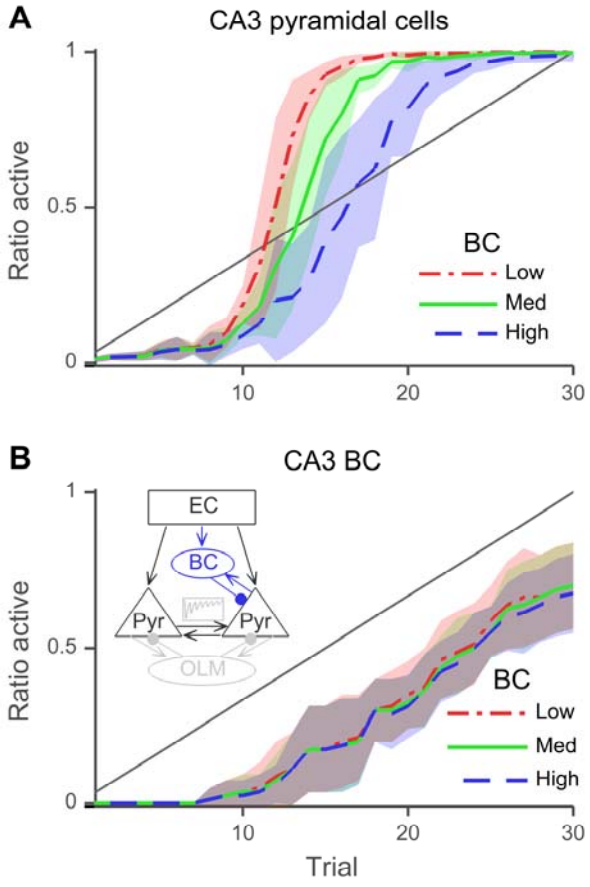

Figure 6 Effects of BC interneurons on the stability of CA3 pyramidal cells.

The ratio of neurons activated was measured in CA3 in response to increasing EC input over 30 trials. Diagonal line in graphs denotes the rate of input increase at EC. Inhibition by BCs was the only stability mechanism in this experiment, and short-term depression at recurrent connections and inhibition by OLM cells were inactivated.

A) Ratio of active pyramidal neurons for three different levels of BC-to-pyramidal inhibition. Compared to low BC inhibition, medium inhibition shifted the activity ratio curve modestly to the right, without a substantial decrease in its maximum slope.

Furthermore, BC inhibition higher than optimized for the pattern separation and completion network did not effectively lower the slope of the curve.

B) The ratio of active BC interneurons showed a linear response with increase in EC inputs, with little difference between the three levels of BC inhibition. Inset shows a schematic with model components used in this experiment. Active components are shown in dark lines, while inactive components are shown in light gray lines.

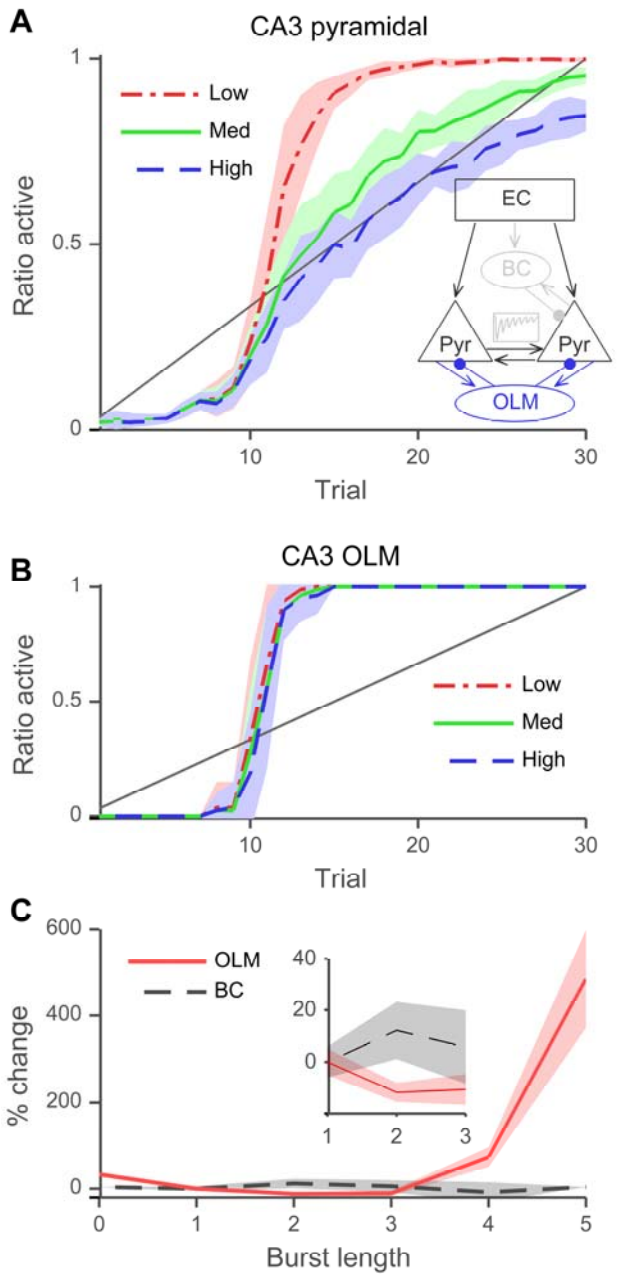

Figure 7 OLM interneurons stabilize CA3 and control burst size.

The network was tested over 30 trials with increasing amounts of EC inputs, denoted by the diagonal line. Short-term depression at recurrent connections was blocked and BC interneurons inactivated.

A) The ratio of active CA3 pyramidal neurons at three different levels of OLM inhibition.

B) The ratio of active OLM interneurons for low, med, and high OLM-to-pyramidal inhibition showed a nonlinear OLM response. The response of OLM cells continued to be nonlinear even with high inhibition where CA3 pyramidal cells show a controlled near linear response.

C) The percentage change in the occurrence of different burst sizes when inhibition level is lowered from high to low, for BC inhibition (dashed line) and OLM inhibition (solid line).

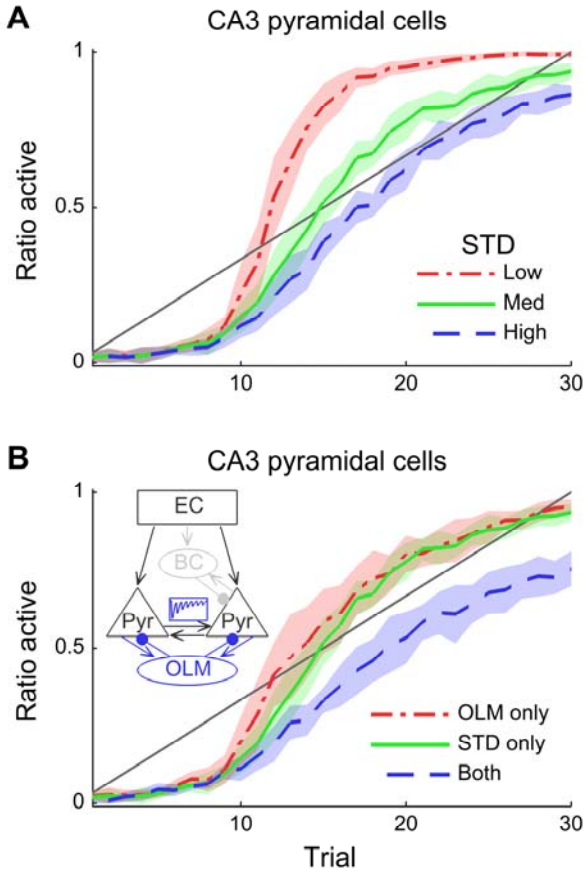

Figure 8 Recurrent connections short-term depression stabilizes CA3 activity.

A) The effect of short-term depression (three levels) at the recurrent connections on the ratio of active cells in CA3 with increasing input from EC. Both OLM and BC were inactivated. Baseline or 'med' values were obtained by matching experimental data (Hoskison et al., 2004) (d1: 0.7, d2: 0.92) and then low (d1: 0.5, d2: 0.86) and high (d1: 0.9, d2: 0.98) levels were created symmetrically around the baseline values. Higher levels of short-term depression stabilized CA3 responses and the curve of ratio of active cells became closer to linear and dropped below the curve for the inputs. (STD: short-term depression).

B) The effects of experimentally matched levels of OLM inhibition or of short-term depression alone compared to the case when both mechanisms were simultaneously active.

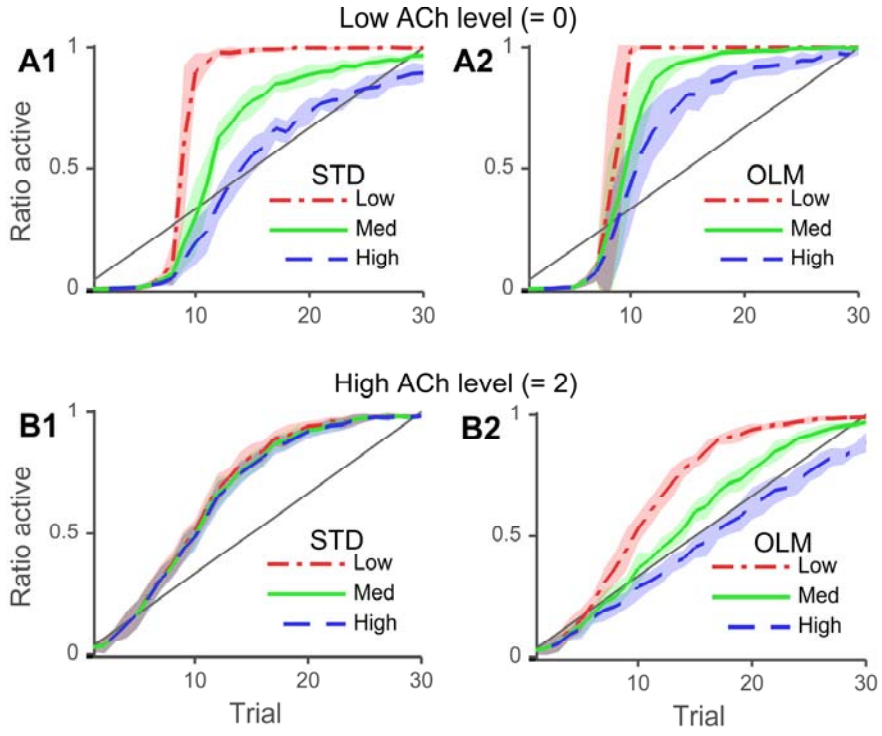

Figure 9 The encoding circuit is stabilized by OLM inhibition and the retrieval circuit is stabilized by short-term depression at the recurrent CA3 connections.

Ratio of active CA3 pyramidal cells was evaluated for low and high ACh levels with either short-term depression or OLM inhibition activated at three levels.

A) The effects of three different levels of short-term depression at the CA3 recurrent connections (A1), and of OLM inhibition (A2) under low levels of ACh.

B) With high ACh, short-term depression at the CA3 recurrent connections had little effect (B1) while OLM inhibition was critical to the stability of the network (B2).

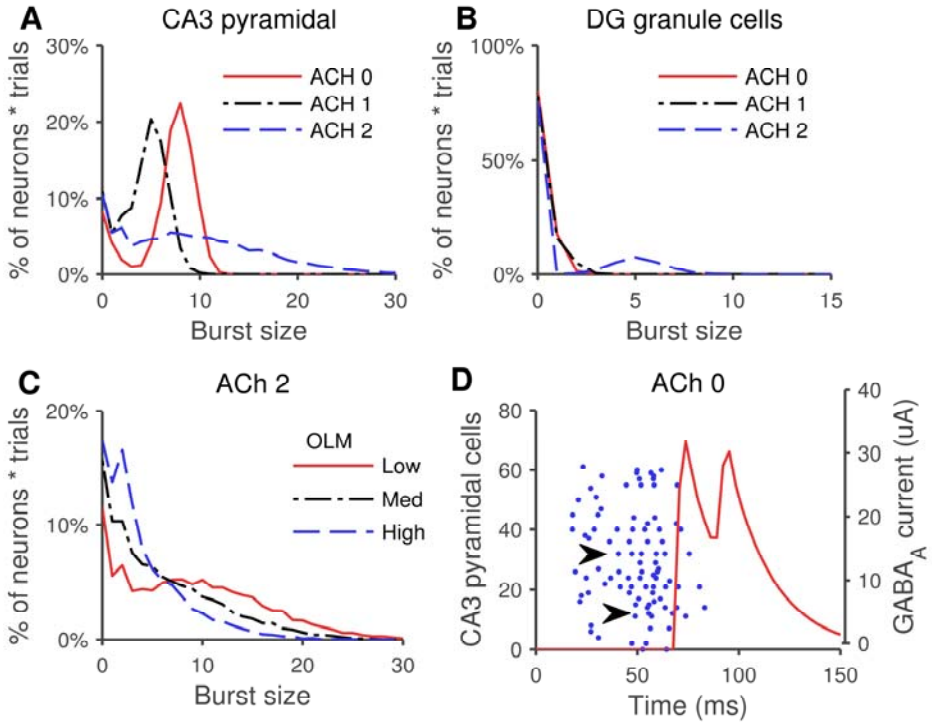

Figure 10 Distinct patterns of excitation during encoding and retrieval levels of ACh.

Both CA3 and DG networks received increasing inputs from EC without the stabilizing effects of short-term depression or inhibition from CA3 interneurons. The occurrence of bursts of different sizes was calculated across neurons and trials, and is presented as a

percentage of all neurons and trials for each burst size. The distribution of burst sizes was considered for low, med, and high levels of ACh.

A) The occurrence of different burst lengths in CA3 under low, med, and high levels of ACh. Low levels of ACh shifted the peak in burst sizes towards longer bursts (peak shifted from five to eight action potentials). Whereas high levels of ACh leads to more distributed burst sizes with a long tail including extended bursts (> 20 action potentials).

B) Same analysis as in (A) applied to DG granule cells revealed that these very long bursts were not simply transmitted from DG. High levels of cholinergic transmission in DG caused an increase in the frequency of short bursts in a limited number of granule cells.

C) OLM interneurons were activated in the encoding network (ACh=2) and the distribution of burst sizes was considered at three different levels of OLM inhibition. Higher levels of OLM inhibition reduced the occurrence of extended bursts.

D) Excitation spread in CA3 network preceded OLM inhibitory current during low ACh levels. One trial is depicted with 20 EC neurons receiving one action potential at time 0. A spike raster plot of CA3 pyramidal cells is shown overlaid with an example of OLM inhibitory current as measured from the soma of a pyramidal cell. Not all pyramidal cells fired in response to the EC stimulus. A few neurons started firing late **(Arrows)**, indicating a di-synaptic source of input from other pyramidal cells. OLM inhibition did not arrive in time to prevent the secondary spread of excitation to these neurons.

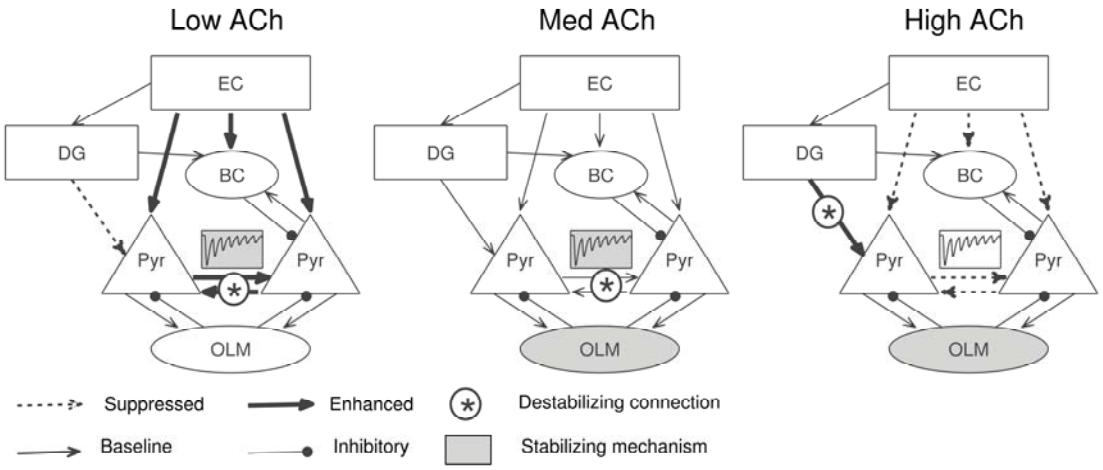

Figure 11 Summary of stabilizing mechanisms in low, med and high cholinergic states.

Connections are suppressed (dotted arrows) or enhanced (thick arrows) from baseline (normal arrows) by ACh levels. Connections promoting runaway excitation (indicated by *) were the recurrent CA3 connections in low and med ACh states, and MF in high ACh states. On the other hand, mechanisms maintaining network stability (indicated by gray shaded area) were short-term depression in low and med ACh states, and OLM in med and high ACh states.

CHAPTER 3: An Integrative Model of the Intrinsic Hippocampal Theta Rhythm

Ali Hummos, PhD student[1], Satish S. Nair, Professor[1, 2]
[1] Informatics Institute, [2] Department of Electrical & Computer Engineering, University of Missouri, Columbia, Missouri.

Abstract

Hippocampal theta oscillations (4-12 Hz) are consistently recorded during memory tasks and spatial navigation. Despite several known circuits and structures that generate hippocampal theta locally *in vitro*, none of them were found to be critical *in vivo*, and the hippocampal theta rhythm is severely attenuated by disruption of external input from medial septum or entorhinal cortex. We investigated these discrepancies that question the sufficiency and robustness of hippocampal theta generation using a biophysical spiking network model of the CA3 region of the hippocampus that included an interconnected network of pyramidal cells, inhibitory basket cells (BC) and oriens-lacunosum moleculare (OLM) cells. The model was developed by matching biological data characterizing neuronal firing patterns, synaptic dynamics, short-term synaptic plasticity, neuromodulatory inputs, and the three-dimensional organization of the hippocampus. The model generated theta power robustly through five cooperating generators: spiking oscillations of pyramidal cells, recurrent connections between them, slow-firing interneurons and pyramidal cells subnetwork, the fast-spiking interneurons and pyramidal cells subnetwork, and non-rhythmic structured external input from entorhinal cortex to CA3. We used the modeling framework to quantify the relative contributions of each of these generators to theta power, across different cholinergic

states. The largest contribution to theta power was that of the divergent input from the entorhinal cortex to CA3, despite being constrained to random Poisson activity. We found that the low cholinergic states engaged the recurrent connections in generating theta activity, whereas high cholinergic states utilized the OLM-pyramidal subnetwork. These findings revealed that theta might be generated differently across cholinergic states, and demonstrated a direct link between specific theta generators and neuromodulatory states.

Introduction

Slow oscillations at theta frequencies (4-12 Hz) are consistently recorded in the hippocampus during working memory tasks, spatial navigation, and storage of episodic memory [for review, see 1,2]. The hippocampus is capable of generating its own theta rhythm when isolated *in vitro* [3,4], and several structures and circuits have been identified as potential intrinsic generators of hippocampal theta [for review, see 1,2]. However, experiments aimed at confirming the role of these structures individually have invariably revealed conditions where the structures made no contribution to hippocampal theta. For instance, the slow firing oriens-lacunosum moleculare (OLM) cells, which lock closely to theta rhythm *in vivo* [5], were proposed as generators of the rhythm, using computational models [3,6]. However, later experiments showed that OLM cells possess modest resonance at theta frequencies [7], and their silencing in vivo did not diminish theta activity [8]. As a second example, computational models have suggested a contribution to hippocampal theta from intrinsic membrane conductances such as the spike-frequency adaptation currents [9–13], or the h-current [3,6,14–17]. Spike-frequency

adaptation currents remain difficult to investigate experimentally, while a genetic knockout of the h-current (HCN1 channels) did not disrupt theta [18,19]. A third theta generator implicated by models is the recurrent excitatory connections between pyramidal cells [9,10,20–23]; experiments again revealed persistent theta oscillations despite disruption of this excitatory glutamatergic transmission in CA1 [24,25]. These observations might indicate a cooperative interaction between the proposed generators of theta, but previous modelling studies have typically focused on a limited set of these generators, and several questions remained unanswered, such as the extent to which each generator contributes to theta power, and whether their relative contributions change in different behavioral or neuromodulatory states.

In addition, despite the presence of these intrinsic hippocampal generators, external input plays a major role and hippocampal theta is severely attenuated *in vivo* by disruption of the input from the medial septum [26–30] and from the entorhinal cortex (EC) [31]. The contribution of input from medial septum and EC to hippocampal theta is assumed to be a consequence, solely, of the rhythmic nature of these external inputs, or the specific delays in the feedback loops formed between these external inputs and the hippocampus [32], but the hippocampus also receives input with less prominent rhythmic modulation, (for e.g. from the lateral EC, compared to the medial EC [33]). Non-rhythmic random spiking arriving through divergent afferent projections to an area has been implicated in oscillations in models [34–36] and in experiments involving the olfactory cortex [37], but has not been investigated for the hippocampus. Modeling allowed us to dissociate and examine how the non-rhythmic component of input from the medial septum and EC might also contribute to hippocampal theta.

We used our previously developed biophysical computational model of the hippocampus [38] that included principal cells and two types of interneurons, to shed light on the cooperative interactions amongst the various intrinsic theta generators, and to examine their relative contributions to the power of hippocampal theta, across neuromodulatory states. The model included neuromodulatory inputs, spatially realistic connectivity, and short-term synaptic plasticity, all constrained by prior experimental observations. To isolate the role of the non-rhythmic component of medial septal and EC inputs in generating theta, we used an input layer of neurons (referred to henceforth as 'EC') excited by random noise constrained by realistic hippocampal unit firing rates. We demonstrated five generators of theta power in our model, as previously reported in the literature, and found that these generators operated simultaneously and cooperatively and no one generator was critical to the theta rhythm. We then quantified their relative contribution to theta power using tractable analysis that maintains relevance to experiments. The non-rhythmic external input had the highest contribution to theta power, which is consistent with the significant drop in theta power following removal of medial septum [29] or EC inputs [31] to the hippocampus *in vivo*. Contributions from two theta generators were dependent on cholinergic state. Low cholinergic states engaged the recurrent connections amongst pyramidal cells for theta generation, while high cholinergic states utilized the OLM-pyramidal cells subnetwork, indicating that the low and the high cholinergic states had distinct mechanisms for theta generation, with specific cholinergic effects fostering the engagement of certain theta generators.

Results

We investigated theta generating mechanisms in the hippocampus using our published biophysical model that included networks for entorhinal cortex (EC), dentate gyrus (DG), and CA3 regions, and their interconnections [38]. The single cell models in the network were developed using the Izhikevich formulation [39] and matched to experimental recordings (Fig. 12, see Methods for references and details). Cells were distributed in 3D space and connected following experimentally reported hippocampal spatial organization with lamellar connectivity between regions (see Methods). Basket cells (BCs) received input from EC, DG and CA3 pyramidal cells, while oriens-lacunosum moleculare (OLM) cells were reciprocally connected to pyramidal cells (Fig. 12A, see Methods). Synaptic currents had values for rise and decay time constants obtained directly from published experiments (see Methods), and also exhibited short-term synaptic plasticity (Fig. 12D-I). The model was constrained further to perform pattern separation and completion, and was validated by its ability to match the effects of acetylcholine (ACh) in biasing the CA3 network towards pattern separation [details in 38].

Results reported below represent data averaged over 10 instantiations of the network with different random seeds for initial cell membrane potentials, synaptic connections, synaptic weights, and random external inputs. To examine the non-rhythmic component of medial septal and EC input, we used an input layer with 30 spiking neurons with no spike-frequency adaptation (referred to as ‘EC’). External input arrived as Poisson spikes to either this layer or directly to pyramidal cells depending on the experiment setup, at rates constrained to produce reported firing rates of hippocampal place cells during active locomotion [44; see Methods for details].

Poisson spikes input generates theta oscillations in the model

The full model (Fig. 13A) generated theta rhythmic activity, in response to external input in the form of Poisson spikes arriving at EC cells. Poisson inputs arrived at a rate of 15 Hz chosen to match experimentally recorded hippocampal firing rates (see Methods, Fig. 12C1), but theta activity was robust over a range of input rates tested (5-100 Hz). Oscillatory activity was discernible in a spike raster plot of CA3 pyramidal cells from an example run, with multiple vertical groupings indicating synchronized firing (Fig. 13B1). The population firing rate, calculated using a 20 ms sliding window (Fig. 13B2), and the membrane voltage traces of two example neurons from the same run showed grossly rhythmic activity (Fig. 13B3, 4). The population power spectrum of CA3 pyramidal cells, averaged across 10 network instantiations, showed a consistent peak in the theta band (Fig. 13C). Spiking activity of both inhibitory slow-spiking oriens-lacunosum moleculare (OLM) cells and fast-spiking basket cells (BC) also had a theta spectral peak (Fig. 13D1, 2), consistent with interneurons locking to theta rhythm in vivo [5]. The power spectrum of EC neurons spikes showed no distinct peaks confirming that the network received random Poisson-distributed inputs from EC (Fig. 13D3). Finally, the DG area of the model, which contains granule cells reciprocally connected to the slow inhibitory HIPP interneurons, and basket cells, also generated its own theta rhythm (Fig. 13D4).

Previous studies have suggested multiple potential theta generators in the hippocampus [1,49], so we examined which generators were engaged in our model by studying sub-networks with only a set of model components active during a specific run. Since rhythmic theta activity was also generated in DG (Fig. 13D4), inputs from DG to

CA3 were also disconnected in the studies reported below. Similarly, since the h-current is capable of producing theta resonance in any model sub-network [50–53], it was also removed, and the remaining cell currents were tuned again to match current injection data in figure 1, without an h-current (cell parameters in Methods, as previously published [38]).

Pyramidal cells display theta spiking oscillations

The simplest case examined had isolated pyramidal CA3 cells (Fig. 14A). The cells were completely disconnected, and each received a distinct train of Poisson spikes, at rates drawn from a lognormal distribution (to reproduce place cells firing rates, Fig. 12C2). While their spiking activity appeared grossly random (Fig. 14B), the power spectrum of the population, averaged over 10 instantiations of the model, peaked in the theta range (Fig. 14C1). To investigate the underlying mechanisms, we considered the relationship between this power spectrum peak and the spike-frequency adaptation of pyramidal cells. The reader is reminded that this version of the model lacks an h-current, but focuses on modeling spike-frequency adaptation. In the Izhikevitch cell model, spike-frequency adaptation current is modeled by the second current ‘u’ (see Methods). A spike-triggered average of this current showed that it builds up after a spike or burst of spikes and decayed slowly going back to its baseline in about 90-100 ms (Fig. 14C2). Hence, these cells had the highest probability of spiking again only after decay of the adaptation current, as confirmed by the inter-spike interval distribution peaking around 90 ms (Fig. 14C3). This predominance of spikes occurring at theta intervals reflects a coherence resonance [54,55], which, in this context, can be defined as an oscillatory response, and a power spectrum peak (resonance), optimized by random perturbation in

an adaptive cell. In other terms, the predominance of theta interval spiking could be interpreted as noise-induced “spiking oscillations”, as opposed to subthreshold oscillations. We will use the term “spiking oscillations” in this manuscript.

To further explore the relationship between spike-frequency adaptation and spiking oscillations, we lowered the time constant of adaptation from 100 ms to 25 ms (the parameter ‘a’ of the Izhikevich cell increased from 0.01 to 0.04, for this experiment, see Methods). We observed that the spiking oscillations shifted to higher frequencies around 17 Hz (Fig. 14D1). The adaptation current decayed faster following a spike and the cells fired at shorter intervals (Fig. 14D2, 3). The adaptation time constant in our model cell (100 ms), chosen to match the current injection data from Brown and Randall [40, Fig 1], was comparable to the time-constant of adaptation recorded from hippocampal pyramidal cells (126 ms) [56]. Increasing the resting membrane potential of the cells had similar effects (not shown), due to the interaction of the potential with the spike-frequency adaptation current.

The reported power spectrum peak (Fig. 14C1), which might be labeled as “spurious correlations” in digital signal processing, closely reflects basic properties of the cells that make up the network. The independent firing of neurons may not be a ‘mechanism’ of theta oscillations, due to absence of coordinated network activity. But such spiking activity can contribute to LFP once received by local cells, and should contribute to theta power measured from neuronal tissue. We next show how other network structures can exploit these spiking oscillations to generate robust theta activity.

Divergent projections from EC produce theta oscillations

A novel finding from the model was that divergent projections from EC exploited the spiking oscillations cited in the previous section to produce theta activity, in a disconnected population of pyramidal cells. In this experiment, CA3 pyramidal cells received inputs from EC, but remained disconnected from each other (Fig. 15A). All other cell types (OLM cells, BCs, and DG granule cells) remained inactivated, so pyramidal cells had no means of communicating with one another. EC cells were devoid of any rhythmicity (see Methods and Fig 3D3) and received Poisson spikes as external input, while CA3 pyramidal cells received input exclusively through the projections from EC. On average, each pair of CA3 pyramidal cells shared 19% of their projecting EC cells.

In this configuration, pyramidal cells spiking patterns appeared remarkably organized (Fig. 15B), despite the absence of local connectivity in CA3. The power spectrum of the cell population confirmed rhythmic activity in the theta range (Fig. 15C), with a power peak much higher than the power peak of independently firing pyramidal cells in figure 14. The spatially divergent projection from EC to CA3 (see methods) causes pyramidal cells in CA3 to have a degree of shared (correlated) input, and synchronizes the theta firing produced by their spiking oscillations. This mechanism has been reported in the generation of gamma oscillations in the piriform cortex [37].

Projections from individual EC cells to CA3 followed a Gaussian function of the longitudinal distance, creating neighborhoods in the longitudinal dimension [see Methods; ,57]. To examine its possible role, we removed the longitudinal organization by allowing EC cells to connect to any CA3 cell irrespective of their longitudinal location,

while keeping the total number of connections constant. This randomization redistributes correlation across neuronal pairs, removing high input correlation between neighboring CA3 cells and the low input correlation for distant ones, and instead produces consistent correlation levels between all pairs of neurons at an average value. We observed the same power spectrum peak in the theta range (not shown), indicating that the specific longitudinal organization was not critical for the synchronized theta firing in CA3. Nonetheless, examining spiking coherence, as a measure of neuronal synchrony, showed that longitudinal organization created local areas of synchrony (Fig. 15D).

Recurrent connections and spike-frequency adaptation interact to generate theta oscillations

We then investigated whether the excitatory connections between pyramidal cells in our model might synchronize their firing, as reported in previous computational studies [9,10,20,22,23,58]. For this experiment, the only active network components were CA3 pyramidal cells and the recurrent synapses connecting them (Fig. 16A), and the h-current in pyramidal cells remained inactivated.

External inputs were applied directly to CA3 pyramidal cells instead of EC cells because the EC-CA3 pathway may have an independent role in the generation of theta rhythms, as discussed above. Power spectra averaged over 10 network instantiations showed a robust peak in the theta band (Fig. 16B). This variation of our model closely resembles previous models [9,10,21,58,59], where spike-frequency adaptation interacts with the recurrent connections to produce theta oscillations.

Pyramidal-Interneuron sub-networks generate theta through two mechanisms

We next examined the role of interneurons in rhythm generation. A sub-network of pyramidal cells reciprocally connected to a population of OLM cells generated robust theta oscillations (Fig. 17), and varying the weight of the synapses from pyramidal to OLM cells illustrated two theta mechanisms in this sub-network. In the first case, with weak pyramidal to OLM cells synapses (weight set to 2, Fig. 17A), OLM cells fired sparsely and sent inhibitory currents to pyramidal cells at a rate much lower than theta frequency (Fig. 17B). However, theta oscillations emerged (Fig. 17C) because of the pyramidal cells spiking oscillations, and the sporadic OLM inhibition acting as a common input [60]. In our model, any two pyramidal cells shared, on average, 32% of their OLM inputs. A spike-triggered average of OLM inhibitory currents showed minimal association with pyramidal cells spikes (Fig. 17D1). Pyramidal cells continued to display the highest probability of firing at around 90 ms after a spike, when their adaptation current decayed to baseline (Fig. 17D1, 2). Similar "excitation-dominated" oscillations were shown in reduced models of this circuit [61].

In the second case, with strong pyramidal to OLM cells synapses (weight set to 6, Fig. 17E), OLM cells fired near theta frequencies and generated theta-locked inhibitory currents in pyramidal cells (Fig. 17F). OLM inhibition associated closely with pyramidal cells spikes, and shifted the pyramidal cells inter-spike interval peak to around 110 ms, to coincide with the trough of OLM inhibition (first trough at 110 ms and second around 220 ms).

In contrast, the BC-pyramidal cells sub-network is viewed as a generator of gamma oscillations [for review, see 62]. In a simulation that had only BCs and pyramidal

cells and their interconnections (Fig. 18A), our first unexpected finding was that this sub-network did not generate any rhythmic activity (Fig. 18B1). We discovered that two characteristics of the connections between BC and pyramidal cells prevented an oscillatory coupling: short-term depression [46,47], and the lower connection probability compared to that of OLM-pyramidal connections [63,64]. We observed that removal of short-term depression and increase of connection probability (doubling) were both required for oscillatory activity (Fig. 18B2-4). The second unexpected finding, however, was that this oscillatory activity was in the theta range (Fig. 18B4).

As demonstrated in the OLM-pyramidal sub-network, weak pyramidal to BC drive can potentially produce sporadic BC inhibition with the sole effect of synchronizing the theta spiking oscillations of pyramidal cells, independent of the specific properties of BC inhibition. But, even with a higher pyramidal to BC connection weight (set to 6), we continued to observe theta oscillations (Fig. 18C-F). To explore the lack of gamma activity, we examined the spike-triggered average of both the adaptation current and the BC inhibitory current in pyramidal cells. To generate gamma activity, pyramidal cells are expected to spike again as BC inhibition decays, however, the ISI distribution showed that cells are most likely to spike again after their own adaptation current decays (Fig. 18F). Thus, pyramidal cells adaptation dominated the dynamics of the sub-network due its slower dynamics, thereby generating oscillations that depend primarily on the dynamics of pyramidal cells rather than the dynamics of inhibitory synapses. Similar pyramidal cells driven oscillations has been seen in a model of the neocortex [65]. Of note, there was an emerging peak at around 17 Hz in the power spectrum of pyramidal cells (Fig. 18E2, indicated with arrow). An upcoming study of this model investigates the

role of background synaptic input in enhancing and shifting this peak to gamma frequencies, similar to the findings of Economo and White [65].

Theta generators have different relative contributions across cholinergic states

Next, we examined the effects of inactivating individual theta generators, across different cholinergic states. We started with the full model with external random inputs arriving at EC (DG area and the h-current remained inactive). We then inactivated each theta generator individually and observed changes in the relative theta power (ratio of power in the 4-12 Hz range to the entire spectrum from 0 to 250 Hz). To inactivate the spiking oscillations of pyramidal cells we removed spike-frequency adaptation by lowering the adaptation time constant to 10 ms (cell parameter 'a' set to 0.1, see Methods) so that it recovered promptly after each spike. The contributions of the recurrent connections, OLM cells, and BCs were removed by inactivating the corresponding synapses. To remove the effects of the projections from EC, we replaced them with direct random inputs to CA3 pyramidal cells that achieved the same firing rate (input rates drawn from a lognormal distribution with mean (± SD) of 50 Hz ± 40 in baseline ACh, 20 Hz ± 20 in low ACh, and 60 Hz ± 50 in high ACh).

In the baseline cholinergic state, removing EC projections had the most profound effect on relative theta power. This large drop in relative theta power suggests a prominent role for the non-rhythmic component of external input from medial septum or EC in the generation of hippocampal theta *in vivo* (Fig. 19A), considering that EC activity was dominated by non-rhythmic input (see Methods). The relative contribution of EC projections was followed by that of the recurrent connections, and then OLM cells (Fig. 19A). Interestingly, inactivating the spiking oscillations of CA3 pyramidal cells had

minimal effects on relative theta (Fig. 19A), presumably due to compensation by the other generators. Removal of BC inhibition slightly raised relative theta (Fig. 19A), due to lowered feedforward inhibition from EC (average pyramidal cell firing rate increased from 7 Hz to 9 Hz).

We repeated the analysis for the low and high cholinergic state networks. Acetylcholine (ACh) state affected the cells and synapses of the network and took values from 0 (lowest) to 2 (highest, see Methods). The low cholinergic state increased the impact of removing the recurrent connections and decreased the impact of removing OLM cells (Fig. 19B). The high cholinergic state produced the opposite effects (Fig. 19C). To focus on CA3 dynamics, DG was not included in the simulations in figure 19. A separate simulation examined the effects of adding DG input and showed a significant increase in CA3 relative theta power only in high cholinergic states (relative theta increase in low cholinergic state: 0.01, $p < 0.5$, med: 0.02, $p < 0.5$, high: 0.15, $p < 0.05$).

These inactivation results are suggestive but not conclusive, due to compensatory changes in the network, so we examined the effects of ACh on these specific theta generators in isolation (Fig. 19D, E). The sub-network of recurrently connected pyramidal cells generated the highest theta power in the low cholinergic states (Fig. 19D2), whereas the OLM-pyramidal cells sub-network had its theta peak in the high cholinergic states (Fig. 19E2). A similar analysis of the EC induced oscillations showed no significant relationship between cholinergic modulation and theta power.

Cholinergic stimulation in the model had several effects on the neurons and synapses of the network (see Methods). We ran simulations by isolating individual cholinergic effects and allowing only one effect to be expressed in each run. Cholinergic

suppression of the recurrent connections, and the cholinergic depolarization of pyramidal cells impaired theta generation in the recurrently connected pyramidal cells sub-network (Fig. 19D3). While it was initially counterintuitive as to why depolarizing pyramidal cells would impair theta generation, we noted that raising the resting potential in our model also controlled the dynamics of the spike-frequency adaptation current (see eq. 2), and adaptation is required for theta generation in a recurrently connected network [9,10,21,58]. Cholinergic effects on OLM cells (depolarization and reduced spike-frequency adaptation) enhanced theta in the OLM-pyramidal cell sub-network, but cholinergic effects on pyramidal cells (depolarization, and enhanced burstiness) had an even steeper effect (Fig. 19E3), presumably due to the short-term facilitation at the pyramidal to OLM synapses. These effects were mediated by enhanced OLM cells firing rates (Fig. 19E4).

In summary, the inactivation of individual theta generators had a variable impact on theta power as a factor of the state of cholinergic neuromodulation. The recurrent connections played a major role in the low cholinergic state while OLM-pyramidal cells sub-network played a more substantial role in the high cholinergic state.

Discussion

A biophysical model of the hippocampus provided an integrative understanding of theta generation and, for the first time, examined five cooperative generators of theta activity. Furthermore, it helped reveal variable engagement of the theta generators in different neuromodulatory states. The model was developed by matching biological data including single cell behavior, synaptic dynamics, connectivity patterns, and short-term synaptic plasticity. In a previous study, the model parameters were constrained to replicate pattern

completion and separation behavior in the hippocampus, and subsequently validated by testing the model's ability to reproduce the effects of ACh in biasing the CA3 network towards pattern separation [38]. The model was used here as previously published with no changes in parameters (available at the public site ModelDB; see Methods). The present study sheds light on several underlying mechanisms involved in theta generation, as discussed below.

Multiple solutions, one rhythm

Earlier reviews speculated several intrinsic theta generators in the hippocampus [1,49]. Our results are consistent with this account, and further provide a tool to examine the relative contributions of each generator and to shed light on how the generators cooperate and compensate for one another. The exceptional robustness of hippocampal theta generation suggested that the rhythm can be considered as an intrinsic property of the network. Consequently, any experimental manipulation or brain state that generates sufficient excitation in the hippocampus may produce theta oscillations, non-specifically. This is consistent with experimental reports of oscillatory activity being generated by simply enhancing neuronal excitability by distributed electrical excitation [66], or by raising extracellular potassium concentration [67].

The abundance of theta generators suggests that designing studies to establish the necessity or the sufficiency of one factor to theta rhythms might be difficult in experiments. For example, in a recent study, optogentic silencing of OLM cells in vivo did not diminish theta activity [8]. In light of our results, this lack of effect on theta rhythm is expected, and is not evidence against a role for OLM cells in theta rhythm generation. In fact, within the integrative framework presented here, disruption of theta

after a particular generator is inactivated would warrant a closer inspection, since causes for the absence might include extreme neuromodulatory states, or diminished excitation below a minimum threshold.

The robustness of theta generation might seem to contradict the presence of other non-theta states. However, it is important to note that we constrained the firing rates distribution to match that of place cells during locomotion, a state characterized by prominent theta activity. In addition, we expect neuromodulation to strongly influence the repertoire of oscillatory states in the hippocampus.

Relative contributions of different generators

We quantified the relative contributions of theta generators by inactivating each individually and assessing the relative drop in theta power (Fig. 19A-C), generating several relevant insights. For example, we found that generators can have a variety of interactions such as compensating for inactivated generators, as exemplified by the network's ability to compensate for the removal of pyramidal cells resonance (Fig. 19A, C). Importantly, we also showed that removal of the divergent projections from EC to CA3 produced the highest drop in theta power (Fig. 19A, C), suggesting that despite the local circuit theta generators, external input amplifies the rhythm substantially. The fact that our model EC neurons lacked rhythmic properties (Fig. 13C3) highlights a role for solely the strength of the external input, i.e., without a frequency-modulated component. This observation is of relevance when considering the substantial drop in hippocampal theta observed after inactivating external input from EC [31] or the medial septum [29]; external input strongly synchronizes hippocampal rhythms. Our results provide a more nuanced interpretation of these experimental findings [29,31], where receiving external

signals, even if randomly distributed, synchronizes hippocampal rhythms. This expands our understanding of the role of these external inputs beyond the interpretation that hippocampal theta is dependent on receiving theta-modulated external input from either the medial septum or EC. Computational modeling in this case allowed us to delineate two effects of external input that might be difficult to dissociate experimentally and suggested that both random input as well as frequency-modulated input have independent contributions to hippocampal theta.

Significantly, this methodology sheds some light on the mechanisms most crucial to theta generation across neuromodulatory states. We previously showed that the low and the high cholinergic states engendered run away excitation via distinct pathways, and also differed in the mechanisms that contained such aberrant excitation [38]. The present study revealed parallel differences and extended this perspective to suggest that the two circuits also differ fundamentally in how they generate rhythmic activity, consistent with the suggested role of neuromodulation in profoundly reconfiguring neuronal circuits [68–70]. This conceptual delineation might be more tied to the underlying mechanisms compared with the categorization of theta into atropine-resistant and atropine-sensitive forms [71]. Furthermore, using this framework, more detailed conductances-based models might reveal how specific neuronal conductances are involved in theta generation across cholinergic states, since these specific currents are the targets of cholinergic modulation either directly (for e.g. m-current) or indirectly (e.g. h-current, through changes in resting potential).

Intrinsic theta generation with no local connectivity

An interesting observation from the model was that a power spectrum peak could be detected in the activity of a population of disconnected and independently firing neurons [Fig. 14; ,72]. Indeed, the power spectrum of summed independent signals is proportional to the autocorrelation function of individual neurons [73, page 184]. A novel finding from the model was to demonstrate that these correlations, though sometimes disregarded as an artifact, had the highest impact on theta power, when entrained by shared extrinsic input from EC (Fig. 19A).

Coordinated activity through input correlations has been observed experimentally in the olfactory cortex [37], but has not been studied in the hippocampus. The spatial divergence of the projections between layers causes cells in the target layer to share many of the same inputs. So, although the EC inputs themselves are not correlated per se, their spatial projection to CA3 pyramidal cells results in the latter having correlated inputs. Since CA3 pyramidal cells had spiking oscillations at theta, this sharing of inputs caused coherent firing at a similar phase, generating coherent theta oscillations [74], despite the absence of any local connectivity. Any resonant process in CA3, such as the h-current in pyramidal or OLM cells or the OLM-pyramidal cell subnetwork [3,6,14,15], can be organized by the shared external input, to generate robust rhythmic activity. While the observed oscillations had a wide-based spectral peak, the architecture of the hippocampus with multiple layers providing divergent projections from one to the next [57] can amplify this effect at each layer, resulting in a robust method for generating rhythms.

The role of pyramidal-interneuron sub-networks in oscillatory activity

Computational models of theta generation emphasized the role of OLM cells, and in particular their h-current, in rhythm generation [3,6,14,15], but recent evidence has suggested a more modest h-current in OLM cells [7]. To reconcile these findings with computational models, we simulated the OLM-pyramidal cells sub-network with inactivated h-current (to take the recent findings to their extreme) but still observed theta generated through two other mechanisms. First, their slow inhibition can form a theta-generating feedback loop with pyramidal cells (Fig. 17A-D) [14,15,20,58]. Second, OLM cells can generate theta by merely synchronizing the activity of the theta resonant pyramidal cells (Fig. 17A-D). Simulating this sub-network with an active h-current enhanced theta power as shown in previous models [3,15,75].

We propose considering these two mechanisms and the h-current as three distinct mechanisms in the OLM-pyramidal sub-network, probably operating simultaneously to maintain theta rhythmic activity. Another mechanism that is relevant to purely inhibitory networks is theta generated by a population of recurrently connected OLM cells sharing inhibitory input [14], but our model lacked the necessary OLM to OLM connections to test the presence of this mechanism.

In the model pyramidal-BCs sub-network, two modifications were necessary to obtain oscillatory activity (Fig. 18A, B). The connection probability between the two cell populations had to be increased above our initial estimates, similar to previous modeling studies [15]. While this might be an issue of modeling at a lower scale compared to biology, it might suggest a lower participation of BCs in oscillatory activity, compared to OLM cells, since they send and receive relatively fewer connections to and from

pyramidal cells [63,64]. In addition, we show that increased connectivity was not sufficient by itself to produce oscillatory activity, but suppression of short-term synaptic depression, a cholinergic effect [76], was also required (Fig. 18B3, 4).

While fast inhibition is associated with the generation of gamma oscillations [61,62,77], a prediction of the model is that the BC-pyramidal cell sub-network can also, indeed, support the generation of ~8 Hz rhythmic activity in states with active spike-frequency adaption in pyramidal cells (Fig. 18). This behavior might be modulated in states where spike-frequency adaptation is suppressed [for e.g., by neuromodulation 78–80]. We also observed an emerging peak around 17 Hz which might be a precursor to gamma-range oscillations when the network is subjected to sufficient background activity [65].

Putting it all together

Rhythmic oscillations in multiple frequency bands are associated with the functioning of most nervous systems, and are a topic of intense research. Underlying such oscillatory activity are complex interactions at multiple levels including individual neurons, local circuits, and neuronal systems. The multitude of generators and interactions amongst areas makes the system particularly difficult to investigate experimentally. We believe that our study contributes to the rapidly growing literature in neural oscillations. Specifically, we suggest how activity in any region could be studied as being comprised of three components, an intrinsic ability of the region to generate oscillations, a random non-rhythmic extrinsic component that coordinates oscillations generated intrinsically in the region, or/and a frequency-modulated rhythmic extrinsic component that specifically entrains neurons in the region to a particular frequency. This idea holds, in general, to both other forms of oscillations

and other brain regions. Moreover, it could be relevant to other biological phenomena involving oscillations.

We suggested how the role of the intrinsic biophysical mechanisms in such complex oscillatory systems can be studied using a biologically realistic model. We devised a simple and experimentally practical approach through serial inactivation of individual rhythm generators across neuromodulatory states. This simplified approach yielded significant insights showing that different neuromodulatory states may engage different theta generators. Additionally, we showed that external input can have a prominent contribution to theta power in the hippocampus, but also that the hippocampus is not solely dependent on this external input being theta-modulated.

The model makes five experimentally testable predictions. First, stimulation of EC in an in vitro preparation of the hippocampus is sufficient for generating oscillatory activity in CA3 even in states with diminished local synaptic transmission in CA3. Second, OLM cells can generate theta activity via at least two mechanisms: synchronizing pyramidal cells with a common inhibitory signal, and pacing theta activity through slow inhibitory feedback loops. Third, BCs reciprocally connected to pyramidal cells are capable of generating theta activity by virtue of spike frequency adaptation in pyramidal cells. Fourth, since the spiking oscillations demonstrated in model pyramidal cells relies on their ubiquitous spike-frequency adaptation, neuromodulators that affect this adaptation should significantly modify resonance characteristics in biological cells. Fifth, while impairment of any single theta generator might not disrupt rhythmic activity, conditions can be set up through neuromodulation to emphasize one generator over the others. For example, inactivation of OLM cells would have a larger effect in high

cholinergic states, while inactivation of recurrent connections would affect theta prominently in low cholinergic states. Modern tools, such as optogentics, with the ability to control specific pathways, would facilitate experimental testing of these predictions.

Methods

Single cell models

The model cells in CA3 were pyramidal cells and two of the most abundant interneuron types, BCs and OLM cells [81]. The two types of interneurons are on extreme ends of many cellular attributes such as spiking patterns, inhibition dynamics and post-synaptic target compartments, and so their inclusion captures a wide range of interneuronal dynamics. The model cells in DG were granule cells, BC, and hilar perforant path-associated (HIPP) cells.

Single cell models were developed using the Izhikevich formulation [39,82]. The equations for a model neuron were as follows:

$$\frac{dv}{dt} = -k(v - v_t)(v - v_r) - u + I \quad (1)$$

$$\frac{du}{dt} = -a(b(v - v_r) - u) \quad (2)$$

$$if\ v > vpeak\ then\ v = c\ and\ u = u + d \quad (3)$$

where v is the membrane potential of the cell, u is a recovery variable, v_t is the 'instantaneous threshold' beyond which the cell will fire an action potential, v_r is the

resting membrane potential, *I* is the current injection, *k* is a constant used to adjust the input resistance and rheobase, *vpeak* is the threshold above which a spike is deemed to have occurred and the membrane potential is reset, and *a*, *b*, *c*, and *d* are parameters used to tune the behavior of the system to model the neuro-computational properties of the desired cell. While the NEURON environment is typically used for Hodgkin-Huxley cell models, we developed a biophysical cell model in NEURON and implemented the Izhikevich formulation by adding a current modeled by the two equations.

This formulation provides a reduced-order model that preserves many of the neuro-computational properties of more detailed biological models. We provide an overview below of how model neurons were developed to match salient features in electrophysiological recordings (Fig. 1), with parameters used listed in table 1. For CA3 pyramidal cells, the resting membrane potential was set to -75 mV, spike threshold to -53 mV, and peak action potential voltage to 29 mV [40]. The remaining cell model parameters were tuned to match responses to both long and brief current injections (Fig. 1) [40]. Similarly, in developing the DG granule cells model, resting membrane potential, threshold, and peak action potential were set using data from Staley et al., [41] and the model was then tuned to match current injection responses (Fig. 1) [41]. Passive properties for the OLM model were estimated from Ali and Thompson [42], and the behavior of the cells was matched to current injection responses from the same study. In particular, we matched the spike frequency adaptation, the prominent slow after-hyperpolarization potential (AHP), sag response, and rebound spikes (Fig. 1). For the BC model, membrane properties, current injection responses (Fig. 1), and finally current vs. firing rate relationship were matched to data reported in Buhl et al., [43]. Due to the

striking similarity of OLM and HIPP cells [83], we used the same model for both cell types. EC cells are known to display theta rhythmicity [31] . So, to examine the non-rhythmic component of EC input and its interaction with the intrinsic generators of theta in the hippocampus, we excluded oscillatory dynamics in EC cells by using generic non-adapting spiking cells [82].

Despite the significant heterogeneity of neurophysiological values reported across studies, our model neurons preserve the most salient cellular features in relative terms. For example, OLM interneurons fire at a slower rate than basket cells [81], and CA3 pyramidal cells burst more than granule cells of the dentate gyrus [84]. Such relative attributes of the cells are well-preserved in our model, irrespective of the particular set of neurophysiological values chosen. Other experimental data considered in developing the single cell models can be found in Hummos et al. [38]. Initial membrane potential values were drawn from a normal distribution with a mean equal to the resting membrane potential and a standard deviation of 10 mV. The h-current in pyramidal and OLM cells is known to have a role in theta generation [for review, see 2], so we added an additional slow current to our pyramidal and OLM cells tuned to match the subthreshold oscillations that the dynamics h-current produces [16]. The additional current equation took the form:

$$\frac{dh}{dt} = -a_h(b_h(v - v_r) - h) \tag{4}$$

where h is the h-current value, and a_h, b_h are parameters used to tune the behavior of the cell and took the values of 0.04 ms^{-1} and 10 for pyramidal cells and 0.03 ms^{-1} and 3.5 for OLM cells. A reset parameters d_h was added to the value of h each time the cell

spiked and took a value of 1 for both pyramidal and OLM cells. These values were chosen to match the subthreshold resonance reported in literature for these two cell types [16].

Network structure and connectivity

The rat hippocampus contains approximately 1.6 million cells [85]. For computational efficiency and to maintain minimum model complexity, the numbers were scaled down while maintaining reported ratios [38], as in our previous models [86–89]. The model DG region had 384 granule cells, 32 BCs, and 32 HIPP interneurons, while the model CA3 region contained 63 pyramidal cells, 8 BCs, and 8 OLM cells [85,90–92]. The model EC region had 30 regular spiking cells.

The entorhinal cortex provides inputs to the hippocampus through the perforant pathway that projects to the entire hippocampal formation. The standard view describes a unidirectional connectivity with a direct path from EC to CA3 and an indirect path through DG (Fig. 12A, B) [57,93]. The perforant path projections follow a lamellar organization across the longitudinal axis of the hippocampus, as follows: Lateral and posterior parts of the EC are connected to the dorsal parts of CA3 and DG, while the more medial and anterior parts of EC project to the ventral parts of CA3 and DG [57]. This lamellar organization transitions gradually from one extreme to the other on the longitudinal axis of the hippocampus, and a single neuron in EC can project to about 25% of the longitudinal length of CA3 [57]. Projections from DG to CA3 also follow a similar longitudinal organization; however, these projections target a more limited longitudinal extent [57].

Model cells were distributed uniformly in 3D space separated into the three regions, EC, DG, and CA3, with dimensions that approximate the respective dimensions of the rat hippocampus [38]. Projections from EC to both pyramidal cells and BCs in DG and CA3 followed a lamellar pattern where neurons were most likely to connect to neurons in of their longitudinal neighborhood with a decreasing probability towards the periphery. This spatial connectivity was modeled using a Gaussian connection probability function that depended on the longitudinal distance between the two connected cells. The Gaussian function had a peak probability of 0.4 and a standard deviation of 3 mm for the perforant path projections to both pyramidal cells and BCs in CA3. Perforant path projections to DG had similar values (see [38]).

Similarly, the mossy fiber projections from DG to CA3 followed the same lamellar pattern but with a more limited longitudinal extent by setting the standard deviation of the Gaussian probability function to 2 mm. In addition, to preserve the sparseness of the mossy fiber connections from DG to CA3 [57], each DG granule cell was limited to contacting two CA3 pyramidal neurons. Projections from DG granule cells to CA3 BCs are more diffuse and out-number projections to CA3 pyramidal neurons by a ratio of 10:1 [94]. Accordingly, DG projections to BC followed a Gaussian distribution with a peak probability of 0.2 and standard deviation of 3 mm. Recurrent CA3 connections reveal relatively more diffuse spatial organization [95,96], and were therefore distributed homogenously with a fixed probability of 0.3.

The dendritic projecting OLM cells are thought to be involved in feedback inhibitory loops [97] and while they have a more limited axonal arborization [98] they make many more synapses compared to BCs [63]. In contrast, BCs have a more diffuse

axonal arborization with the highest connection probability to pyramidal cells in their immediate neighborhood and a decreasing connection probability towards the periphery of their axonal arbors [63]. Similarly, BCs project to neighboring OLM cells [99]. As before, we used a Gaussian function to approximate these spatial probabilities. We also assumed that BC projections to both pyramidal cells and to OLM cells shared the same spatial domain (Remove statement or add to figures or explain why it did not contribute much?). In the reverse direction, OLMs receive reciprocal connections from the same pyramidal cells they projected to, in line with their function as local feedback cells [97]. On the other hand, granule cells in DG and pyramidal cells in CA3 projected homogenously to BCs with a fixed probability of 0.15, consistent with the lack of specific topography reported at these projections [100].

The network was constructed by generating connections randomly between cells while maintaining the connection probabilities and spatial patterns of connectivity described above. The spatial connectivity patterns and parameter values are summarized in table 2 (also see [38]).

Synaptic currents

Synaptic currents were modeled using the kinetic model described in Destexhe et al. [101]. AMPA, NMDA, $GABA_A$, and $GABA_B$ currents were modeled and their dynamics such as rise and decay time constants and delays were matched to available literature [38]. In particular, CA3 pyramidal cell AMPA currents were fastest for the mossy fiber inputs from DG and slowest for perforant path inputs from EC, while recurrent CA3 inputs from other pyramidal cells had intermediate values [48,102], as

summarized in table 2. Additionally, inhibitory currents from OLM had slower dynamics compared to those from BC (Table 2) [99,103].

Synaptic weights were assigned in accordance with literature where available. The mossy fiber synapses were adjusted so that a train of spikes arriving at the synapse could cause a CA3 pyramidal cell to fire while a single spike could not [109]. Recurrent CA3 connections were assigned a low initial weight, as an approximation of data showing that the transmission of action potentials had a probability of 4% at those synapses [110]. Synapses from CA3 pyramidal cells to interneurons were set at a higher level to reflect the fact that action potential transmission occurs at a ~60% success rate [111,112]. Connections between granule cells and DG interneurons were adjusted to achieve sparse DG firing [113]. Synapses had initial weights chosen from a uniform random distribution of values between 50% and 100% of the assigned weight value. All associated equations and parameter values are described in Hummos et al. [38].

Activity-dependent plasticity

For this study, long-term plasticity was excluded from the synapses. Model synapses, however, exhibited short-term synaptic plasticity that used the formulation proposed by Varela et al. [114]. We modeled the pronounced short-term facilitation at mossy fibers [45] and the frequency-dependent synaptic depression reported at the recurrent CA3 connections [Fig. 13D-I; ,48]. We extrapolated from data in CA1 where projections from pyramidal cells display short-term facilitation at synapses contacting OLM cells [42], and short-term depression at those contacting BC cells [46]. In the other direction, inhibitory currents from OLM cells to pyramidal cells show no short-term facilitation or depression [97], while inhibitory currents from BCs to pyramidal cells

show depression [47]. Model traces are compared with available experimental recordings in figure 12. Additional details and equations related to the implementation of short-term synaptic plasticity can be found in Hummos et al [38].

Acetylcholine effects

The hippocampus receives widespread volume transmission of cholinergic inputs from the septum-diagonal band complex [115]. To implement the effects of ACh on model neurons and synapses, we used a variable 'ACh' to represent the ACh state. The variable ACh had values of 0 (low), 1 (baseline), and 2 (high).

Cholinergic stimulation has differential effects on synaptic transmission of different pathways in the hippocampus [116]. Synaptic transmission through the perforant pathway projections to CA3 is suppressed by 50%, compared to a suppression by 85% at the recurrent connections in CA3 [107,117]. On the other hand, the mossy fibers transmission is enhanced by 49% [118]. To model ACh effects on synapses, AMPA synaptic currents were scaled by the value of ACh. A parameter bACh determined the direction and magnitude of ACh effects on a particular synapse. Values of bACh for different synapses were set according to experimental results as summarized in table 2 (also see Hummos et al. [38]).

In addition to the synapse specific effects, cholinergic stimulation enhanced cellular excitability and depolarized the resting membrane potential of principal cells, eliminated AHP, decreased spike frequency adaptation and induced rhythmic burst activity [78,79]. Furthermore, effects on interneurons were subtype-dependent [119,120]. Muscarinic stimulation of OLM interneurons depolarized the resting membrane potential, and lowered both spike frequency adaptation and AHP [121]. In contrast, PV-BCs

respond to muscarinic receptor activation with a limited depolarization in resting membrane potential [122,123]. Effects of ACh on neurons were modeled by linearly scaling the neuronal model parameters by the ACh state as detailed in Hummos et al. (see fig. S4 in [38]). Considering the slow dynamics of ACh effects [onset time constant approximated between 1 and 2 s; ,124], ACh state was set to a given value at the beginning of each experiment and had no dynamics.

Inputs and data analysis

For the full model and sub-circuit cases considered, either EC cells or CA3 pyramidal cells (identified in the figures) received external input as trains of Poisson-distributed spikes, triggering an influx of AMPA and NMDA currents into the cell. We studied two model cases: one with external input arriving at EC, and the other with input arriving directly at CA3 pyramidal cells. The two types of inputs differed in the weight of the associated input synapses, and the base rate of the Poisson spike trains arriving at these synapses. Input to EC arrived at synapses with a 100% spike transmission rate to ensure that EC firing pattern was dictated by the Poisson input, whereas input to CA3 pyramidal cells had a lower weight value with parameters matching the EC to CA3 synapses (Table 2).

To determine the base rates of the Poisson processes generating these input trains, we considered place cells in CA3. Place cells respond to certain areas in the environment and their firing rates approximate a lognormal distribution [44] with an average of ~7 Hz [125]. In our model case where external inputs arrived at EC, each EC cell received a unique train of Poisson input spikes at a base rate of 15 Hz, which produced firing rates in CA3 pyramidal cells with a lognormal distribution and an average of 7 Hz (Fig. 12C1).

In the model case where external inputs arrived directly to CA3 pyramidal cells, the input rates to different cells had to be drawn from a lognormal distribution (average: 50 Hz, standard deviation: 40 Hz), to produce firing rates with a lognormal distribution (Fig. 12C2) that matched experimental data.

For spectral analysis, we summed the spikes of all cells of each type in a region (e.g., CA3 pyramidal cells) in 0.1 ms bins and computed the fast-Fourier transform of the resulting vector, using the Matlab function psautospk.m [126], with a moving window of size 1024 ms, and overlap of 512 ms. Spike data was used in spectral calculations as a proxy for LFP as used in network models [e.g., 127–129], with the assumption that these spikes are received by a downstream local neuron and translated into membrane currents that generate an LFP signal.

The coherence measure used was implemented as described by Wang and Buzsaki [72]. Briefly, the coherence measure reflects synchrony between the spike trains of two neurons (two spikes are synchronous if occurring within 5 ms of each other). The population coherence is the average coherence across all neuron pairs to give a measure between zero (minimum synchrony) and one (maximum network synchrony). Oscillatory activity tends to synchronize the network making coherence a good measure of oscillations.

The model was developed using the NEURON software package [130] and run on a PC with an Intel i7-core processor with an integration time-step of 0.1 ms (key results were also verified with a time-step of 0.01 ms). The code is available as part of our previous publication via the public database ModelDB at Yale University. The recorded spike times were then analyzed using MATLAB (Mathworks, Inc.). All simulations ran

for 5 seconds except for the experiment in figure 14, where single neuron spike data was analyzed over a 30 second period.

Tables

Table 1: Model cells parameter values

Parameters **Cell types**	**C** **(pF)**	**k**	**a** **(1/ms)**	**b**	**c** **(mV)**	**d**	**v_r** **(mV)**	**v_t** **(mV)**	**v_{peak}** **(mV)**
CA3 pyr	24	1.5	0.01	2	-63 [a]	60	-75	-58	29
GC	24	1	0.015	3	-62	3	-73	-53	32
O-LM	80	1.5	0.003	10	-65 [b]	30	-68	-53	30 [b]
BC	16	1.5	0.9	2	-80	400	-65	-50	28

[a] for the burst response to brief current pulse, c was -53

[b] for OLM interneurons, c and v_{peak} were dependent on the recovery variable u, where c was incremented by (10 * u) and v_{peak} was decremented by (30 * u) to produce the stereotypical shape of OLM firing.

Table 2: Summary of synaptic properties used in the CA3 network model.

	EC input	*Recurrent*	*Pyr to OLM*	*Pyr to BC*	*OLM to pyr*	*BC to pyr*
Spatial connectivity	Diffuse [57]	Homogenous [96]	Reciprocal [97]	Homogenous [100]	Dense, compact [102]	Light, diffuse [98]

Synaptic Delay (ms)	5 [104,105]	2 [48]	0.9 [103]	0.9 [103]	0.8 [103]	0.8 [103]
AMPA or $GABA_A$ rise/decay time constants (ms)	1.7/10.9 [102] [a]	1.1/5 [48]	0.27/0.57 [103]	0.27/0.57 [103]	2.8/20.8 [99] [a]	0.21/3.3 [99] [a]
NMDA or $GABA_B$ rise/decay time constants (ms)	25/300 [102]	25/300 [102]	25/150 [102,106]	25/150 [102,106]	11.1/125 [101]	11.1/125 [101]
Weight	2	0.4	3	3	3	3
Short-term synaptic plasticity	None	Depressing [48]	Facilitating [46]	Depressing [46]	None	Depressing [47]
bACh	-0.5[107]	-0.85 [107]	None	None	None	-0.5 [108]

bACh: a unit-less value determining the direction and magnitude of ACh effects on synapses (see Methods)

[a] We calculated the rise time constant from the reported 20-80% rise time or 10-90% rise time, see Hummos et al. [38].

Figures

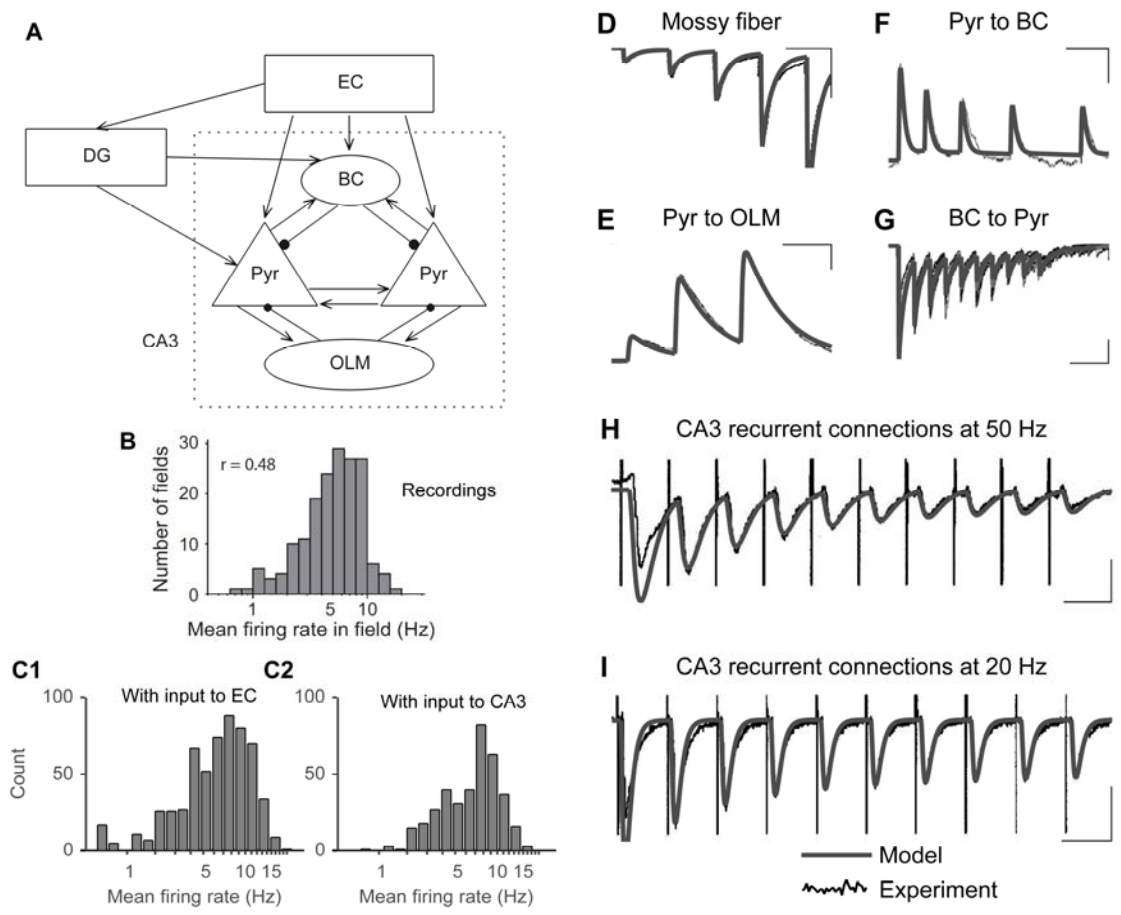

Figure 12: Network synaptic connections, titration of external input synapses, and the dynamics of short-term plasticity.

A) Schematic showing the full model. Abbreviations: Pyr, pyramidal cells; OLM, oriens-lacunosum moleculare cells; BC, basket cells; EC, Entorhinal cortex; DG, dentate gyrus. B) *In vivo* distribution of CA3 place cells firing rates as the rat crossed their place field. Reproduced from [44]. C1) The distribution of CA3 pyramidal cells firing rates in the model case where random trains of synaptic inputs arrived at EC cells at a base rate of 15 Hz. C2) The distribution of CA3 pyramidal cells firing rates in the model case where random trains of synaptic inputs arrived at CA3 pyramidal cells at base rates drawn from a lognormal distribution with an average of 50 Hz and a standard deviation of 40 Hz. D-I:

Synaptic model responses match those in experimental recordings. D) Mossy fiber synaptic facilitation [45]. (Scale bars: 50 ms, 100 pA). Parameter values used to reproduce data are listed in Hummos et al. [38]. E) CA3 Pyramidal cell to OLM interneuron [42]. (Scale bars: 20 ms, 1 mV). F) CA3 Pyramidal cell to BC interneuron [46]. (Scale bars: 30 ms, 0.5 mV). G) BC interneuron to CA3 pyramidal cell [47]. (Scale bars: 50 ms, 100 pA). H, I) Recurrent CA3 connections stimulated at 50 Hz, and 20 Hz, respectively [48]. Note that these connections displayed paired pulse facilitation, a phenomenon not included in our synapse model. Therefore, responses to the first stimulus in the train appear larger than in the recordings. (Scale bars: 20 ms, 0.5 mV in E; 50 ms, 0.5 mV in F).

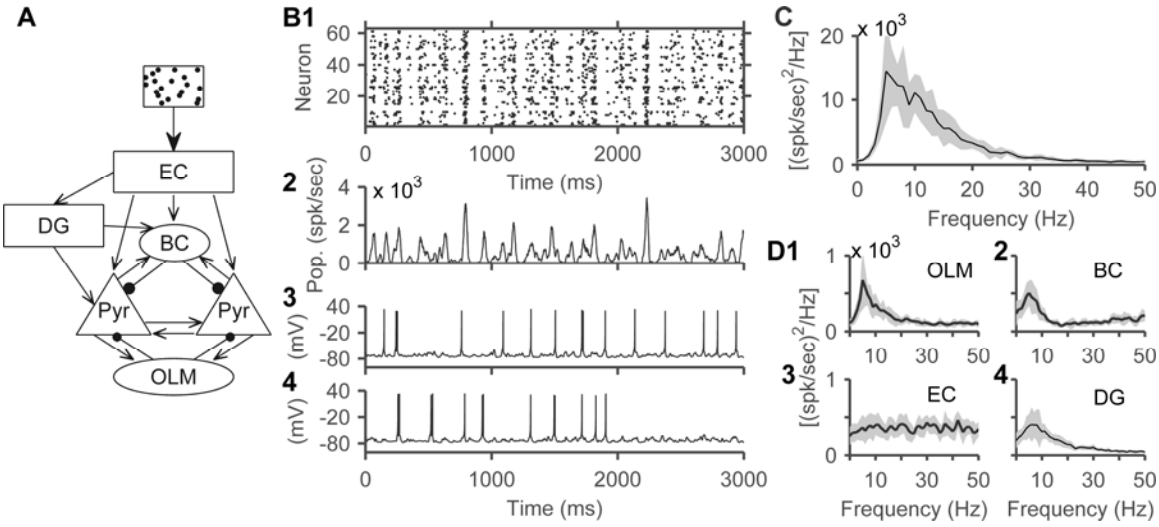

Figure 13 Model network displayed theta rhythmicity.

External inputs arrived at EC cells in the form of Poisson spikes with a base rate of 15 Hz, chosen to reproduce place cells firing rates (see Methods). A) Network schematic

showing the entire model. External input represented by box with random spike trains. B1) Spike raster plot from an example instantiation of the network. B2) Population firing rate calculated using a 20 ms sliding window and B3, 4) two membrane potential traces of neurons from the same network instantiation. C) The population power spectrum of CA3 pyramidal cells averaged from 10 network instantiations showing a peak at around 6 Hz. We sampled spike counts from the cell types considered, in 0.1 ms bins, and calculated the Fourier transform of the resulting vector, using a window length of 1024 ms. Shaded areas represent SD. D) Power spectra from four populations of cells in the model showed a peak around 6 Hz: (D1) OLM cells, (D2) BCs, (D3) EC, and (D4) DG.

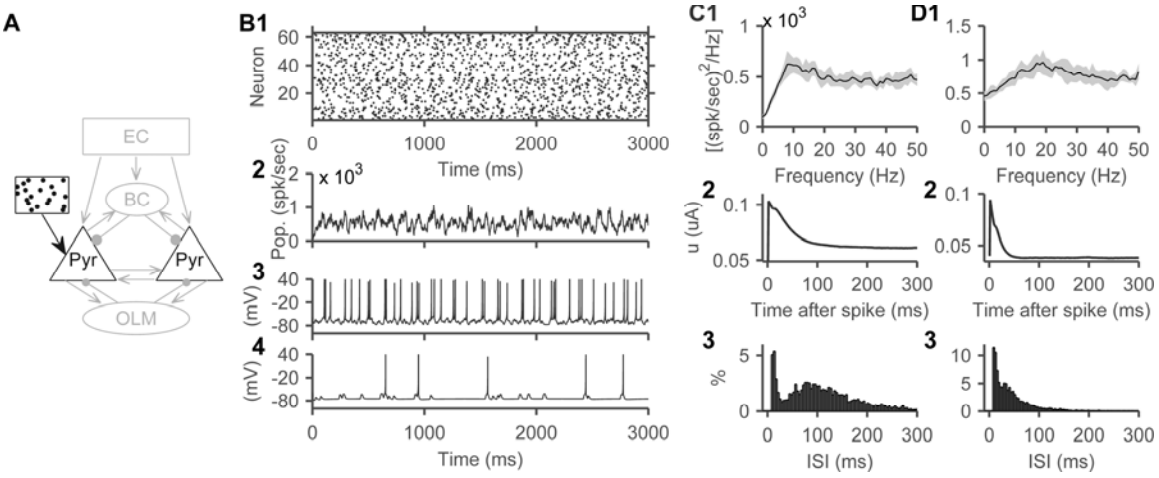

Figure 14 Disconnected pyramidal cells show theta spiking oscillations.

A) Schematic of this experiment with isolated pyramidal cells each receiving a unique train of Poisson spikes with base rates derived from a lognormal distribution (mean 50 Hz SD 40 Hz, chosen to reproduce place cells firing rates). B1) Spike raster plot of pyramidal cells showing grossly random firing. B2) Population firing rate calculated using a 20 ms sliding window. B3, 4) Example membrane voltage traces from two neurons. C1) The power spectrum of the spiking activity of pyramidal cells as a

population showing a peak at 8 Hz. C2) the spike-triggered average of the 'u' current of the Izhikevich model that captures the spike-frequency adaptation of the cells. C3) The inter-spike interval distribution of pyramidal cells. D) Same as in C, but with the time-constant of adaptation lowered from 100 ms to 25 ms, resulting in a power spectrum peak at 17 Hz, to demonstrate the relationship between the spiking oscillations, adaptation current, and the spiking dynamics of pyramidal cells.

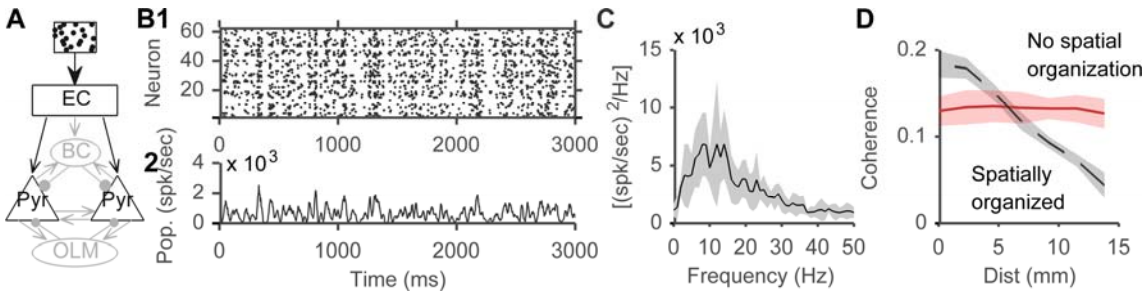

Figure 15 Divergent projections from EC to CA3 produced theta oscillations.
A) Schematic of this experiment where the only active connections were the projections from EC to CA3 pyramidal cells. Model EC neurons lacked any rhythmicity and on average, each EC neuron projected to about 20% of CA3 pyramidal cells (see Methods). B1) Spike raster plot and (B2) population firing rate from one example network. C) The population power spectrum of CA3 pyramidal cells averaged over 10 network instantiations showed a wide based peak in the theta band centered around 9 Hz. D) Pairwise coherence between pyramidal cells is inversely related to the distance separating them (dashed black line), but this relationship is lost when EC neurons were connected to pyramidal cells randomly irrespective of the longitudinal distance (solid red line).

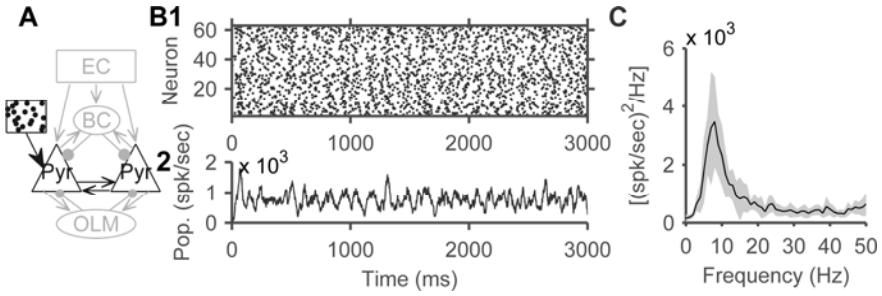

Figure 16 Recurrent connections produced theta oscillations.

A) Schematic of the minimal network used for this experiment with only pyramidal cells and the synapses connecting them. B1) Spike raster plot and (B2) population firing rate from one example network. Note that in this sub-circuit, the oscillations are easier to identify visually in the firing rate plot. C) The population power spectrum of CA3 pyramidal cells averaged over 10 network instantiations shows a peak at 8 Hz.

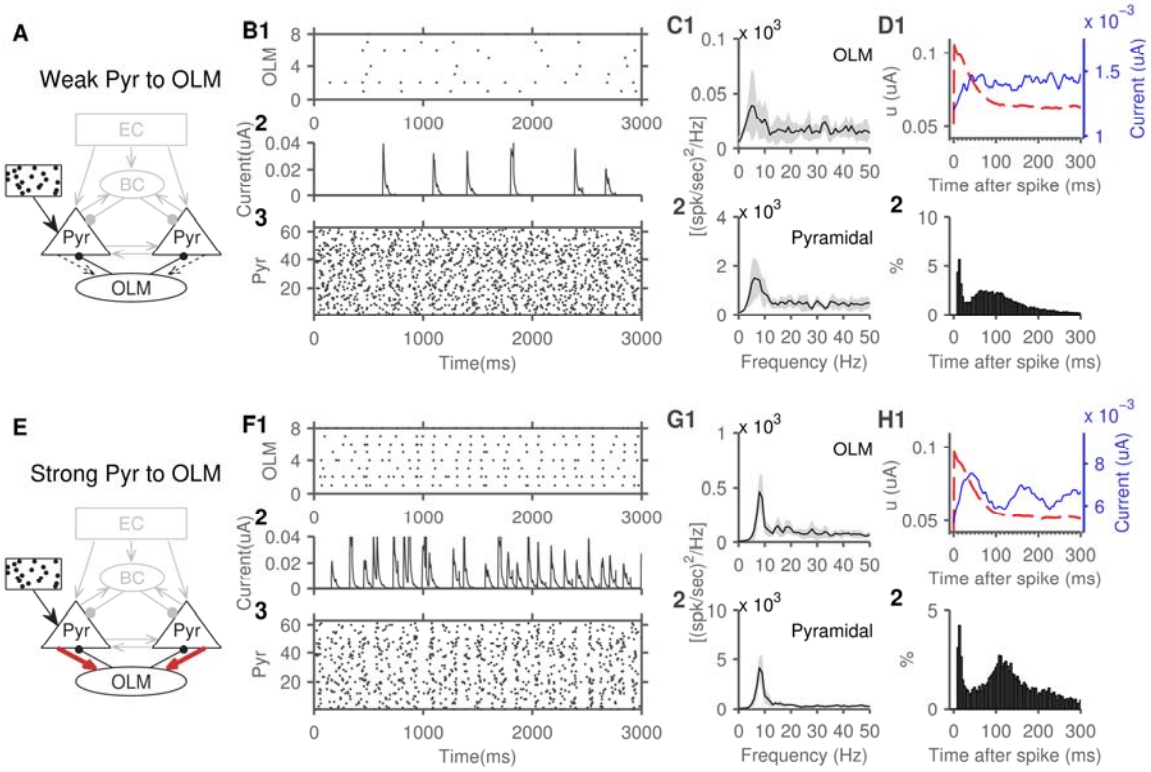

Figure 17 Pyramidal-OLM cells network generates theta through two mechanisms. A) Schematic showing the pyramidal-OLM cells network with weak pyramidal to OLM synapses (weight set to 2), used in panels B-D. B) Spike raster plot of OLM spikes (B1). The OLM inhibitory currents received by one example pyramidal cell (B2). Note that inhibitory currents occur at a frequency much lower than theta. Spike raster plot of pyramidal cells spikes (B3). C) The population power spectrum of OLM cells (C1), and pyramidal cells (C2). Spectrum averaged from 10 instantiations of the network, shaded areas represent SD. D1) The pyramidal cell spike-triggered average of the adaptation current (dashed red line) and received OLM inhibition (solid blue line). Note that OLM inhibition showed a poor association with pyramidal cells spikes. D2) the inter-spike interval distribution of pyramidal cells remains largely unchanged from freely spiking pyramidal cells (compare with Fig. 14C3). E) Schematic showing the network with

strong pyramidal to OLM synapses (weight set to 6), used in panels F-H. F1) Spike raster plot of OLM spikes. F2) The OLM inhibitory currents received by one example pyramidal cell. F3) Spike raster plot of pyramidal cells spikes. G) The population power spectrum of OLM cells (G1), and pyramidal cells (G2). H) The pyramidal cell spike-triggered average (H1) of the adaptation current (dashed red line) and received OLM inhibition (solid blue line). Note the close association between OLM inhibition and pyramidal cells spikes. Note that OLM inhibition changes the distribution of the pyramidal cells inter-spike intervals (H2), creating a peak around 110 ms. Power spectrum peaks: C1,2: 6 Hz. G1,2: 8 Hz.

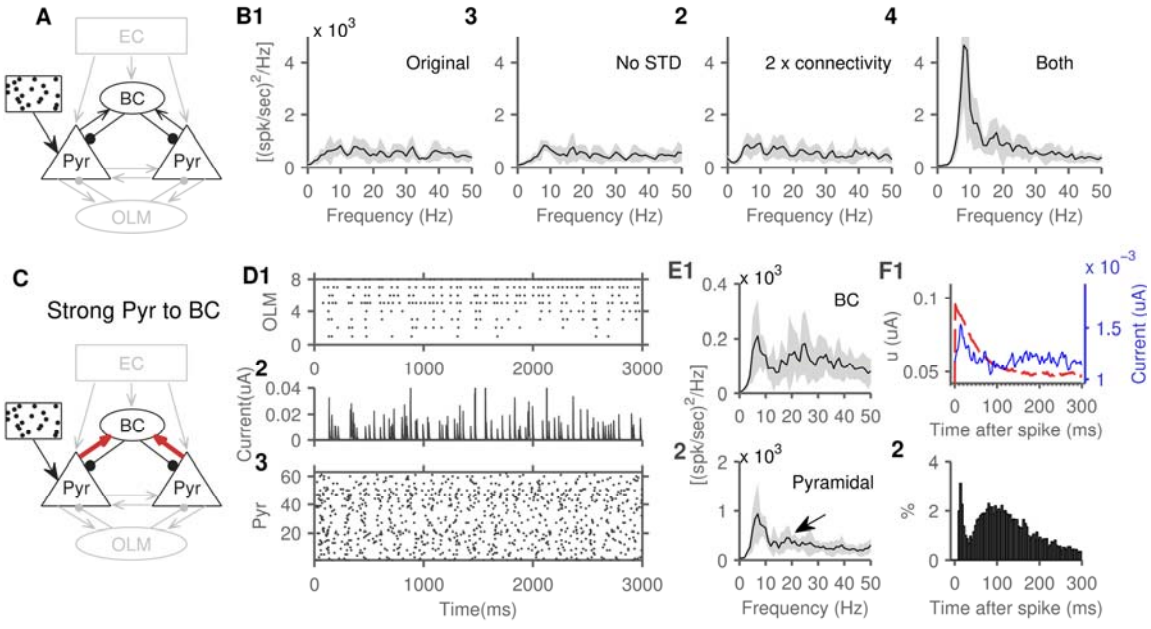

Figure 18 The role of BCs in theta rhythm generation.

A) Schematic of this network with only pyramidal and basket cells active. B) In the original state, the sub-network failed to generate a significant spectral peak (B1, beyond the small theta peak expected from isolated pyramidal cells activity, see Fig. 14). Oscillations remained absent after either removing short-term depression (B2) or doubling connection probability in both directions (B3). Both interventions were necessary to produce robust oscillatory activity (B4). C) Schematic of the network with strong pyramidal to basket cells synapses (weight set to 6), used in panels D-F. Note that short-term depression remained inactivated, and connectivity doubled for this experiment as well. D) Spike raster plot of BC spikes (D1). The BC inhibitory currents received by one example pyramidal cell (D2). The spike raster plot of pyramidal cells spikes (D3). E) The population power spectrum of BCs (E1), and pyramidal cells (E2), arrow pointing to a small emerging 18 Hz peak. F) The pyramidal cell spike-triggered average (F1) of the adaptation current (dashed red line) and received BC inhibition (solid blue line). Note the BC inhibitory current peaking sharply and then decaying back to average around 40 ms. F2) The inter-spike interval distribution of pyramidal cells. Power spectrum peaks: B1-3: 8 Hz. B4: 8 Hz, 18 Hz. E1: 6 Hz, 23 Hz. E2: 6 Hz, 18 Hz.

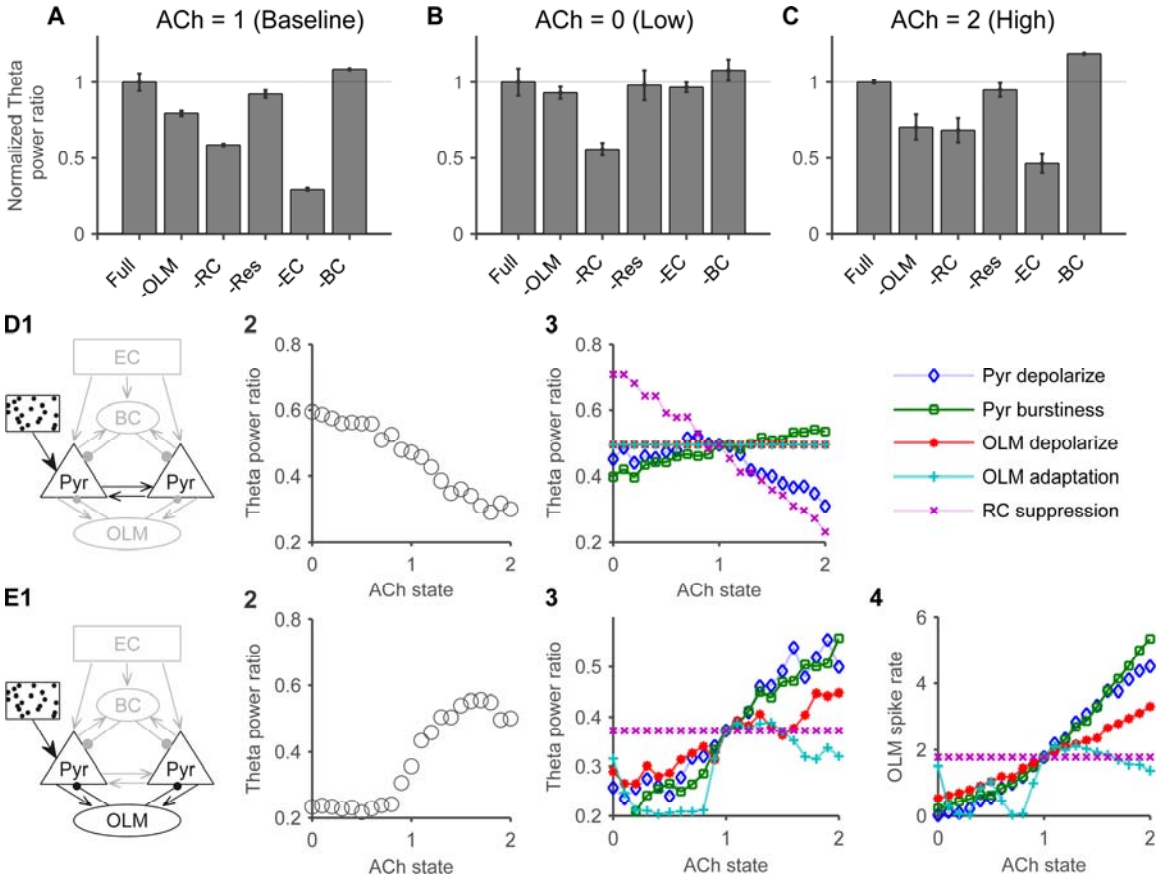

Figure 19 Relative contributions of individual theta generators across cholinergic states. A) Starting with the full EC and CA3 circuits we inactivated each individual generator and observed the changes in relative theta power (power in the 4 to 12 Hz range divided by the entire spectrum 0 to 250 Hz). To normalize, all values were divided by the relative theta power in the full model. Error bars indicate SD. B) The effects of inactivating individual generators in the low cholinergic state, and C) high cholinergic state. D) In the recurrent connections sub-network (D1), relative theta power decreased with higher cholinergic states (D2). A breakdown of cholinergic effects (D3) revealed that this was mainly mediated by the cholinergic suppression of the recurrent connection transmission (RC suppression) in addition to the cholinergic depolarization of pyramidal cells (Pyr depolarize). ACh in increments of 0.1. E) Schematic of the OLM-pyramidal cells

network (E1). Relative theta increased with cholinergic state (E2) and a breakdown of cholinergic effects (E3) shows that cholinergic suppression of spike-frequency adaptation in OLM cells (OLM adaptation), and OLM cells depolarization (OLM depolarize) enhanced theta power in the network. In addition, the cholinergic pyramidal cells depolarization (Pyr depolarize) and enhanced burstiness (Pyr burstiness, lower c and d parameters of Izhikevitch model) enhanced theta in this network with a steeper slope. These effects were associated with enhanced OLM cells firing rates (E4).

CHAPTER 4: Interplay of resonant and synchronizing generators in a hippocampal theta model

Ali Hummos, PhD student[1], Satish S. Nair, Professor[1, 2]
[1] Informatics Institute, [2] Department of Electrical & Computer Engineering, University of Missouri, Columbia, Missouri.

Abstract

Rhythmic activity characterizes neuronal processing in multiple brain areas. Study of rhythms indicate the involvement of a multitude of rhythm generators, likely through a variety of mechanisms. Considering the multitude of involved mechanisms in rhythm generation, inactivation of circuit components can produce complex and unpredictable results. We use computational modeling to examine interaction between circuit components that participate in rhythm generation. We distinguish between resonant components and synchronizing components and demonstrate that this categorization permits predicting the rules of which components can interfere with one another and which can substitute for one another. Resonant mechanisms inherently produce rhythmic signals as a product of their dynamics and include spike-frequency adaptation, slow inhibition, rhythmic external input, and slow neuronal currents. Synchronizing mechanisms promote coordinated activity and include inhibitory feedback, non-rhythmic external input, and recurrent excitatory connections. Some circuit components can provide both resonance and synchronization. We found the most robust rhythm generation to require at least one resonant component and one synchronizing component. We found that pyramidal cells adaptation can interfere with theta produced by slow inhibition, and fast inhibition can either substitute for or interfere with rhythm generation

by slow inhibition, depending on the cholinergic state. These results begin to shed light on the conflicting evidence produced by studies inactivating circuit components, and also predicts circuit states where inactivating a component known to participate in rhythm generation might paradoxically enhance rhythmic activity. We conclude that effects of component inactivation can only be predicted in the context of what other components are present and on the neuromodulatory state of the circuit.

Introduction

The hippocampus is a well-studied and easily accessible part of the brain with a wealth of physiological data and computational models. It displays a prominent slow rhythmic activity in the theta band (4-12 Hz) (Vanderwolf, 1969). In rodents, evidence points to a hippocampal role in navigation, both spatial (O'Keefe and Dostrovsky, 1971) and temporal (Pastalkova et al., 2008; MacDonald et al., 2011), but also in encoding and retrieval of episodic-like memories (Steckler et al., 1998; Mumby et al., 2002; Eacott and Norman, 2004; Fortin et al., 2004).

The hippocampal theta rhythm is understood to be generated intrinsically, through a number of mechanisms (Kocsis et al., 1999; Buzsáki, 2002; Hummos and Nair, 2017), and also entrained from external input. Theta oscillations can be driven by medial septal and entorhinal cortex input in vivo, as found in experiments that inactivated the external input altogether, i.e., both its non-rhythmic and its rhythmic components (Petsche et al., 1962; Brazhnik and Vinogradova, 1986; Stewart and Fox, 1990; Vinogradova, 1995; Boyce et al., 2016). While multiple mechanisms are suspected, biological and theoretical studies of hippocampal oscillations have typically focused on individual intrinsic

oscillatory mechanisms, and the individual contributions of the multiple intrinsic mechanisms to theta activity are not well understood.

The rise of optogentic tools, and detailed realistic computer models, popularized inactivation studies that aim to 'dissect' rhythm generating circuits in the hippocampus, by inactivating one component at a time and observing changes rhythmic activity. While these studies generated multiple insights, divergent findings have been reported (Table 1). For instance, despite in vitro reports of a role for the slow inhibition from oriens-lacunosum moleculare cells (OLM cells) in theta generation (Pouille and Scanziani, 2004; Gloveli et al., 2005), *in vivo* optogentic inactivation of slow and fast inhibitory cells (OLM, and BC) revealed no role in ongoing theta activity (Royer et al., 2012). However, an in vitro study showed no role for OLM cells but rather inactivation of BCs severely attenuated theta activity (Amilhon et al., 2015). Nagode and colleagues (2014), on the other hand, found no effect from inactivating BCs on CA1 theta activity, but a reduction in CA3 gamma activity. A highly detailed model of CA1 region confirmed attenuation of theta with BCs inactivation but found no contribution from OLM cells (Bezaire et al., 2016). Computational models have suggested a contribution to hippocampal theta from intrinsic membrane conductances such as the spike-frequency adaptation currents (Crook et al., 1998; Fuhrmann et al., 2002; Hu et al., 2002; Gigante et al., 2007; Augustin et al., 2013), or the h-current (Gloveli et al., 2005; Rotstein et al., 2005; Orbán et al., 2006; Zemankovics et al., 2010; Neymotin et al., 2013a; Rotstein, 2015). Spike-frequency adaptation currents remain difficult to inactivate experimentally, while a genetic knockout of the h-current (HCN1 channels) did not disrupt theta (Nolan et al., 2004; Giocomo et al., 2011).

These inconsistent results highlight the need for a deeper understanding of how the multiple mechanisms of theta interact. We used our previously developed model, that showed a multitude of interacting theta generators, to discover more specific rules that govern how the generators might substitute for others in some cases, and under what conditions. For this, we suggest that the approach should distinguish between network components that generate oscillatory resonance from those that synchronize neuronal activity (Table 2). By considering this distinction, we were able to better describe the effects of inactivating one component, in the presence of other components, and to describe several minimal circuits for robust rhythm generation. We also found that theta generators can also compete and interfere with each other, and the model predicts conditions under which inactivation of one theta generator can paradoxically enhance the power of ongoing theta activity.

Results

We used our previously published computational model of the hippocampal CA3 network that included pyramidal, OLM, and basket cells, modeled using the Izhikevich formulation (Izhikevich, 2003), with cellular characteristics matched to physiological data. The model had synapses with realistic dynamics and short-term plasticity. Physiologically recorded place cells showed firing rates that were lognormally distributed (Mizuseki and Buzsáki, 2013), so our model pyramidal cells received Poisson inputs at rates drawn from a lognormal distribution, to match physiological firing patterns. The model reproduced the physiological aspects of theta rhythmic activity in the hippocampus (Mizuseki et al., 2012; Mizuseki and Buzsáki, 2013).

In the present study, we inactivated components of the circuit individually or in combination, to discern their effect on the theta rhythm. Expectedly, these inactivation runs led to variations in firing rates. To allow for an interpretable comparison of spectral power peaks across experimental conditions, we added a constant current injection to each cell to bias their activity level. The amplitude of these current injections was adjusted across experiments to maintain a realistic average firing rate for pyramidal cells as a population, keeping it within the reported 7 Hz reported for place cell activity *in vivo* (Mizuseki and Buzsáki, 2013). The application of a bias current maintained the lognormal distribution of firing rates and we only matched the average firing rate for the population (see Methods, current injection values are given in figure legends).

In examining as many potential network components involved in rhythm generation, we found it useful to describe components as either resonance generators or synchronizing mechanisms. This distinction has parallels with current understanding of rhythmic activity generation in a single neuron where neuronal currents are categorized into resonant and amplifying currents. Another helpful distinction between 'resonance generators' and 'current generators' was previously considered in literature (Buzsáki, 2002).

OLMs and slow currents in pyramidal cells are the resonant mechanisms in CA3

To identify the resonant components of our model, we began with isolated pyramidal cells, with their slow currents (adaptation and h-current) inactivated. Pyramidal cells also received unique Poisson input and had no correlations in their external input. We then ran simulations with only one model component activated including the recurrent connections, BCs, non-rhythmic correlated external input from EC, OLM cells, and

pyramidal cells slow currents. The results showed that only OLM cells and the pyramidal cells slow currents produced a peak in theta range (Fig. 21), indicating that the two components are the resonant components in this network. Recurrent connections, and input from EC enhanced power in the delta range (2-6 Hz).

Resonant mechanisms can substitute for or compete with one another

Resonant mechanisms are defined as network components possessing dynamics consistent with rhythmic activity at certain frequencies. It follows from this definition that one resonant mechanism, at a minimum, is critical for the generation of oscillatory activity in the corresponding oscillatory band. To test this hypothesis in our model, we considered that the OLM-pyramidal cells loop and the slow currents in pyramidal cells (adaptation and h-current) are the only two active resonant mechanisms.

We ran experiments with four combinations of model components. First, the full model with all components of the CA3 network active. Second, we inactivated OLM cells (denoted "-OLM"), and third we activated OLM cells back on again and inactivated slow currents in pyramidal cells (denoted "-sPYR"), through decreasing the time constant of the adaptation current to 10 ms (from 100 ms), and removing the h-current. The last experiment was to inactivate both OLM cells and slow currents together (denoted "-Both"). Power spectra of these experiments showed that the presence of either resonant mechanisms, OLM-pyramidal cells or slow current, was sufficient to produce theta rhythmic activity, whereas inactivating both abolished all theta activity (Fig. 22B). These results are made more evident by calculating the relative power in the theta band (Fig. 22C, power in the 4-12 Hz range divided by power in the 0-50 Hz range). The firing rate

was kept within 0.5 Hz of the physiologically reported value of 7 Hz (Fig. 22D, see Methods).

In this experiment other synchronizing mechanisms of theta remained intact, such as the recurrent connections and the reciprocal inhibition to BCs. But in the absence of any resonant mechanisms rhythm generation fails. This suggests a rule of a minimum of one resonant mechanism to generate rhythms. An interesting interaction observed indicated that pyramidal cells slow currents has the potential to compete with OLM-pyramidal cell ability to generate rhythmic activity. The observation that theta power increases with the activation of pyramidal cells slow currents indicates potential interference between resonating mechanisms (Fig. 22B, C)

Cholinergic states separate resonant mechanisms functionally, and reduce interference.

We found that there is a potential for interference between the two resonant mechanisms in our model. Our previous findings indicated that different cholinergic states engage different theta mechanisms (Hummos and Nair, 2017), accordingly, we theorized that by functionally separating the two mechanisms, cholinergic modulation might reduce the interference between the two resonant mechanisms.

For this experiment, we performed the four experimental conditions (full model, OLM inactivated, slow currents inactivated, both inactivated) in three cholinergic states, low, med, and high (by setting the ACh variable to 0, 1, and 2 respectively, see Methods). Examination of relative theta power in these conditions revealed that in the extremes of cholinergic modulation (low and high), the pattern of slow currents interfering with OLM generated theta disappeared (Fig. 23).

Interactions between slow and fast inhibitory cells in theta generation

We next considered interactions between interneuronal subtypes in theta generation across cholinergic states. We examined the OLM-pyramidal cells and the BC-pyramidal cells subnetworks and ran experiments with other synchronizing mechanisms inactivated (recurrent connections were inactivated, and non-rhythmic external input was substituted with direct Poisson inputs to pyramidal cells).

In the baseline cholinergic state, both mechanisms appeared to have an additive effect on producing theta spectral peak. Inactivating either subtype of interneurons produced a moderate drop in theta power. We have previously shown that the OLM-pyramidal cells subnetwork becomes increasingly engaged in theta generation in high cholinergic states (Hummos and Nair, 2017). Here we observed that at increasing cholinergic levels, OLM-pyramidal subnetwork is becoming more engaged in generating higher levels of theta power, meanwhile, BCs effects remained the same. In high cholinergic states, interestingly, BCs began to interfere with the theta activity generated through the OLM-pyramidal subnetwork, and their inactivation increased rhythmic power in the theta range (Fig. 24). A similar analysis with a circuit including the recurrent connections and basket cells revealed little interaction between the two synchronizing mechanisms (Fig. 25). Specifically, recurrent connections appeared to have the most significant role in lower cholinergic states, while BCs had a consistent role with little change across cholinergic states.

Discussion

We used our previously developed model of the hippocampal CA3 to provide in-depth concepts to assimilate what is known about hippocampal theta generation, in a well-

grounded conceptual framework. Our study shows a complex interaction between theta generators. The effects of inactivating one theta component can be complex and dependent on other generators present and on neuromodulatory states.

Multiple interacting mechanisms

Comprehensive models have been developed recently allowing the examination of a number of these generators in one model (Neymotin et al., 2013a; Bezaire et al., 2016; Ferguson et al., 2017; Hummos and Nair, 2017). We here used our biologically realistic model, with many theta generating components, to show that theta generators act to provide a context in which inactivation of one component can be interpreted. Inactivation of on component can have no effect, reduce or even enhance rhythmic activity, depending on which other components are active. Our previous study showed that results of component inactivation can also depend strongly cholinergic neuromodulation (Hummos and Nair, 2017). Here we also extend these results to show a complex interaction between the component inactivated, other active components, in addition to the cholinergic state, to determine the effects of inactivation on the power spectrum. These insights can be used to interpret results from experiments. For example, our results are consistent with findings by Royer et al., where optogentic inactivation of either BCs or OLM did not impact theta generation significantly. As far as can be gleaned from their Methods, the animals were not exposed to any novel stimuli or environments during testing, and because cholinergic modulation is tied to novelty (Miranda et al., 2000; Giovannini et al., 2001), one can assume a low cholinergic state in this study. Their results are consistent with our inactivation results, where, in low cholinergic states, BCs and OLMs were able to compensate for one another to generate theta (Fig. 24A).

However, our model predicts that in a high cholinergic state, the same experiment could show a dramatic drop in theta with OLM inactivation, and an increase in theta power with BCs inactivation (Fig. 24C); this remains to be shown in experiments.

Resonant and synchronizing mechanisms act in concert to generate rhythms

We here provide a broad stroke conceptualization by distinguishing between resonant mechanisms and synchronizing mechanisms. We note another distinction between 'resonance generators', and 'current generators' suggested by Buzsaki (2002). BCs have recently been shown in a computational model to be significant current generators, even if not directly involved in rhythm generation (Neymotin et al., 2013b).

Parallels can be seen between this conceptual division and the requirements for generating subthreshold membrane oscillations in a single cell. Individual neurons were described to require at least one resonant current and at least one amplifying current to display significant membrane oscillations (Hutcheon et al., 2000).

Recently another comprehensive model of CA1 showed that theta power was sensitive to silencing several of the interneuronal cell types including silencing PV+ BCs, CCK+ BCs, neurogliaform, bistratified, and axo-axonic cells (Bezaire et al., 2016). Our work suggests that almost any interneuronal population, if reciprocally connected to pyramidal cells, can participate in rhythm generation, as a synchronizing component. The sensitivity of the theta rhythm in that study to the inactivation of as many types of interneurons might be related to changes in the levels of network excitability, as the study indicates theta was sensitive to level of excitation. A contribution of our study was to examine effects of inactivating interneurons while maintaining excitation levels within physiological limits. We provided pyramidal cells with a constant current injection to

offset the effects of inactivating inhibitory interneurons on level of excitation. Isolating effect of interneurons on excitation level, revealed their role in rhythm generation by acting as synchronizing mechanisms.

Most interneuronal types are capable of participating in theta rhythm generation, including OLM cells. We here emphasized the role of the OLM-pyramidal cells sub-network in providing resonance in theta frequency, however OLM cells also do participate, as do many interneurons, as a synchronizing mechanism.

Fast spiking basket cells as synchronizing component for theta generation

Inhibition by fast spiking basket cells, which tightly controls the timing of pyramidal cells firing, was proposed to play a role in theta generation (Buzsaki 2002), but later studies focused on the role of the pyramidal-basket cells sub-network as a generator of gamma power (for review, see Buzsáki and Wang, 2012). However, recent experimental and computational findings have highlighted a role for basket cells in the generation of theta activity. Inactivation of PV+ basket cells diminished theta activity in an intact hippocampus preparation (Amilhon et al., 2015), and in a detailed computational model of CA1 (Bezaire et al., 2016), and a minimal circuit with pyramidal cells and BCs was found sufficient to produce theta activity (Stark et al., 2013; Ferguson et al., 2017; Hummos and Nair, 2017).

Two more recent modeling studies, Hummos et al. (2017) and Ferguson et al. (2017), demonstrated a role for BCs in synchronizing a population of excitatory pyramidal cells to generate theta activity. In these models, pyramidal cells had spike frequency adaptation matched to experimental data, and generated theta spiking oscillations, i.e. a predominance of theta interval spikes in pyramidal cells (ISI peak ~ 90 ms), robustly at a

wide range of input levels (Hummos and Nair, 2017). Through reciprocal connections, BCs synchronize these theta spikes. Intuitively, we theorize that BCs can synchronize pyramidal cells spikes to a degree where BCs themselves begins to receive increasingly synchronized excitation from pyramidal cells, and in turn provides theta rhythmic inhibition, thus amplifying the rhythmic activity. This mechanism is relatively independent of the specific properties of BCs or their connections to pyramidal cells, but is rather a general property of pyramidal-interneuronal interactions. Considering that pyramidal cells have both subthreshold and spiking oscillations in the theta range, any common input might add sufficient synchrony in their activity to create more coherent rhythmic activity (Cobb et al., 1995). This common input can come from any type of inhibitory cells reciprocally connected to pyramidal cells, independent from the specific dynamics of the inhibitory cells or their inhibitory current, although faster inhibitory currents might control pyramidal cells spiking with higher precision.

We demonstrate this effect in a simulation with two populations of BCs and pyramidal cells and their interconnections (Fig. 20E). This subnetwork is capable of generating theta rhythmic activity that is robust to a range of input levels to pyramidal cells. This current study extends these results and show that the role of BCs in ongoing theta oscillations is dependent on the involvement of OLM cells, and on the neuromodulatory state of the circuit.

Competition and interference

This study provides examples of interference and competition amongst resonant mechanisms and amongst synchronizing mechanisms, in a biologically realistic model. The results accordingly predict conditions were inactivation of a resonant or a

synchronizing mechanism might enhance rhythmic activity, indicating that their presence interfered with other active generators. We note, however, that interference is not a destructive phenomenon in this context. Indeed, interference between oscillators has been theorized to encode the location of an animal by producing grid cells firing patterns in EC (Burgess, 2008). In addition, competition of multiple peripheral oscillators to synchronization with a central oscillator have been theorized to serve as a mechanism for attention controlled by executive function (Kazanovich et al., 2013).

Limitation and future direction

As discussed above, theta appears to be generated in the hippocampus due to the effects of external input, both its rhythmic and non-rhythmic components, and a consortium of intrinsic mechanisms. Our model falls short of representing the diversity of these theta generators and analyzing more complex interactions that involve a larger number of rhythm generators. With the current community effort to make more detailed models increasingly available, these complexities can be examined comprehensively. In addition to complexity added by more theta generators, neuromodulators (such as endocannabinoids, and serotonin) have effects of theta generation and likely have a role in determining which theta generators are actively engaged. The h-current model used matched experiments of subthreshold resonance in pyramidal cells (see Methods), however it remained mathematically difficult to separate from the adaptation current in pyramidal cells. A more detailed model of the h-current can allow examination of its role specifically and separate from spike-frequency adaptation.

Another area of future interest would be to examine how individual theta generators interact with rhythmic external input. Results can vary from competition and interference

to synergy. Combinations of intrinsic theta generators might also respond differently than individual ones. These questions in addition to cholinergic dependence can help future conceptualization of how the hippocampus responds to its rhythmic inputs.

CONCLUSIONS

- As a conceptual framework for hippocampal theta generation, we propose a useful distinction between resonant and synchronizing components.
- Many interneuronal types can be involved in theta generation through a general role for interneurons as synchronizing mechanisms. These effects can be more evident if inactivation studies would compensate for variation in excitation levels.
- We predict conditions when inactivation of a rhythm generator might paradoxically raise the power in the particular rhythmic band.

Methods

Single cell models

The model cells in CA3 were pyramidal cells and two of the most abundant interneuron types, BCs and OLM cells (Vida, 2010). The two types of interneurons are on extreme ends of many cellular attributes such as spiking patterns, inhibition dynamics and post-synaptic target compartments, and so their inclusion captures a wide range of interneuronal dynamics. The model cells in DG were granule cells, BC, and hilar perforant path-associated (HIPP) cells.

Single cell models were developed using the Izhikevich formulation (Izhikevich, 2003, 2010). The equations for a model neuron were as follows:

$$\frac{dv}{dt} = -k(v - v_t)(v - v_r) - u + I \quad (1)$$

$$\frac{du}{dt} = -a(b(v - v_r) - u) \quad (2)$$

$$if\ v > vpeak\ then\ v = c\ and\ u$$

$$= u + d \quad (3)$$

where v is the membrane potential of the cell, u is a recovery variable, v_t is the 'instantaneous threshold' beyond which the cell will fire an action potential, v_r is the resting membrane potential, I is the current injection, k is a constant used to adjust the input resistance and rheobase, *vpeak* is the threshold above which a spike is deemed to have occurred and the membrane potential is reset, and a, b, c, and d are parameters used to tune the behavior of the system to model the neuro-computational properties of the desired cell. While the NEURON environment is typically used for Hodgkin-Huxley cell models, we developed a biophysical cell model in NEURON and implemented the Izhikevich formulation by adding a current modeled by the two equations.

This formulation provides a reduced-order model that preserves many of the neuro-computational properties of more detailed biological models. We provide an overview below of how model neurons were developed to match salient features in electrophysiological recordings, with parameters used listed in table 3. For CA3 pyramidal cells, the resting membrane potential was set to -75 mV, spike threshold to -53 mV, and peak action potential voltage to 29 mV (Brown and Randall, 2009). The remaining cell model parameters were tuned to match responses to both long and brief current injections (Brown and Randall, 2009). Similarly, in developing the DG granule cells model, resting membrane potential, threshold, and peak action potential were set

using data from Staley et al., (1992) and the model was then tuned to match current injection responses (1992). Passive properties for the OLM model were estimated from Ali and Thompson (1998), and the behavior of the cells was matched to current injection responses from the same study. In particular, we matched the spike frequency adaptation, the prominent slow after-hyperpolarization potential (AHP), sag response, and rebound spikes. For the BC model, membrane properties, current injection responses, and finally current vs. firing rate relationship were matched to data reported in Buhl et al., (1996). Due to the striking similarity of OLM and HIPP cells (Katona et al., 1999), we used the same model for both cell types. EC cells are known to display theta rhythmicity (Alonso and García-Austt, 1987) . So, to examine the non-rhythmic component of EC input and its interaction with the intrinsic generators of theta in the hippocampus, we excluded oscillatory dynamics in EC cells by using generic non-adapting spiking cells (Izhikevich, 2010). More details in figure 1 of Hummos and Nair (2017).

Despite the significant heterogeneity of neurophysiological values reported across studies, our model neurons preserve the most salient cellular features in relative terms. For example, OLM interneurons fire at a slower rate than basket cells (Vida, 2010), and CA3 pyramidal cells burst more than granule cells of the dentate gyrus (Jung and McNaughton, 1993). Such relative attributes of the cells are well-preserved in our model, irrespective of the particular set of neurophysiological values chosen. Other experimental data considered in developing the single cell models can be found in Hummos et al. (Hummos et al., 2014). Initial membrane potential values were drawn from a normal distribution with a mean equal to the resting membrane potential and a standard deviation of 10 mV. The h-current in pyramidal and OLM cells is known to have a role in theta

generation (for review, see Colgin, 2013), so we added an additional slow current to our pyramidal and OLM cells tuned to match the subthreshold oscillations that the dynamics h-current produces (Zemankovics et al., 2010). The additional current equation took the form:

$$\frac{dh}{dt} = -a_h(b_h(v - v_r) - h) \tag{4}$$

where h is the h-current value, and a_h, b_h are parameters used to tune the behavior of the cell and took the values of 0.04 ms^{-1} and 10 for pyramidal cells and 0.03 ms^{-1} and 3.5 for OLM cells. A reset parameters d_h was added to the value of h each time the cell spiked and took a value of 1 for both pyramidal and OLM cells. These values were chosen to match the subthreshold resonance reported in literature for these two cell types (Zemankovics et al., 2010).

Network structure and connectivity

The rat hippocampus contains approximately 1.6 million cells (Hosseini-Sharifabad and Nyengaard, 2007). For computational efficiency and to maintain minimum model complexity, the numbers were scaled down while maintaining reported ratios (Hummos et al., 2014), as in our previous models (Li et al., 2011; Kim et al., 2013a, 2013b; Pendyam et al., 2013). The model DG region had 384 granule cells, 32 BCs, and 32 HIPP interneurons, while the model CA3 region contained 63 pyramidal cells, 8 BCs, and 8 OLM cells (Seress and Pokorny, 1981; Kosaka et al., 1987; Baude et al., 2007; Hosseini-Sharifabad and Nyengaard, 2007). The model EC region had 30 regular spiking cells.

The entorhinal cortex provides inputs to the hippocampus through the perforant pathway that projects to the entire hippocampal formation. The standard view describes a unidirectional connectivity with a direct path from EC to CA3 and an indirect path through DG (Fig. 21 in Hummos and Nair, 2017) (Naber et al., 1997; Witter, 2010). The perforant path projections follow a lamellar organization across the longitudinal axis of the hippocampus, as follows: Lateral and posterior parts of the EC are connected to the dorsal parts of CA3 and DG, while the more medial and anterior parts of EC project to the ventral parts of CA3 and DG (Witter, 2010). This lamellar organization transitions gradually from one extreme to the other on the longitudinal axis of the hippocampus, and a single neuron in EC can project to about 25% of the longitudinal length of CA3 (Witter, 2010). Projections from DG to CA3 also follow a similar longitudinal organization; however, these projections target a more limited longitudinal extent (Witter, 2010).

Model cells were distributed uniformly in 3D space separated into the three regions, EC, DG, and CA3, with dimensions that approximate the respective dimensions of the rat hippocampus (Hummos et al., 2014). Projections from EC to both pyramidal cells and BCs in DG and CA3 followed a lamellar pattern where neurons were most likely to connect to neurons in of their longitudinal neighborhood with a decreasing probability towards the periphery. This spatial connectivity was modeled using a Gaussian connection probability function that depended on the longitudinal distance between the two connected cells. The Gaussian function had a peak probability of 0.4 and a standard deviation of 3 mm for the perforant path projections to both pyramidal cells and BCs in CA3. Perforant path projections to DG had similar values (see (Hummos et al., 2014)).

Similarly, the mossy fiber projections from DG to CA3 followed the same lamellar pattern but with a more limited longitudinal extent by setting the standard deviation of the Gaussian probability function to 2 mm. In addition, to preserve the sparseness of the mossy fiber connections from DG to CA3 (Witter, 2010), each DG granule cell was limited to contacting two CA3 pyramidal neurons. Projections from DG granule cells to CA3 BCs are more diffuse and out-number projections to CA3 pyramidal neurons by a ratio of 10:1 (Acsady et al., 1998). Accordingly, DG projections to BC followed a Gaussian distribution with a peak probability of 0.2 and standard deviation of 3 mm. Recurrent CA3 connections reveal relatively more diffuse spatial organization (Ishizuka et al., 1990; Wittner et al., 2007), and were therefore distributed homogenously with a fixed probability of 0.3.

The dendritic projecting OLM cells are thought to be involved in feedback inhibitory loops (Maccaferri, 2005) and while they have a more limited axonal arborization (Buhl and Whittington, 2007) they make many more synapses compared to BCs (Sik et al., 1995). In contrast, BCs have a more diffuse axonal arborization with the highest connection probability to pyramidal cells in their immediate neighborhood and a decreasing connection probability towards the periphery of their axonal arbors (Sik et al., 1995). Similarly, BCs project to neighboring OLM cells (Bartos et al., 2010). As before, we used a Gaussian function to approximate these spatial probabilities. We also assumed that BC projections to both pyramidal cells and to OLM cells shared the same spatial domain (Remove statement or add to figures or explain why it did not contribute much?). In the reverse direction, OLMs receive reciprocal connections from the same pyramidal cells they projected to, in line with their function as local feedback cells (Maccaferri,

2005). On the other hand, granule cells in DG and pyramidal cells in CA3 projected homogenously to BCs with a fixed probability of 0.15, consistent with the lack of specific topography reported at these projections (Wittner et al., 2006).

The network was constructed by generating connections randomly between cells while maintaining the connection probabilities and spatial patterns of connectivity described above. The spatial connectivity patterns and parameter values are summarized in table 4 (also see (Hummos et al., 2014)).

Synaptic currents

Synaptic currents were modeled using the kinetic model described in Destexhe et al. (1998). AMPA, NMDA, $GABA_A$, and $GABA_B$ currents were modeled and their dynamics such as rise and decay time constants and delays were matched to available literature (Hummos et al., 2014). In particular, CA3 pyramidal cell AMPA currents were fastest for the mossy fiber inputs from DG and slowest for perforant path inputs from EC, while recurrent CA3 inputs from other pyramidal cells had intermediate values (Hoskison et al., 2004; Tóth, 2010), as summarized in table 4. Additionally, inhibitory currents from OLM had slower dynamics compared to those from BC (Table 4) (Geiger et al., 1997; Bartos et al., 2010). Synaptic weights were assigned in accordance with literature where available (for details, see Hummos and Nair, 2017).

Activity-dependent plasticity

For this study, long-term plasticity was excluded from the synapses. Model synapses, however, exhibited short-term synaptic plasticity that used the formulation proposed by Varela et al. (1997). We modeled the pronounced short-term facilitation at mossy fibers (Toth et al., 2000) and the frequency-dependent synaptic depression

reported at the recurrent CA3 connections (see Fig. 3 in Hummos and Nair, 2017; Hoskison et al., 2004). We extrapolated from data in CA1 where projections from pyramidal cells display short-term facilitation at synapses contacting OLM cells (Ali and Thomson, 1998), and short-term depression at those contacting BC cells (Ali et al., 1998). In the other direction, inhibitory currents from OLM cells to pyramidal cells show no short-term facilitation or depression (Maccaferri, 2005), while inhibitory currents from BCs to pyramidal cells show depression (Hefft and Jonas, 2005). Additional details and equations related to the implementation of short-term synaptic plasticity can be found in Hummos et al (Hummos et al., 2014).

Acetylcholine effects

The hippocampus receives widespread volume transmission of cholinergic inputs from the septum-diagonal band complex (Woolf, 1991). To implement the effects of ACh on model neurons and synapses, we used a variable 'ACh' to represent the ACh state. The variable ACh had values of 0 (low), 1 (baseline), and 2 (high).

Cholinergic stimulation has differential effects on synaptic transmission of different pathways in the hippocampus (Barry et al., 2012). Synaptic transmission through the perforant pathway projections to CA3 is suppressed by 50%, compared to a suppression by 85% at the recurrent connections in CA3 (Hasselmo et al., 1995; Kremin and Hasselmo, 2007). On the other hand, the mossy fibers transmission is enhanced by 49% (Vogt and Regehr, 2001). To model ACh effects on synapses, AMPA synaptic currents were scaled by the value of ACh. A parameter bACh determined the direction and magnitude of ACh effects on a particular synapse. Values of bACh for different

synapses were set according to experimental results as summarized in table 4 (also see Hummos et al. (Hummos et al., 2014)).

In addition to the synapse specific effects, cholinergic stimulation enhanced cellular excitability and depolarized the resting membrane potential of principal cells, eliminated AHP, decreased spike frequency adaptation and induced rhythmic burst activity (Madison and Nicoll, 1984; Misgeld et al., 1989). Furthermore, effects on interneurons were subtype-dependent (McQuiston and Madison, 1999a, 1999b). Muscarinic stimulation of OLM interneurons depolarized the resting membrane potential, and lowered both spike frequency adaptation and AHP (Lawrence et al., 2006). In contrast, PV-BCs respond to muscarinic receptor activation with a limited depolarization in resting membrane potential (Cea-del Rio et al., 2010; Cobb and Lawrence, 2010). Effects of ACh on neurons were modeled by linearly scaling the neuronal model parameters by the ACh state as detailed in Hummos et al. (see fig. S4 in (Hummos et al., 2014)). Considering the slow dynamics of ACh effects (onset time constant approximated between 1 and 2 s; Hasselmo and Fehlau, 2001), ACh state was set to a given value at the beginning of each experiment and had no dynamics.

Inputs and data analysis

For the full model and sub-circuit cases considered, either EC cells or CA3 pyramidal cells (identified in the figures) received external input as trains of Poisson-distributed spikes, triggering an influx of AMPA and NMDA currents into the cell. We studied two model cases: one with external input arriving at EC, and the other with input arriving directly at CA3 pyramidal cells. The two types of inputs differed in the weight of the associated input synapses, and the base rate of the Poisson spike trains arriving at

these synapses. Input to EC arrived at synapses with a 100% spike transmission rate to ensure that EC firing pattern was dictated by the Poisson input, whereas input to CA3 pyramidal cells had a lower weight value with parameters matching the EC to CA3 synapses (Table 4).

To determine the base rates of the Poisson processes generating these input trains, we considered place cells in CA3. Place cells respond to certain areas in the environment and their firing rates approximate a lognormal distribution (Mizuseki and Buzsáki, 2013) with an average of ~7 Hz (Mizuseki et al., 2012). In our model case where external inputs arrived at EC, each EC cell received a unique train of Poisson input spikes at a base rate of 15 Hz, which produced firing rates in CA3 pyramidal cells with a lognormal distribution and an average of 7 Hz. In the model case where external inputs arrived directly to CA3 pyramidal cells, the input rates to different cells had to be drawn from a lognormal distribution (average: 50 Hz, standard deviation: 40 Hz), to produce firing rates with a lognormal distribution that matched experimental data. Following titration of the Poisson input, a constant current injection was added to the voltage equation and the current amplitude was adjusted to maintain the physiologically reported average firing rate and lognormal distribution of firing rates. The current values used for each experimental condition are listed in the corresponding figure legend.

For spectral analysis, we summed the spikes of all cells of each type in a region (e.g., CA3 pyramidal cells) in 0.1 ms bins and computed the fast-Fourier transform of the resulting vector, using the Matlab function psautospk.m (Koch and Segev, 1998), with a moving window of size 1024 ms, and overlap of 512 ms. Spike data was used in spectral calculations as a proxy for LFP as used in network models (e.g., Brunel and Wang, 2003;

Hoseini and Wessel, 2016; Samarth et al., 2016), with the assumption that these spikes are received by a downstream local neuron and translated into membrane currents that generate an LFP signal.

The model was developed using the NEURON software package (Carnevale and Hines, 2009) and run on a PC with an Intel i7-core processor with an integration time-step of 0.1 ms (key results were also verified with a time-step of 0.01 ms). The code is available as part of our previous publication via the public database ModelDB at Yale University. The recorded spike times were then analyzed using MATLAB (Mathworks, Inc.). All simulations ran for 5 seconds.

Tables

Table 3: Summary of inactivation studies

Study	Type	Component inactivated	Evidence for	Evidence against	Cholinergic effects	Region
(Amilhon et al., 2015)	*In vitro* intact preparation	Optogentic BCs and OLM inactivation	Role of BCs	OLM cells	Not considered	CA1
(Wulff et al., 2009)	In vivo	$GABA_A$ receptors on BCs	Role for inhibition of BCs in theta	Role for inhibition of BCs in gamma	Not considered	CA1
(Gillies et al., 2002)	In vitro	AMPA transmission	Inhibitory currents	Recurrent connections (But not in CA3)	Inhibition based theta was atropine-resistant	CA1, CA3
(Nolan et al., 2004)	In vivo	HCN1		h-current	Not considered	CA1
(Leung and Shen, 2004)	In vivo	AMPA transmission	None	Recurrent connections	Not considered.	CA1, theta dropped by 47%
(Nagode et al., 2014)	in vitro		Role of CCK cells	Role of BCs	Rhythms cholinergically induced	CA1
(Royer et al., 2012)	In vivo	OLM cells and BCs	None	OLM cells or BCs cells	Not considered, but animals not	CA3

					exposed to novelty.	
(Buzsáki et al., 1983)	In vivo	EC input	Rhythmic EC input		Inactivating EC input made the remaining theta atropine-sensitive	Theta dropped but more markedly became atropine sensitive.

Table 4: Classification of theta rhythm mechanisms as resonant, synchronizing, or both.

Mechanism	**Resonant**	**Synchronizing**	
E-E		X	
E-Slow I	X	X	
E-Fast I		X	
Adaptation	X		
h-current	X		
Non-rhythmic external input		X	
Rhythmic external input	X	X	

Figures

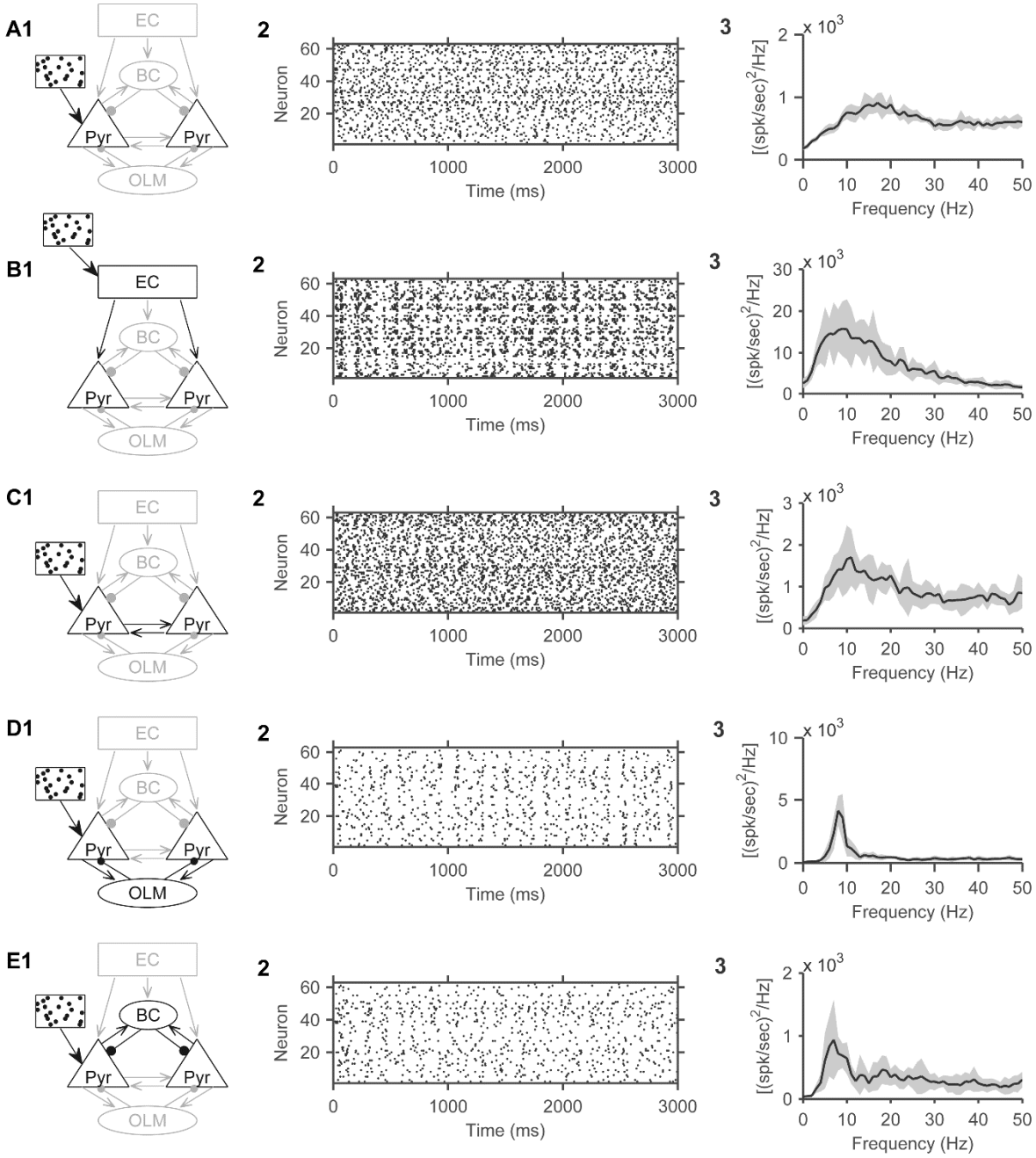

Figure 20: Multiple generators of theta oscillations in the hippocampal CA3 network.

Adapted from Hummos and Nair (2017).

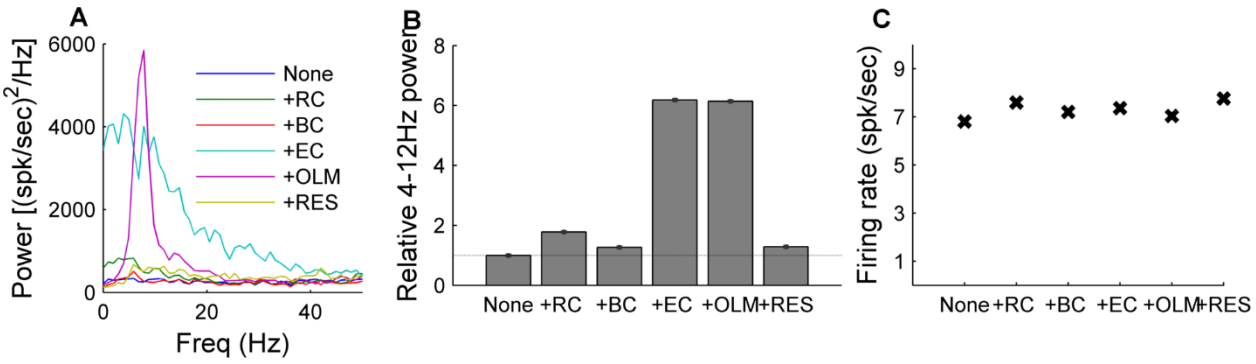

Figure 21: Pyramidal cells slow currents and OLM-pyramidal cells loop are the two resonant mechanisms.

A) The power spectra of 6 simulations. The 'None' experiment had no theta generating components with isolated pyramidal cells with no slow currents, and direct unique Poisson input with no correlations. The following experiments activated one theta component at a time and examined the power spectrum. The recurrent connections were activated in '+RC' and produced a small bump in the 2-4 Hz range. BCs activated in '+BC' produced no spectral peaks. Routing input through the EC added correlations in the external input and shift the power to low frequencies but did not produce theta peaks. Adding OLM cells '+OLM' produced a robust theta peak. Activating the slow currents in pyramidal cells also produced a small but significant peak in theta frequencies '+RES'. B) relative theta calculations. '+RC', '+EC' increased relative theta due to a less specific increase in slow frequency power. C) firing rates were kept within physiological range using the following current injections. None: 7 mA, +RC 8 mA, +BC 5 mA, +EC 10 mA, +OLM 1 mA, +RES 1 mA.

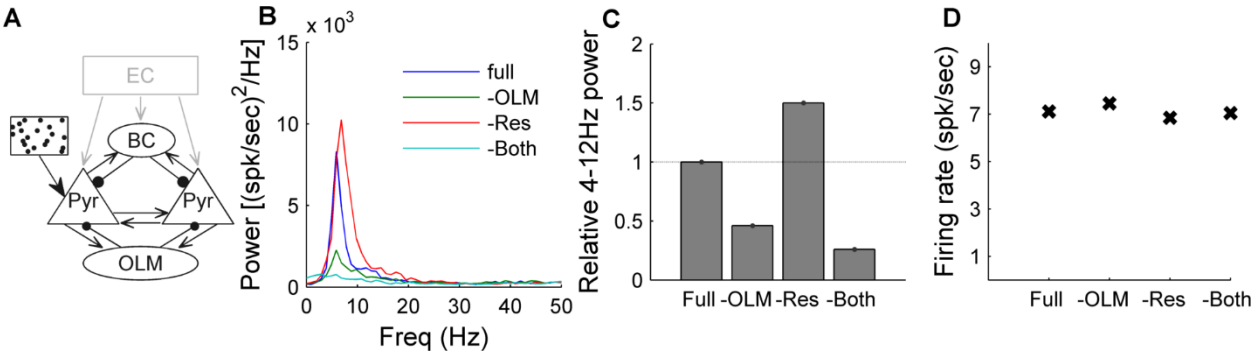

Figure 22: Resonant mechanisms can substitute for and compete with each other.

A) Schematic of this experiment with EC inactivated and input directly arriving at CA3 pyramidal cells. Both OLM cells, BCs, and the recurrent excitatory connections were active.

B) The power spectra of four experiments as follows: "full" simulated with both OLM cells and adaptation in pyramidal cells intact, "-OLM" was run with OLM cells inactivated, "-sPYR" had OLM cells intact but adaptation and h-current were removed from pyramidal cells, and finally "-both" had both pyramidal cells slow currents and OLM cells inactivated. The power spectra indicate that theta activity persisted with at least one resonant mechanism intact, but also interestingly showed that pyramidal cells adaptation as a resonant component may have interfered with the OLM-pyramidal cells resonator.

C) Relative power in the theta band (4-12 Hz) divided by total power (0-50 Hz) and normalized to the value of the "full" model run.

D) Shows the results of our procedure using constant current injections to cells to maintain a population average firing rate consistent with physiological data, to

compensate for the variation in firing rates resulting from inactivating various network components. Current injections to pyramidal cells in the different experiments were as follows. Full: 3.5 mA, -OLM: 4.2 mA, -sPYR: 3 mA, -Both: 8.2 mA.

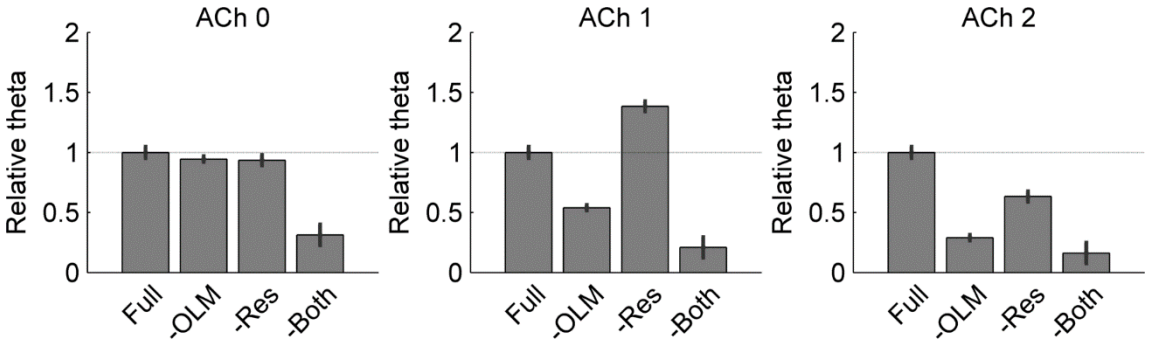

Figure 23: Functional separation at the extremes of cholinergic modulation minimizes interference between resonating mechanisms.

Current injections to compensate for variation in firing rates: ACh 0: Full: -2 mA, -OLM: -2 mA, -sPYR: 0 mA, -Both: 2 mA. ACh 1: Full: 3.5 mA, -OLM: 4.2 mA, -sPYR: 3 mA, -Both: 8.2 mA. ACh 2: Full: 4 mA, -OLM: 5 mA, -sPYR: 3.5 mA, -Both: 8.5 mA.

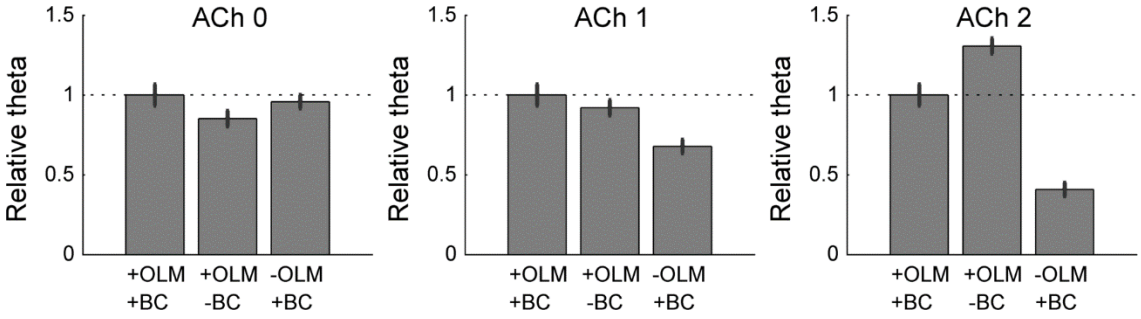

Figure 24: Synchronizing mechanisms can substitute for or interfere with one another

Recurrent connections and EC were inactivated, leaving the two synchronizing mechanisms in the model, OLM cells and BC cells. We tested three conditions, first with both OLM and BC cells active (+OLM +BC), and then with BCs inactivated (+OLM -BC) and finally, with OLM cells inactivated (-OLM +BC). Running the three conditions under three different cholinergic states revealed different interaction modes between the two synchronizing mechanisms. In low ACh, they were equally effective at generating theta, and only one mechanism appeared necessary. With increasing cholinergic levels, BCs contribution to theta diminished, and in high cholinergic states they interfered with OLM generated theta. Current injections to compensate for variation in firing rates: ACh 0: +both: -7 mA, -BC: -6.5 mA, -OLM: -7.5 mA. ACh 1: +both: -3 mA, -BC: 1 mA, -OLM: -6.1 mA. ACh 2: +both: -1 mA, -BC: 2.8 mA, -OLM: 1.4 mA.

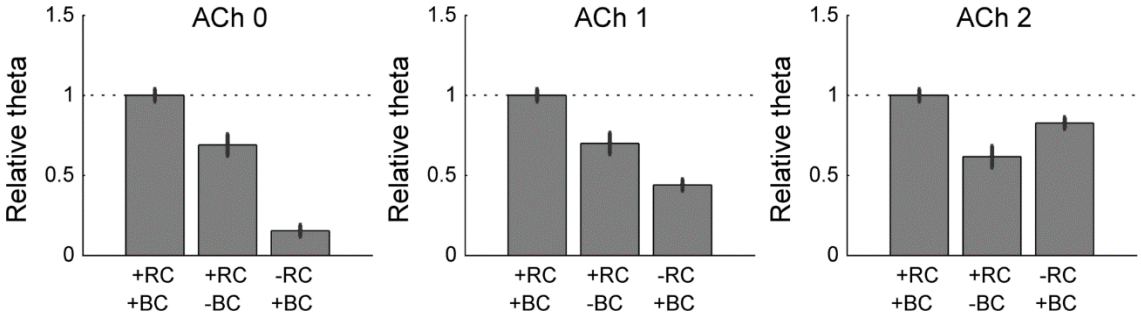

Figure 25: Recurrent connections and BCs cooperatively synchronize theta oscillations.

OLM cells and EC were inactivated, leaving the two synchronizing mechanisms in the model, recurrent connections and BC cells. We tested three conditions, first with both recurrent connections and BC cells active (+RC +BC), and then with BCs inactivated (+RC -BC) and finally, with recurrent connections inactivated (-RC +BC). Running the

three conditions under three different cholinergic states revealed a stable engagement of BCs in theta generation while recurrent connection had a stronger engagement in lower cholinergic states. Current injections to compensate for variation in firing rates: ACh 0: +both: 5 mA, -BC: 6 mA, -RC: 1 mA. ACh 1: +both: 2 mA, -BC: 5 mA, -RC: -2 mA. ACh 2: +both: -2 mA, -BC: 5 mA, -RC: -2 mA

CHAPTER 5 − SUMMARY, CONTRIBUTIONS, AND FUTURE WORK

Summary

Biological neuronal systems are complex and highly nonlinear dynamical systems that have defied our understanding for decades. While we remain relatively far from understanding the underpinnings of traumatic memories in the brain, we are making significant progress in understanding the functional aspects of the hippocampus, the brain area intimately associated with the storage of personal episodic memories.

This dissertation builds on existing knowledge about hippocampal function, and extends this knowledge, through computational modelling, to investigate how the hippocampus maintains its level of excitation and how it generates oscillatory activity. Both of these functional aspects are important for understanding the role the hippocampus plays in the storage of traumatic memories. We hope to see our work contribute to the efforts of the neuroscientific community to understand the nature of traumatic memories and eventually discover practical ways to influence them. We summarize the contributions of our three research projects below.

Chapter 2

In Chapter 2, we expanded upon previous work that identified memory encoding and memory retrieval circuits in the mammalian hippocampus regulated by the neuromodulator Acetylcholine. We first began by reproducing the known behavior of the hippocampus as it attempts to separate new learned information from previously stored memories and to

give the new information a separate representational neuronal activity pattern. We then examined mechanisms that maintain the stability of the network against runaway excitation. This runaway activity produces seizures in animals. Our results indicated that different mechanisms are responsible for preventing seizure activity during memory encoding and memory retrieval. Our work was the first to categorize seizures according to the functional state of the brain. We hope that these new distinctions will allow more targeted treatment options for these different kinds of seizures.

Future work:

- A future goal is to collaborate with experimental biologists to test our hypothesis in rodents. Literature review showed that a certain chemical lesion causes rats to develop seizures when placed in a novel maze that they needed to learn. We make specific predictions about the type of deficit at a neuronal level based on our model findings, and we seek to test these predictions.

Chapter 3

In Chapter 3, we used the hippocampal model to examine the origins and mechanisms of the theta rhythmic activity observed in the hippocampus during spatial navigation and active exploration. Our results revealed a wealth of mechanisms capable of generating theta. We again found parallel differences between the memory encoding and the memory retrieval circuits. The memory encoding circuits depended primarily on the activity of inhibitory interneurons to generate theta activity, while the memory retrieval depended on the recurrent connections between pyramidal cells. The differences between the two

circuits extends their conceptualization as two distinct circuits despite their sharing of many of the physical components.

Future work:

- By combining our work in Chapter 2 and Chapter 3, theta rhythmic activity that can be easily recorded, might possibly help discern the computational state of the hippocampal circuit, whether it is in memory encoding or memory retrieval mode. That knowledge can be extended to predict what pathology might gender seizure episodes and what specific treatments would be recommended based on the current functional state of the hippocampus.

Chapter 4

In Chapter 4, the model describes a more elaborate conceptualization of theta generation mechanisms. Their complex interactions and ability to substitute for one another and even interfere with each other are examined.

Future work:

- The framework presented in this paper, if examined in full detail, can generate a model that can predict the results of inactivation experiments. Such biological experiments usually inactivate circuit components and observe changes in the power spectrum. Currently these results are divergent, and our conceptual framework promises to unify these conflicted results in one theoretical framework.

REFERENCES:

Abbott, L. F, and S. B Nelson. 2000. "Synaptic Plasticity: Taming the Beast." *Nature Neuroscience* 3:1178–1183.

Acker, Corey D., Nancy Kopell, and John A. White. 2003. "Synchronization of Strongly Coupled Excitatory Neurons: Relating Network Behavior to Biophysics." *Journal of Computational Neuroscience* 15 (1):71–90.

Acsady, Laszlo, Anita Kamondi, Attila Sik, Tamas Freund, and Gyorgy Buzsaki. 1998. "GABAergic Cells Are the Major Postsynaptic Targets of Mossy Fibers in the Rat Hippocampus." *J. Neurosci.* 18 (9):3386–3403.

Ali, A B, J Deuchars, H Pawelzik, and A M Thomson. 1998. "CA1 Pyramidal to Basket and Bistratified Cell EPSPs: Dual Intracellular Recordings in Rat Hippocampal Slices." *The Journal of Physiology* 507 (February):201–17.

Ali, A B, and A M Thomson. 1998. "Facilitating Pyramid to Horizontal Oriens-Alveus Interneurone Inputs: Dual Intracellular Recordings in Slices of Rat Hippocampus." *The Journal of Physiology* 507 (February):185–99.

Alonso, A., and E. García-Austt. 1987. "Neuronal Sources of Theta Rhythm in the Entorhinal Cortex of the Rat. II. Phase Relations between Unit Discharges and Theta Field Potentials." *Experimental Brain Research* 67 (3):502–9.

Asghar, Aziz U. R., Paul F. Cilia La Corte, Fiona E. N. LeBeau, Mutaz Al Dawoud, Siobhan C. Reilly, Eberhard H. Buhl, Miles A. Whittington, and Anne E. King. 2005. "Oscillatory Activity within Rat Substantia Gelatinosa in Vitro: A Role for Chemical and Electrical Neurotransmission." *The Journal of Physiology* 562 (1):183–98. https://doi.org/10.1113/jphysiol.2004.076398.

Augustin, Moritz, Josef Ladenbauer, and Klaus Obermayer. 2013. "How Adaptation Shapes Spike Rate Oscillations in Recurrent Neuronal Networks." *Frontiers in Computational Neuroscience* 7:9. https://doi.org/10.3389/fncom.2013.00009.

Bakker, Arnold, C. Brock Kirwan, Michael Miller, and Craig E. L. Stark. 2008. "Pattern Separation in the Human Hippocampal CA3 and Dentate Gyrus." *Science* 319 (5870):1640–42. https://doi.org/10.1126/science.1152882.

Barkai, E, R E Bergman, G Horwitz, and M E Hasselmo. 1994. "Modulation of Associative Memory Function in a Biophysical Simulation of Rat Piriform Cortex." *Journal of Neurophysiology* 72 (2):659–77.

Barry, Caswell, James G. Heys, and Michael E. Hasselmo. 2012. "Possible Role of Acetylcholine in Regulating Spatial Novelty Effects on Theta Rhythm and Grid Cells." *Frontiers in Neural Circuits* 6 (5). https://doi.org/10.3389/fncir.2012.00005.

Bartos, Marlene, Jonas-Frederic Sauer, Imre Vida, and Ákos Kulik. 2010. “Fast and Slow GABAergic Transmission in Hippocampal Circuits.” In *Hippocampal Microcircuits*, edited by Vassilis Cutsuridis, Bruce Graham, Stuart Cobb, and Imre Vida, 5:129–61. New York: Springer.

Baude, Agnès, Catherine Bleasdale, Yannis Dalezios, Peter Somogyi, and Thomas Klausberger. 2007. “Immunoreactivity for the GABAA Receptor A1 Subunit, Somatostatin and Connexin36 Distinguishes Axoaxonic, Basket, and Bistratified Interneurons of the Rat Hippocampus.” *Cerebral Cortex* 17 (9):2094–2107. https://doi.org/10.1093/cercor/bhl117.

Berger, T., H.-R. Lüscher, and M. Giugliano. 2006. “Transient Rhythmic Network Activity in the Somatosensory Cortex Evoked by Distributed Input in Vitro.” *Neuroscience* 140 (4):1401–13.

Beyeler, Anna, Aude Retailleau, Colin Molter, Amine Mehidi, Janos Szabadics, and Xavier Leinekugel. 2013. “Recruitment of Perisomatic Inhibition during Spontaneous Hippocampal Activity in Vitro.” *PloS One* 8 (6):e66509. https://doi.org/10.1371/journal.pone.0066509.

Bezaire, Marianne J., and Ivan Soltesz. 2013. “Quantitative Assessment of CA1 Local Circuits: Knowledge Base for Interneuron-Pyramidal Cell Connectivity.” *Hippocampus* 23 (9):751–85. https://doi.org/10.1002/hipo.22141.

Bianchi, R., and R. K. Wong. 1994. “Carbachol-Induced Synchronized Rhythmic Bursts in CA3 Neurons of Guinea Pig Hippocampus in Vitro.” *Journal of Neurophysiology* 72 (1):131–38.

Bliss, T V, and T Lomo. 1973. “Long-Lasting Potentiation of Synaptic Transmission in the Dentate Area of the Anaesthetized Rabbit Following Stimulation of the Perforant Path.” *The Journal of Physiology* 232 (2):331–56.

Bliss, Tim, Graham Collingridge, and Richard Morris. 2007. “Synaptic Plasticity in the Hippocampus.” In *Andersen P, Morris RGM, Amaral DG, Bliss TVP, O’Keefe J, Editors. The Hippocampus Book.*, 133–242. New York: Oxford University Press.

Bower, Mark R., and Paul S. Buckmaster. 2008. “Changes in Granule Cell Firing Rates Precede Locally Recorded Spontaneous Seizures by Minutes in an Animal Model of Temporal Lobe Epilepsy.” *Journal of Neurophysiology* 99 (5):2431–42. https://doi.org/10.1152/jn.01369.2007.

Boyce, Richard, Stephen D. Glasgow, Sylvain Williams, and Antoine Adamantidis. 2016. “Causal Evidence for the Role of REM Sleep Theta Rhythm in Contextual Memory Consolidation.” *Science* 352 (6287):812–16. https://doi.org/10.1126/science.aad5252.

Brazhnik, E S, and O S Vinogradova. 1986. “Control of the Neuronal Rhythmic Bursts in the Septal Pacemaker of Theta-Rhythm: Effects of Anaesthetic and Anticholinergic Drugs.” *Brain Research* 380 (1):94–106.

Brown, Jon T., and Andrew D. Randall. 2009. “Activity-Dependent Depression of the Spike after-Depolarization Generates Long-Lasting Intrinsic Plasticity in Hippocampal CA3 Pyramidal Neurons.” *The Journal of Physiology* 587 (6):1265–81. https://doi.org/10.1113/jphysiol.2008.167007.

Brunel, Nicolas, and Xiao-Jing Wang. 2003. “What Determines the Frequency of Fast Network Oscillations with Irregular Neural Discharges? I. Synaptic Dynamics and Excitation-Inhibition Balance.” *Journal of Neurophysiology* 90 (1):415–30. https://doi.org/10.1152/jn.01095.2002.

Buhl, E H, T Szilágyi, K Halasy, and P Somogyi. 1996. “Physiological Properties of Anatomically Identified Basket and Bistratified Cells in the CA1 Area of the Rat Hippocampus in Vitro.” *Hippocampus* 6 (3):294–305. https://doi.org/10.1002/(SICI)1098-1063(1996)6:3<294::AID-HIPO7>3.0.CO;2-N.

Buhl, Eberhard, and Miles Whittington. 2007. “Local Circuits.” In *The Hippocampus Book*, edited by Per Andersen, Richard Morris, David Amaral, Tim Bliss, and John O’Keefe, 297–320. New York: Oxford University Press.

Buzsáki, György. 2002. “Theta Oscillations in the Hippocampus.” *Neuron* 33 (3):325–40. https://doi.org/10.1016/S0896-6273(02)00586-X.

Buzsáki, György, and Xiao-Jing Wang. 2012. “Mechanisms of Gamma Oscillations.” *Annual Review of Neuroscience* 35:203–25. https://doi.org/10.1146/annurev-neuro-062111-150444.

Carnevale, Nicholas T., and Michael L. Hines. 2009. *The NEURON Book.* UK: Cambridge University Press.

Cea-del Rio, Christian A, J Josh Lawrence, Ludovic Tricoire, Ferenc Erdelyi, Gabor Szabo, and Chris J McBain. 2010. “M3 Muscarinic Acetylcholine Receptor Expression Confers Differential Cholinergic Modulation to Neurochemically Distinct Hippocampal Basket Cell Subtypes.” *The Journal of Neuroscience* 30 (17):6011–24. https://doi.org/10.1523/JNEUROSCI.5040-09.2010.

Cobb, S. R., E. H. Buhl, K. Halasy, O. Paulsen, and P. Somogyi. 1995. “Synchronization of Neuronal Activity in Hippocampus by Individual GABAergic Interneurons.” *Nature* 378 (6552):75–78. https://doi.org/10.1038/378075a0.

Cobb, Stuart, and J. Josh Lawrence. 2010. “Neuromodulation of Hippocampal Cells and Circuits.” In *Hippocampal Microcircuits.*, edited by Vassilis Cutsuridis, Bruce Graham, Stuart Cobb, and Imre Vida, 187–246. 5. New York: Springer.

Colgin, Laura Lee. 2013. “Mechanisms and Functions of Theta Rhythms.” *Annual Review of Neuroscience* 36 (July):295–312. https://doi.org/10.1146/annurev-neuro-062012-170330.

Cossart, Rosa, Christophe Bernard, and Yehezkel Ben-Ari. 2005. “Multiple Facets of GABAergic Neurons and Synapses: Multiple Fates of GABA Signalling in Epilepsies.” *Trends in Neurosciences* 28 (2):108–15. https://doi.org/10.1016/j.tins.2004.11.011.

Crook, S. M., G. B. Ermentrout, and J. M. Bower. 1998. “Spike Frequency Adaptation Affects the Synchronization Properties of Networks of Cortical Oscillations.” *Neural Computation* 10 (4):837–54.

Cutsuridis, Vassilis, Stuart Cobb, and Bruce P Graham. 2010. “Encoding and Retrieval in a Model of the Hippocampal CA1 Microcircuit.” *Hippocampus* 20 (3):423–46. https://doi.org/10.1002/hipo.20661.

Denham, Michael J., and Roman M. Borisyuk. 2000. “A Model of Theta Rhythm Production in the Septal-Hippocampal System and Its Modulation by Ascending Brain Stem Pathways.” *Hippocampus* 10 (6):698–716. https://doi.org/10.1002/1098-1063(2000)10:6<698::AID-HIPO1008>3.0.CO;2-Z.

Deshmukh, Sachin S., D. Yoganarasimha, Horatiu Voicu, and James J. Knierim. 2010. “Theta Modulation in the Medial and the Lateral Entorhinal Cortices.” *Journal of Neurophysiology* 104 (2):994–1006. https://doi.org/10.1152/jn.01141.2009.

Destexhe, A., Z. F. Mainen, and T. J. Sejnowski. 1998. “Kinetic Models of Synaptic Transmission.” *Methods in Neuronal Modeling* 2:1–26.

Dickson, C. T., J. Magistretti, M. H. Shalinsky, E. Fransén, M. E. Hasselmo, and A. Alonso. 2000. “Properties and Role of I(h) in the Pacing of Subthreshold Oscillations in Entorhinal Cortex Layer II Neurons.” *Journal of Neurophysiology* 83 (5):2562–79.

Do, Viet H., Carlo O. Martinez, Joe L. Martinez, and Brian E. Derrick. 2002a. “Long-Term Potentiation in Direct Perforant Path Projections to the Hippocampal CA3 Region in Vivo.” *Journal of Neurophysiology* 87 (2):669–78.

———. 2002b. “Long-Term Potentiation in Direct Perforant Path Projections to the Hippocampal CA3 Region In Vivo.” *J Neurophysiol* 87 (2):669–78.

Doucette, T A, P B Bernard, H Husum, M A Perry, C L Ryan, and R A Tasker. 2004. “Low Doses of Domoic Acid during Postnatal Development Produce Permanent Changes in Rat Behaviour and Hippocampal Morphology.” *Neurotoxicity Research* 6 (7–8):555–63.

Economo, Michael N., and John A. White. 2012. “Membrane Properties and the Balance between Excitation and Inhibition Control Gamma-Frequency Oscillations

Arising from Feedback Inhibition." *PLoS Computational Biology* 8 (1):e1002354. https://doi.org/10.1371/journal.pcbi.1002354.

Eichenbaum, Howard. 2000. "A Cortical–hippocampal System for Declarative Memory." *Nature Reviews Neuroscience* 1 (1):41–50. https://doi.org/10.1038/35036213.

Eisen, J S, and E Marder. 1984. "A Mechanism for Production of Phase Shifts in a Pattern Generator." *Journal of Neurophysiology* 51 (6):1375–93.

Freeman, Walter J. 1968. "Analog Simulation of Prepyriform Cortex in the Cat." *Mathematical Biosciences* 2 (1):181–90. https://doi.org/10.1016/0025-5564(68)90017-5.

Fuhrmann, Galit, Henry Markram, and Misha Tsodyks. 2002. "Spike Frequency Adaptation and Neocortical Rhythms." *Journal of Neurophysiology* 88 (2):761–70.

Gaiarsa, Jean-Luc, Olivier Caillard, and Yehezkel Ben-Ari. 2002. "Long-Term Plasticity at GABAergic and Glycinergic Synapses: Mechanisms and Functional Significance." *Trends in Neurosciences* 25 (11):564–70. https://doi.org/10.1016/S0166-2236(02)02269-5.

Galán, Roberto F., Nicolas Fourcaud-Trocmé, G. Bard Ermentrout, and Nathaniel N. Urban. 2006. "Correlation-Induced Synchronization of Oscillations in Olfactory Bulb Neurons." *Journal of Neuroscience* 26 (14):3646–55. https://doi.org/10.1523/JNEUROSCI.4605-05.2006.

Geiger, Jörg R.P, Joachim Lübke, Arnd Roth, Michael Frotscher, and Peter Jonas. 1997. "Submillisecond AMPA Receptor-Mediated Signaling at a Principal Neuron–interneuron Synapse." *Neuron* 18 (6):1009–23. https://doi.org/10.1016/S0896-6273(00)80339-6.

Gerstner, Wulfram, Werner Kistler, Richard Naud, and Liam Paninski. 2014. *Neuronal Dynamics: From Single Neurons to Networks and Models of Cognition*. 1 edition. Cambridge, United Kingdom: Cambridge University Press.

Getting, P A. 1989. "Emerging Principles Governing the Operation of Neural Networks." *Annual Review of Neuroscience* 12:185–204. https://doi.org/10.1146/annurev.ne.12.030189.001153.

Gigante, Guido, Paolo Del Giudice, and Maurizio Mattia. 2007. "Frequency-Dependent Response Properties of Adapting Spiking Neurons." *Mathematical Biosciences*, BIOCOMP2005 Special Issue, 207 (2):336–51. https://doi.org/10.1016/j.mbs.2006.11.010.

Gillies, M J, R D Traub, F E N LeBeau, C H Davies, T Gloveli, E H Buhl, and M A Whittington. 2002. "A Model of Atropine-Resistant Theta Oscillations in Rat Hippocampal Area CA1." *The Journal of Physiology* 543 (Pt 3):779–93.

Giocomo, Lisa M., Syed A. Hussaini, Fan Zheng, Eric R. Kandel, May-Britt Moser, and Edvard I. Moser. 2011. "Grid Cells Use HCN1 Channels for Spatial Scaling." *Cell* 147 (5):1159–70. https://doi.org/10.1016/j.cell.2011.08.051.

Gloveli, Tengis, Tamar Dugladze, Horacio G Rotstein, Roger D Traub, Hannah Monyer, Uwe Heinemann, Miles A Whittington, and Nancy J Kopell. 2005. "Orthogonal Arrangement of Rhythm-Generating Microcircuits in the Hippocampus." *Proceedings of the National Academy of Sciences of the USA* 102 (37):13295–300. https://doi.org/10.1073/pnas.0506259102.

Goutagny, Romain, Jesse Jackson, and Sylvain Williams. 2009. "Self-Generated Theta Oscillations in the Hippocampus." *Nature Neuroscience* 12 (12):1491–93. https://doi.org/10.1038/nn.2440.

Gulyás, A I, R Miles, A Sík, K Tóth, N Tamamaki, and T F Freund. 1993. "Hippocampal Pyramidal Cells Excite Inhibitory Neurons through a Single Release Site." *Nature* 366 (6456):683–87. https://doi.org/10.1038/366683a0.

Hansel, D., G. Mato, and C. Meunier. 1995. "Synchrony in Excitatory Neural Networks." *Neural Computation* 7 (2):307–37.

Hasselmo, M E, E Schnell, and E Barkai. 1995. "Dynamics of Learning and Recall at Excitatory Recurrent Synapses and Cholinergic Modulation in Rat Hippocampal Region CA3." *The Journal of Neuroscience* 15 (7 Pt 2):5249–62.

Hasselmo, M E, and B P Wyble. 1997. "Free Recall and Recognition in a Network Model of the Hippocampus: Simulating Effects of Scopolamine on Human Memory Function." *Behavioural Brain Research* 89 (1–2):1–34.

Hasselmo, ME, E Schnell, and E Barkai. 1995. "Dynamics of Learning and Recall at Excitatory Recurrent Synapses and Cholinergic Modulation in Rat Hippocampal Region CA3." *J. Neurosci.* 15 (7):5249–62.

Hasselmo, Michael E, Clara Bodelón, and Bradley P Wyble. 2002. "A Proposed Function for Hippocampal Theta Rhythm: Separate Phases of Encoding and Retrieval Enhance Reversal of Prior Learning." *Neural Computation* 14 (4):793–817. https://doi.org/10.1162/089976602317318965.

Hasselmo, Michael E., and Brian P. Fehlau. 2001. "Differences in Time Course of ACh and GABA Modulation of Excitatory Synaptic Potentials in Slices of Rat Hippocampus." *J Neurophysiol* 86 (4):1792–1802.

Hasselmo, Michael E., Bradley P. Wyble, and Gene V. Wallenstein. 1996. "Encoding and Retrieval of Episodic Memories: Role of Cholinergic and GABAergic Modulation in the Hippocampus." *Hippocampus* 6 (6):693–708. https://doi.org/10.1002/(SICI)1098-1063(1996)6:6<693::AID-HIPO12>3.0.CO;2-W.

Hefft, Stefan, and Peter Jonas. 2005. “Asynchronous GABA Release Generates Long-Lasting Inhibition at a Hippocampal Interneuron–principal Neuron Synapse.” *Nature Neuroscience* 8 (10):1319–28. https://doi.org/10.1038/nn1542.

Henze, Darrell A., Lucia Wittner, and Gyorgy Buzsaki. 2002. “Single Granule Cells Reliably Discharge Targets in the Hippocampal CA3 Network in Vivo.” *Nat Neurosci* 5 (8):790–95. https://doi.org/10.1038/nn887.

Hoseini, Mahmood S., and Ralf Wessel. 2016. “Coherent and Intermittent Ensemble Oscillations Emerge from Networks of Irregular Spiking Neurons.” *Journal of Neurophysiology* 115 (1):457–69. https://doi.org/10.1152/jn.00578.2015.

Hoskison, M.M, J.A Connor, and C.W Shuttleworth. 2004. “GABAB-Receptor Modulation of Short-Term Synaptic Depression at an Excitatory Input to Murine Hippocampal CA3 Pyramidal Neurons.” *Neuroscience Letters* 365 (1):48–53. https://doi.org/10.1016/j.neulet.2004.04.050.

Hosseini-Sharifabad, Mohammad, and Jens Randel Nyengaard. 2007. “Design-Based Estimation of Neuronal Number and Individual Neuronal Volume in the Rat Hippocampus.” *Journal of Neuroscience Methods* 162 (1–2):206–14. https://doi.org/10.1016/j.jneumeth.2007.01.009.

Hu, Hua, Koen Vervaeke, and Johan F Storm. 2002. “Two Forms of Electrical Resonance at Theta Frequencies, Generated by M-Current, h-Current and Persistent Na+ Current in Rat Hippocampal Pyramidal Cells.” *The Journal of Physiology* 545 (Pt 3):783–805.

Hummos, Ali, Charles C. Franklin, and Satish S. Nair. 2014. “Intrinsic Mechanisms Stabilize Encoding and Retrieval Circuits Differentially in a Hippocampal Network Model.” *Hippocampus* 24 (12):1430–48. https://doi.org/10.1002/hipo.22324.

Hunsaker, Michael R, and Raymond P Kesner. 2013. “The Operation of Pattern Separation and Pattern Completion Processes Associated with Different Attributes or Domains of Memory.” *Neuroscience and Biobehavioral Reviews* 37 (1):36–58. https://doi.org/10.1016/j.neubiorev.2012.09.014.

Ikonen, Sami, Robert McMahan, Michela Gallagher, Howard Eichenbaum, and Heikki Tanila. 2002. “Cholinergic System Regulation of Spatial Representation by the Hippocampus.” *Hippocampus* 12 (3):386–97. https://doi.org/10.1002/hipo.1109.

Ishizuka, Norio, Janet Weber, and David G. Amaral. 1990. “Organization of Intrahippocampal Projections Originating from CA3 Pyramidal Cells in the Rat.” *The Journal of Comparative Neurology* 295 (4):580–623. https://doi.org/10.1002/cne.902950407.

Izhikevich, E M. 2003. “Simple Model of Spiking Neurons.” *IEEE Transactions on Neural Networks* 14 (6):1569–72. https://doi.org/10.1109/TNN.2003.820440.

Izhikevich, Eugene M. 2010. *Dynamical Systems in Neuroscience: The Geometry of Excitability and Bursting.* London: MIT Press.

Jung, M W, and B L McNaughton. 1993. "Spatial Selectivity of Unit Activity in the Hippocampal Granular Layer." *Hippocampus* 3 (2):165–82. https://doi.org/10.1002/hipo.450030209.

Katona, I, L Acsády, and T.F Freund. 1999. "Postsynaptic Targets of Somatostatin-Immunoreactive Interneurons in the Rat Hippocampus." *Neuroscience* 88 (1):37–55. https://doi.org/10.1016/S0306-4522(98)00302-9.

Kim, Dongbeom, Denis Paré, and Satish S Nair. 2013a. "Mechanisms Contributing to the Induction and Storage of Pavlovian Fear Memories in the Lateral Amygdala." *Learning & Memory* 20 (8):421–30. https://doi.org/10.1101/lm.030262.113.

———. 2013b. "Assignment of Model Amygdala Neurons to the Fear Memory Trace Depends on Competitive Synaptic Interactions." *The Journal of Neuroscience* 33 (36):14354–58. https://doi.org/10.1523/JNEUROSCI.2430-13.2013.

Kispersky, Tilman J, Fernando R Fernandez, Michael N Economo, and John A White. 2012. "Spike Resonance Properties in Hippocampal O-LM Cells Are Dependent on Refractory Dynamics." *The Journal of Neuroscience* 32 (11):3637–51. https://doi.org/10.1523/JNEUROSCI.1361-11.2012.

Kitajima, Tatsuo, and Ken-Ichi Hara. 1997. "An Integrated Model for Activity-Dependent Synaptic Modifications." *Neural Networks* 10 (3):413–21. https://doi.org/10.1016/S0893-6080(96)00095-0.

Klausberger, Thomas, Peter J Magill, László F Márton, J David B Roberts, Philip M Cobden, György Buzsáki, and Peter Somogyi. 2003. "Brain-State- and Cell-Type-Specific Firing of Hippocampal Interneurons in Vivo." *Nature* 421 (6925):844–48. https://doi.org/10.1038/nature01374.

Klink, R., and A. Alonso. 1993. "Ionic Mechanisms for the Subthreshold Oscillations and Differential Electroresponsiveness of Medial Entorhinal Cortex Layer II Neurons." *Journal of Neurophysiology* 70 (1):144–57.

Koch, Christof, and Idan Segev. 1998. *Methods in Neuronal Modeling: From Ions to Networks.* London: MIT Press.

Kocsis, Bernat, Anatol Bragin, and György Buzsáki. 1999. "Interdependence of Multiple Theta Generators in the Hippocampus: A Partial Coherence Analysis." *The Journal of Neuroscience* 19 (14):6200–6212.

Kopell, N., C. Börgers, D. Pervouchine, P. Malerba, and A. Tort. 2010. "Gamma and Theta Rhythms in Biophysical Models of Hippocampal Circuits." In *Hippocampal Microcircuits*, edited by Vassilis Cutsuridis, Bruce Graham, Stuart Cobb, and Imre Vida, 423–57. 5. New York: Springer.

Kosaka, T, H Katsumaru, K Hama, J Y Wu, and C W Heizmann. 1987. “GABAergic Neurons Containing the Ca2+-Binding Protein Parvalbumin in the Rat Hippocampus and Dentate Gyrus.” *Brain Research* 419 (1–2):119–30.

Kremin, T., and M.E. Hasselmo. 2007. “Cholinergic Suppression of Glutamatergic Synaptic Transmission in Hippocampal Region CA3 Exhibits Laminar Selectivity: Implication for Hippocampal Network Dynamics.” *Neuroscience* 149 (4):760–67. https://doi.org/doi: DOI: 10.1016/j.neuroscience.2007.07.007.

Kunec, Steve, Michael E. Hasselmo, and Nancy Kopell. 2005. “Encoding and Retrieval in the CA3 Region of the Hippocampus: A Model of Theta-Phase Separation.” *J Neurophysiol* 94 (1):70–82. https://doi.org/10.1152/jn.00731.2004.

Lawrence, J Josh, and Chris J McBain. 2003. “Interneuron Diversity Series: Containing the Detonation--Feedforward Inhibition in the CA3 Hippocampus.” *Trends in Neurosciences* 26 (11):631–40.

Lawrence, J Josh, Jeffrey M Statland, Zachary M Grinspan, and Chris J McBain. 2006. “Cell Type-Specific Dependence of Muscarinic Signalling in Mouse Hippocampal Stratum Oriens Interneurones.” *The Journal of Physiology* 570 (Pt 3):595–610. https://doi.org/10.1113/jphysiol.2005.100875.

Lee, Inah, and Raymond P. Kesner. 2004. “Encoding versus Retrieval of Spatial Memory: Double Dissociation between the Dentate Gyrus and the Perforant Path Inputs into CA3 in the Dorsal Hippocampus.” *Hippocampus* 14 (1):66–76. https://doi.org/10.1002/hipo.10167.

Lee, Sang-Gui, Alexander Neiman, and Seunghwan Kim. 1998. “Coherence Resonance in a Hodgkin-Huxley Neuron.” *Physical Review E* 57 (3):3292.

Leung, L. Stan, and Bixia Shen. 2004. “Glutamatergic Synaptic Transmission Participates in Generating the Hippocampal EEG.” *Hippocampus* 14 (4):510–25. https://doi.org/10.1002/hipo.10199.

Leutgeb, Jill K., Stefan Leutgeb, May-Britt Moser, and Edvard I. Moser. 2007. “Pattern Separation in the Dentate Gyrus and CA3 of the Hippocampus.” *Science* 315 (5814):961–66. https://doi.org/10.1126/science.1135801.

Li, Guoshi, Taiju Amano, Denis Pare, and Satish S. Nair. 2011. “Impact of Infralimbic Inputs on Intercalated Amygdala Neurons: A Biophysical Modeling Study.” *Learning & Memory* 18 (4):226–40. https://doi.org/10.1101/lm.1938011.

Li, Guoshi, Satish S. Nair, and Gregory J. Quirk. 2009. “A Biologically Realistic Network Model of Acquisition and Extinction of Conditioned Fear Associations in Lateral Amygdala Neurons.” *J Neurophysiol* 101 (3):1629–46. https://doi.org/10.1152/jn.90765.2008.

Liljenstrom, H., and M. E. Hasselmo. 1995. “Cholinergic Modulation of Cortical Oscillatory Dynamics.” *Journal of Neurophysiology* 74 (1):288–97.

Maccaferri, Gianmaria. 2005. “Stratum Oriens Horizontal Interneurone Diversity and Hippocampal Network Dynamics.” *The Journal of Physiology* 562 (1):73–80. https://doi.org/10.1113/jphysiol.2004.077081.

Madison, D V, and R A Nicoll. 1984. “Control of the Repetitive Discharge of Rat CA 1 Pyramidal Neurones in Vitro.” *The Journal of Physiology* 354 (1):319–31. https://doi.org/10.1113/jphysiol.1984.sp015378.

Maffei, Arianna. 2011. “The Many Forms and Functions of Long Term Plasticity at GABAergic Synapses.” *Neural Plasticity* 2011:1–9. https://doi.org/10.1155/2011/254724.

Marder, Eve. 2012. “Neuromodulation of Neuronal Circuits: Back to the Future.” *Neuron* 76 (1):1–11. https://doi.org/10.1016/j.neuron.2012.09.010.

Marr, D. 1971. “Simple Memory: A Theory for Archicortex.” *Philosophical Transactions of the Royal Society of London. B, Biological Sciences* 262 (841):23–81. https://doi.org/10.1098/rstb.1971.0078.

Martin, Chris B, Seyed M Mirsattari, Jens C Pruessner, Sandra Pietrantonio, Jorge G Burneo, Brent Hayman-Abello, and Stefan Köhler. 2012. “Déjà vu in Unilateral Temporal-Lobe Epilepsy Is Associated with Selective Familiarity Impairments on Experimental Tasks of Recognition Memory.” *Neuropsychologia* 50 (13):2981–91. https://doi.org/10.1016/j.neuropsychologia.2012.07.030.

McClelland, J L, and N H Goddard. 1996. “Considerations Arising from a Complementary Learning Systems Perspective on Hippocampus and Neocortex.” *Hippocampus* 6 (6):654–65. https://doi.org/10.1002/(SICI)1098-1063(1996)6:6<654::AID-HIPO8>3.0.CO;2-G.

McMahon, David B.T., and German Barrionuevo. 2002. “Short- and Long-Term Plasticity of the Perforant Path Synapse in Hippocampal Area CA3.” *J Neurophysiol* 88 (1):528–33.

McQuiston, A. Rory, and Daniel V. Madison. 1999a. “Nicotinic Receptor Activation Excites Distinct Subtypes of Interneurons in the Rat Hippocampus.” *The Journal of Neuroscience* 19 (8):2887–96.

———. 1999b. “Muscarinic Receptor Activity Has Multiple Effects on the Resting Membrane Potentials of CA1 Hippocampal Interneurons.” *J. Neurosci.* 19 (14):5693–5702.

Meeter, M., J.M.J. Murre, and L.M. Talamini. 2004. “Mode Shifting between Storage and Recall Based on Novelty Detection in Oscillating Hippocampal Circuits.” *Hippocampus* 14 (6):722–41. https://doi.org/10.1002/hipo.10214.

Miles, R. 1990. “Synaptic Excitation of Inhibitory Cells by Single CA3 Hippocampal Pyramidal Cells of the Guinea-Pig in Vitro.” *The Journal of Physiology* 428 (September):61–77.

Miles, R, and R K Wong. 1983. “Single Neurones Can Initiate Synchronized Population Discharge in the Hippocampus.” *Nature* 306 (5941):371–73.

———. 1986. “Excitatory Synaptic Interactions between CA3 Neurones in the Guinea-Pig Hippocampus.” *The Journal of Physiology* 373 (April):397–418.

———. 1987. “Inhibitory Control of Local Excitatory Circuits in the Guinea-Pig Hippocampus.” *The Journal of Physiology* 388 (July):611–29.

Misgeld, U, W Müller, and H R Polder. 1989. “Potentiation and Suppression by Eserine of Muscarinic Synaptic Transmission in the Guinea-Pig Hippocampal Slice.” *The Journal of Physiology* 409 (1):191–206.

Mizuseki, Kenji, and György Buzsáki. 2013. “Preconfigured, Skewed Distribution of Firing Rates in the Hippocampus and Entorhinal Cortex.” *Cell Reports* 4 (5):1010–21. https://doi.org/10.1016/j.celrep.2013.07.039.

Mizuseki, Kenji, Sebastien Royer, Kamran Diba, and György Buzsáki. 2012. “Activity Dynamics and Behavioral Correlates of CA3 and CA1 Hippocampal Pyramidal Neurons.” *Hippocampus* 22 (8):1659–80. https://doi.org/10.1002/hipo.22002.

Morin, F., C. Beaulieu, and J. C. Lacaille. 1996. “Membrane Properties and Synaptic Currents Evoked in CA1 Interneuron Subtypes in Rat Hippocampal Slices.” *Journal of Neurophysiology* 76 (1):1–16.

Naber, P A, M Caballero-Bleda, B Jorritsma-Byham, and M P Witter. 1997. “Parallel Input to the Hippocampal Memory System through Peri- and Postrhinal Cortices.” *Neuroreport* 8 (11):2617–21.

Nakao, Hiroya, Ken-suke Arai, Ken Nagai, Yasuhiro Tsubo, and Yoshiki Kuramoto. 2005. “Synchrony of Limit-Cycle Oscillators Induced by Random External Impulses.” *Physical Review E* 72 (2):026220. https://doi.org/10.1103/PhysRevE.72.026220.

Netoff, Theoden I., Corey D. Acker, Jonathan C. Bettencourt, and John A. White. 2005. “Beyond Two-Cell Networks: Experimental Measurement of Neuronal Responses to Multiple Synaptic Inputs.” *Journal of Computational Neuroscience* 18 (3):287–95. https://doi.org/10.1007/s10827-005-0336-9.

Neunuebel, Joshua P, and James J Knierim. 2014. “CA3 Retrieves Coherent Representations from Degraded Input: Direct Evidence for CA3 Pattern Completion and Dentate Gyrus Pattern Separation.” *Neuron* 81 (2):416–27. https://doi.org/10.1016/j.neuron.2013.11.017.

Newman, Ehren L, Kishan Gupta, Jason R Climer, Caitlin K Monaghan, and Michael E Hasselmo. 2012. "Cholinergic Modulation of Cognitive Processing: Insights Drawn from Computational Models." *Frontiers in Behavioral Neuroscience* 6:24. https://doi.org/10.3389/fnbeh.2012.00024.

Neymotin, Samuel A., Markus M. Hilscher, Thiago C. Moulin, Yosef Skolnick, Maciej T. Lazarewicz, and William W. Lytton. 2013. "Ih Tunes Theta/Gamma Oscillations and Cross-Frequency Coupling in an in Silico CA3 Model." *PloS One* 8 (10):e76285. https://doi.org/10.1371/journal.pone.0076285.

Nolan, Christopher R, Gordon Wyeth, Michael Milford, and Janet Wiles. 2010. "The Race to Learn: Spike Timing and STDP Can Coordinate Learning and Recall in CA3." *Hippocampus* 21 (6):647–60. https://doi.org/10.1002/hipo.20777.

Nolan, Matthew F., Gaël Malleret, Josh T. Dudman, Derek L. Buhl, Bina Santoro, Emma Gibbs, Svetlana Vronskaya, et al. 2004. "A Behavioral Role for Dendritic Integration: HCN1 Channels Constrain Spatial Memory and Plasticity at Inputs to Distal Dendrites of CA1 Pyramidal Neurons." *Cell* 119 (5):719–32. https://doi.org/10.1016/j.cell.2004.11.020.

O'Keefe, J, and J Dostrovsky. 1971. "The Hippocampus as a Spatial Map. Preliminary Evidence from Unit Activity in the Freely-Moving Rat." *Brain Research* 34 (1):171–75.

Orbán, Gergo, Tamás Kiss, and Péter Erdi. 2006. "Intrinsic and Synaptic Mechanisms Determining the Timing of Neuron Population Activity during Hippocampal Theta Oscillation." *Journal of Neurophysiology* 96 (6):2889–2904. https://doi.org/10.1152/jn.01233.2005.

O'Reilly, Randall C., and James L. McClelland. 1994. "Hippocampal Conjunctive Encoding, Storage, and Recall: Avoiding a Trade-Off." *Hippocampus* 4 (6):661–82. https://doi.org/10.1002/hipo.450040605.

Pendyam, Sandeep, Christian Bravo-Rivera, Anthony Burgos-Robles, Francisco Sotres-Bayon, Gregory J. Quirk, and Satish S. Nair. 2013. "Fear Signaling in the Prelimbic-Amygdala Circuit: A Computational Modeling and Recording Study." *Journal of Neurophysiology* 110 (4):844–61. https://doi.org/10.1152/jn.00961.2012.

Perry, Melissa A, Catherine L Ryan, and R Andrew Tasker. 2009. "Effects of Low Dose Neonatal Domoic Acid Administration on Behavioural and Physiological Response to Mild Stress in Adult Rats." *Physiology & Behavior* 98 (1–2):53–59. https://doi.org/10.1016/j.physbeh.2009.04.009.

Petsche, H., C. Stumpf, and G. Gogolak. 1962. "The significance of the rabbit's septum as a relay station between the midbrain and the hippocampus. I. The control of hippocampus arousal activity by the septum cells." *Electroencephalography and Clinical Neurophysiology* 14 (April):202–11.

Pikovsky, Arkady S., and Jürgen Kurths. 1997. “Coherence Resonance in a Noise-Driven Excitable System.” *Physical Review Letters* 78 (5):775.

Pitler, T A, and B E Alger. 1992. “Cholinergic Excitation of GABAergic Interneurons in the Rat Hippocampal Slice.” *The Journal of Physiology* 450 (May):127–42.

Podlogar, M., and Dirk Dietrich. 2006. “Firing Pattern of Rat Hippocampal Neurons: A Perforated Patch Clamp Study.” *Brain Research* 1085 (1):95–101. https://doi.org/10.1016/j.brainres.2006.02.050.

Poldrack, Russell A, and Paul Rodriguez. 2003. “Sequence Learning: What’s the Hippocampus to Do?” *Neuron* 37 (6):891–93. https://doi.org/10.1016/S0896-6273(03)00159-4.

Rogers, Jason L., and Raymond P. Kesner. 2003. “Cholinergic Modulation of the Hippocampus during Encoding and Retrieval.” *Neurobiology of Learning and Memory* 80 (3):332–42. https://doi.org/doi: DOI: 10.1016/S1074-7427(03)00063-7.

———. 2004. “Cholinergic Modulation of the Hippocampus during Encoding and Retrieval of Tone/Shock-Induced Fear Conditioning.” *Learning & Memory* 11 (1):102–7. https://doi.org/10.1101/lm.64604.

Rolls, Edmund T., and Raymond P. Kesner. 2006. “A Computational Theory of Hippocampal Function, and Empirical Tests of the Theory.” *Progress in Neurobiology* 79 (1):1–48. https://doi.org/10.1016/j.pneurobio.2006.04.005.

Rotstein, Horacio G. 2015. “Subthreshold Amplitude and Phase Resonance in Models of Quadratic Type: Nonlinear Effects Generated by the Interplay of Resonant and Amplifying Currents.” *Journal of Computational Neuroscience* 38 (2):325–54. https://doi.org/10.1007/s10827-014-0544-2.

Rotstein, Horacio G., Tim Oppermann, John A. White, and Nancy Kopell. 2006. “The Dynamic Structure Underlying Subthreshold Oscillatory Activity and the Onset of Spikes in a Model of Medial Entorhinal Cortex Stellate Cells.” *Journal of Computational Neuroscience* 21 (3):271–92. https://doi.org/10.1007/s10827-006-8096-8.

Rotstein, Horacio G, Dmitri D Pervouchine, Corey D Acker, Martin J Gillies, John A White, Eberhardt H Buhl, Miles A Whittington, and Nancy Kopell. 2005. “Slow and Fast Inhibition and an H-Current Interact to Create a Theta Rhythm in a Model of CA1 Interneuron Network.” *Journal of Neurophysiology* 94 (2):1509–18. https://doi.org/10.1152/jn.00957.2004.

Royer, Sébastien, Boris V Zemelman, Attila Losonczy, Jinhyun Kim, Frances Chance, Jeffrey C Magee, and György Buzsáki. 2012. “Control of Timing, Rate and Bursts of Hippocampal Place Cells by Dendritic and Somatic Inhibition.” *Nature Neuroscience* 15 (5):769–75. https://doi.org/10.1038/nn.3077.

Samarth, Pranit, John M. Ball, Gunes Unal, Denis Paré, and Satish S. Nair. 2016. "Mechanisms of Memory Storage in a Model Perirhinal Network." *Brain Structure and Function*, March. https://doi.org/10.1007/s00429-016-1210-4.

Seress, L, and J Pokorny. 1981. "Structure of the Granular Layer of the Rat Dentate Gyrus. A Light Microscopic and Golgi Study." *Journal of Anatomy* 133 (Pt 2):181–95.

Shouval, Harel Z., Mark F. Bear, and Leon N Cooper. 2002. "A Unified Model of NMDA Receptor-Dependent Bidirectional Synaptic Plasticity." *Proceedings of the National Academy of Sciences of the USA* 99 (16):10831–36. https://doi.org/10.1073/pnas.152343099.

Sik, A., M. Penttonen, A. Ylinen, and G. Buzsaki. 1995. "Hippocampal CA1 Interneurons: An in Vivo Intracellular Labeling Study." *The Journal of Neuroscience* 15 (10):6651–65.

Springer, Michael, and Johan Paulsson. 2006. "Biological Physics: Harmonies from Noise." *Nature* 439 (7072):27–28. https://doi.org/10.1038/439027a.

Staley, K J, T S Otis, and I Mody. 1992. "Membrane Properties of Dentate Gyrus Granule Cells: Comparison of Sharp Microelectrode and Whole-Cell Recordings." *Journal of Neurophysiology* 67 (5):1346–58.

Stark, Eran, Ronny Eichler, Lisa Roux, Shigeyoshi Fujisawa, Horacio G. Rotstein, and György Buzsáki. 2013. "Inhibition-Induced Theta Resonance in Cortical Circuits." *Neuron* 80 (5):1263–76. https://doi.org/10.1016/j.neuron.2013.09.033.

Stewart, M., and S. E. Fox. 1990. "Do Septal Neurons Pace the Hippocampal Theta Rhythm?" *Trends in Neurosciences* 13 (5):163–68.

Sussillo, David, Taro Toyoizumi, and Wolfgang Maass. 2007. "Self-Tuning of Neural Circuits through Short-Term Synaptic Plasticity." *Journal of Neurophysiology* 97 (6):4079–95. https://doi.org/10.1152/jn.01357.2006.

Szabadics, János, and Ivan Soltesz. 2009. "Functional Specificity of Mossy Fiber Innervation of GABAergic Cells in the Hippocampus." *The Journal of Neuroscience* 29 (13):4239–51. https://doi.org/10.1523/JNEUROSCI.5390-08.2009.

Szabo, Gergely G, Noemi Holderith, Attila I Gulyas, Tamas F Freund, and Norbert Hajos. 2010. "Distinct Synaptic Properties of Perisomatic Inhibitory Cell Types and Their Different Modulation by Cholinergic Receptor Activation in the CA3 Region of the Mouse Hippocampus." *The European Journal of Neuroscience* 31 (12):2234–46. https://doi.org/10.1111/j.1460-9568.2010.07292.x.

Teramae, Jun-nosuke, and Dan Tanaka. 2004. “Robustness of the Noise-Induced Phase Synchronization in a General Class of Limit Cycle Oscillators.” *Physical Review Letters* 93 (20):204103. https://doi.org/10.1103/PhysRevLett.93.204103.

Tóth, Katalin. 2010. “Glutamatergic Neurotransmission in the Hippocampus.” In *Hippocampal Microcircuits.*, edited by Vassilis Cutsuridis, Bruce Graham, Stuart Cobb, and Imre Vida, 99–128. New York: Springer.

Toth, Katalin, Gregory Suares, J. Josh Lawrence, Emily Philips-Tansey, and Chris J. McBain. 2000. “Differential Mechanisms of Transmission at Three Types of Mossy Fiber Synapse.” *The Journal of Neuroscience* 20 (22):8279–89.

Traub, R. D., R. Miles, and G. Buzsáki. 1992. “Computer Simulation of Carbachol-Driven Rhythmic Population Oscillations in the CA3 Region of the in Vitro Rat Hippocampus.” *The Journal of Physiology* 451:653–72.

Traub, R D, R Miles, and R K Wong. 1987. “Models of Synchronized Hippocampal Bursts in the Presence of Inhibition. I. Single Population Events.” *Journal of Neurophysiology* 58 (4):739–51.

———. 1989. “Model of the Origin of Rhythmic Population Oscillations in the Hippocampal Slice.” *Science (New York, N.Y.)* 243 (4896):1319–25.

Treves, A, and E T Rolls. 1992. “Computational Constraints Suggest the Need for Two Distinct Input Systems to the Hippocampal CA3 Network.” *Hippocampus* 2 (2):189–99. https://doi.org/10.1002/hipo.450020209.

Vanderwolf, C. H. 1969. “Hippocampal Electrical Activity and Voluntary Movement in the Rat.” *Electroencephalography and Clinical Neurophysiology* 26 (4):407–18.

Varela, Juan A., Kamal Sen, Jay Gibson, Joshua Fost, L. F. Abbott, and Sacha B. Nelson. 1997. “A Quantitative Description of Short-Term Plasticity at Excitatory Synapses in Layer 2/3 of Rat Primary Visual Cortex.” *The Journal of Neuroscience* 17 (20):7926–40.

Vida, Imre. 2010. “Morphology of Hippocampal Neurons.” In *Hippocampal Microcircuits.*, edited by Vassilis Cutsuridis, Bruce Graham, Stuart Cobb, and Imre Vida, 27–67. 5. New York: Springer.

Vinogradova, O. S. 1995. “Expression, Control, and Probable Functional Significance of the Neuronal Theta-Rhythm.” *Progress in Neurobiology* 45 (6):523–83. https://doi.org/10.1016/0301-0082(94)00051-I.

Vogt, Kaspar E., and Wade G. Regehr. 2001. “Cholinergic Modulation of Excitatory Synaptic Transmission in the CA3 Area of the Hippocampus.” *J. Neurosci.* 21 (1):75–83.

Wang, X. J, and G. Buzsaki. 1996. “Gamma Oscillation by Synaptic Inhibition in a Hippocampal Interneuronal Network Model.” *Journal of Neuroscience* 16 (20):6402.

Wang, Xiao-Jing. 2010. “Neurophysiological and Computational Principles of Cortical Rhythms in Cognition.” *Physiological Reviews* 90 (3):1195–1268. https://doi.org/10.1152/physrev.00035.2008.

White, J. A., T. Budde, and A. R. Kay. 1995. “A Bifurcation Analysis of Neuronal Subthreshold Oscillations.” *Biophysical Journal* 69 (4):1203–17. https://doi.org/10.1016/S0006-3495(95)79995-7.

Witter, Menno P. 2010. “Connectivity of the Hippocampus.” In *Hippocampal Microcircuits.*, edited by Vassilis Cutsuridis, Bruce Graham, Stuart Cobb, and Imre Vida, 5–26. 5. New York: Springer.

Wittner, Lucia, Darrell A Henze, László Záborszky, and György Buzsáki. 2006. “Hippocampal CA3 Pyramidal Cells Selectively Innervate Aspiny Interneurons.” *The European Journal of Neuroscience* 24 (5):1286–98. https://doi.org/10.1111/j.1460-9568.2006.04992.x.

Wittner, Lucia, Darrell Henze, László Záborszky, and György Buzsáki. 2007. “Three-Dimensional Reconstruction of the Axon Arbor of a CA3 Pyramidal Cell Recorded and Filled in Vivo.” *Brain Structure and Function* 212 (1):75–83. https://doi.org/10.1007/s00429-007-0148-y.

Woodin, Melanie A, Karunesh Ganguly, and Mu-ming Poo. 2003. “Coincident Pre- and Postsynaptic Activity Modifies GABAergic Synapses by Postsynaptic Changes in Cl- Transporter Activity.” *Neuron* 39 (5):807–20.

Woolf, N J. 1991. “Cholinergic Systems in Mammalian Brain and Spinal Cord.” *Progress in Neurobiology* 37 (6):475–524.

Wyeth, Megan S, Nianhui Zhang, Istvan Mody, and Carolyn R Houser. 2010. “Selective Reduction of Cholecystokinin-Positive Basket Cell Innervation in a Model of Temporal Lobe Epilepsy.” *The Journal of Neuroscience* 30 (26):8993–9006. https://doi.org/10.1523/JNEUROSCI.1183-10.2010.

Yeckel, M F, and T W Berger. 1990. “Feedforward Excitation of the Hippocampus by Afferents from the Entorhinal Cortex: Redefinition of the Role of the Trisynaptic Pathway.” *Proceedings of the National Academy of Sciences of the United States of America* 87 (15):5832–36.

Zemankovics, Rita, Szabolcs Káli, Ole Paulsen, Tamás F. Freund, and Norbert Hájos. 2010. “Differences in Subthreshold Resonance of Hippocampal Pyramidal Cells and Interneurons: The Role of h-Current and Passive Membrane Characteristics: Impedance Characteristics and h-Current of Hippocampal Neurons.” *The Journal of Physiology* 588 (12):2109–32. https://doi.org/10.1113/jphysiol.2009.185975.

VITA

Ali Hummos graduated the university of Jordan medical school in Amman, Jordan. He started training as a psychiatry resident physician in 2006 at the University of Missouri-Columbia Department of Psychiatry. During his training in psychiatry, he started a research project that eventually matured into a PhD candidacy with Dr. Satish Nair at the Informatics Institute.

The work focused on building a biologically realistic spiking neuron model of the rat hippocampus under the mentorship of Dr. Satish Nair in the Electrical and Computer Engineering department.

Work in computational neuroscience shaped an understanding of mammalian brain circuits, and continued work with psychiatric patients provided an end goal for studying brain science. However, the gap remained too wide to bridge in this decade. Promising fields, such as computational psychiatry, are beginning to take shape, and offer a path towards integrating basic neuroscience and clinical psychiatry.

Publications (Peer-reviewed):

Hummos A, Nair S., (2017) An integrative model of the intrinsic hippocampal theta rhythm. PLoS ONE 12:e0182648.

Hummos A, Franklin CC, Nair SS (2014) Intrinsic mechanisms stabilize encoding and retrieval circuits differentially in a hippocampal network model. Hippocampus 24:1430–1448.

Hummos A, Nair S. (In preparation) Interplay of resonant and synchronizing generators in a hippocampal theta model

Franklin CC, Hummos AH, Guntu V, Nair SS (in revision), Cellular and synaptic correlates of pattern formation in a hippocampal model

Ball JM, Hummos AM, Nair SS (2012) Role of sensory input distribution and intrinsic connectivity in lateral amygdala during auditory fear conditioning: A computational study. Neuroscience 224:249–267

Grants Funded:

Primary-Investigator, SBIR grant Phase I, 2010 “Medication IconoGraphs: Visualization of Complex Medication Regimens” Grant number: 1R43MH081446-01A2 revised; Sponsor: National Institute of Mental Health. Company: IconicHealth LLC. Duties: Direct software development to meet clinical standards and HIPAA requirements, user interface usability and testing.

Primary-Investigator, SBIR USDA phase I grant, 2010 “Transformational Approach to Managing Major Depressive Disorder Among College Students from Rural Communities”. Award No.: 2010-33610-20853

Presentations:

Hummos, A., (2016). “Hippocampal theta, an integrative model”, Computational and systems neuroscience, Salt Lake city, Utah. Presentation type: Poster.

Hummos, A., (2015). “*Stabilizing a model of the rat hippocampus*”, Dr. Wulfram, Gerstner Lab EPFL Lausanne, Switzerland. Presentation type: Oral Session.

Hummos, A., Nair, S., (2015). “*Multiple theta mechanisms in a hippocampal model*.” Computational Neuroscience Meeting, Prague, Czech Republic. Presentation type: Oral Session. Conference type: National/International 7/2015

Hummos, A., Nair, S., (2014). "*A comprehensive theory for brain rhythms*." Society for Neuroscience Presentation type: Poster Presentation Conference type: National/International 10/2014

Hummos, A., Franklin, C., Nair, S., (2010). "*Erasing fear memories through Neuromodulation*." Society for Neuroscience Presentation type: Poster Presentation Conference type: National/International 10/2009

Hummos, A., Nair, S., (2009). "Firing rate model of the fear network." Society for Neuroscience
Presentation type: Poster Presentation Conference type: National/International 10/2009

Hummos, A., Nair, S., (2009). "Firing-rate model of the Lateral Nucleus of Amygdala: Towards a Firing-Rate model of the fear circuit." University of Missouri Life Sciences week Presentation type: Poster Presentation Conference type: Local 3/2009